Spring 2018

Imaging and mitigating karst features

Kenneth Joseph Bansah

Department: Mining and Nuclear Engineering

IMAGING AND MITIGATING KARST FEATURES

by

KENNETH JOSEPH BANSAH

A DISSERTATION

Presented to the Faculty of the Graduate School of the

MISSOURI UNIVERSITY OF SCIENCE AND TECHNOLOGY

In Partial Fulfillment of the Requirements for the Degree

DOCTOR OF PHILOSOPHY

in

MINING ENGINEERING

2018

Approved by:

Neil Anderson, Advisor
Grzegorz Galecki
Nassib Aouad
Ralph Flori
Lesley Sneed

ABSTRACT

Over the last three years, a comprehensive subsurface investigation that combines both conventional and geophysical techniques has been conducted near Springfield in southwest Missouri, United States. This study, which forms part of the comprehensive subsurface investigation, aimed to (1) image and characterize the subsurface, (2) map variations in engineering properties of soil/rock, (3) map variable depth to top of rock, (4) explore the utility of the geophysical techniques, (5) determine the factors contributing to karst processes, and (6) propose karst mitigation. Electrical resistivity tomography (ERT) and multichannel analysis of surface waves (MASW) were employed for the acquisition of subsurface geophysical data. Borehole controls were used to verify and constrain the geophysical interpretation.

In some instances, the ERT and MASW techniques produced complementary, high quality, and reliable data consistent with borehole control. Bedrock was pervasively fractured and extensively weathered with pronounced uneven surface. The topography of the surface was observed to depict the topography of the karst bedrock in many of the investigative areas. Moisture content was the major parameter influencing resistivity of the subsurface. A pervasive and systematic network of discontinuities characterizing the bedrock could serve as conduits for percolating acidic waters, ultimately resulting in distinct karst features. Anthropogenic activities were observed as a major contributor to the karst processes. Minimizing the amounts and rate of percolating acidic waters can significantly reduce karst processes and mitigate related features.

ACKNOWLEDGMENTS

I am most grateful to Dr. Neil Anderson for his financial support, excellent academic guidance, and fatherly care. I extend profound gratitude to the advisory committee members: Dr. Grzegorz Galecki, Dr. Nassib Aouad, Dr. Ralp Flori, and Dr. Lesley Sneed, for their support and intellectual input. Dr. Evgeniy Torgashov and the team of graduate students who forfeited the comforts of their beds and offices to help acquire the field data under unfriendly weather conditions are also appreciated.

I extend special gratitude to my wife, Elsie, for her contributions and to my children, Esi, Ekua, and Kweku for their understanding and sacrifices. Many thanks to Ms. Emily Seals, Ms. Tina Alobaidan, Ms. Barbara Robertson, Ms. Shirley Hall, Ms. Stacey Fuller, Ms. Jennifer Schafler, and persons, including staff and colleague graduate students who supported me.

I acknowledge funding support from the Mining and Nuclear Engineering Department and the Rock Mechanics and Explosives Research Center of Missouri S&T towards my PhD program and research. The following scholarship awards are also acknowledged: Tau Beta Pi Scholarship from the Engineering Honor Society, the Tau Beta Pi Association and the Grand Canyon SME Scholarship from the Grand Canyon Section of the Society for Mining, Metallurgy & Exploration Inc. (SME).

I wish also to state that some of the models in this dissertation have been presented at conferences and published in conference proceedings.

TABLE OF CONTENTS

Page

LIST OF ILLUSTRATIONS

Page

LIST OF TABLES

Page

NOMENCLATURE

Symbol	Description
β	Shear-wave Velocity
α	Compressional Wave Velocity
V_R	Rayleigh Wave Velocity
Vs	Shear-wave Velocity
I	Current (amperes)
ΔV	Potential Difference (volts)
c	Conductance(Siemens)
R	Resistance (ohm)
ρ	Resistivity (ohm.m)
$\Omega \cdot m$	Ohm-Meter (ohm.m)
K	Geometric Factor
ρ_w	Resistivity of Fluid saturating the Rock
ϕ	Fraction of Rock filled with Fluid
a	Empirical Parameter (1 for most rocks)
m	Empirical Parameter (2 for most rocks)
L	Length of Cylindrical Rock Sample
A	Cross-sectional Area of Cylindrical Rock Sample

1. INTRODUCTION

1.1. BACKGROUND AND PROBLEM STATEMENT

Karst terrain, a unique environment underlain by carbonate or evaporite bedrock presents complex geologic and morphologic subsurface conditions. It is formed by the gradual dissolution of the carbonate or evaporite bedrock by percolating acidic waters and piping of fine-grained sediments. Karst terrain is characterized by ground failures, sinkholes, sinking streams, closed depressions, subsidence, subterranean drainage, suffusion processes, and caves/caverns (Martínez-Moreno et al., 2014; Pueyo-Anchuela et al., 2010). The heterogeneous nature and complex characteristics of karst terrain pose challenges to safety, groundwater, engineering projects, and the natural environment (Andreychouk & Tyc, 2013; Doerfliger et al., 1999; Peterson et al., 2000). Thus, karst terrain has been a subject of increasing environmental, geological, and geotechnical investigations or studies (Currens et al., 2012; Debeglia et al., 2006; Gómez-Ortiz & Martín-Crespo, 2012).

Different methods, broadly categorized into conventional and geophysical techniques, are used to characterize the soils or subsurface for environmental and geotechnical purposes. Conventional investigation techniques, including inspection, pitting, trenching, probing, and boring/drilling have been used to characterize the subsurface over many decades. Except inspection, the conventional investigation techniques are invasive, more expensive, and time-consuming. Additionally, adopting the pitting, trenching, probing, or boring/drilling method of investigation in karst terrain can

be hazardous to working crew or tools due to potential risk posed by cover-collapse sinkholes or unstable ground.

Geophysical techniques such as ground penetrating radar (GPR), gravity, electromagnetic (EM), and seismic surveys have typically been used to complement conventional investigation techniques for more than three decades (Anderson & Torgashov, 2010; Anderson et al., 2003; Cook, 1965; Daily et al., 1992; Kašpar & Pecen, 1975; Lange; 1999; Moore & Stewart, 1983). More recently, the electrical resistivity tomography (ERT) and multichannel analysis of surface waves (MASW) techniques, which are noninvasive, less expensive, and less time-consuming, have often commonly been used to acquire geophysical data in karst terrain (Baines et al., 2002; Kidanu et al. 2016; Stepišnik, 2008; Yassin et al., 2013). Kidanu et al. (2016) used the ERT and MASW techniques to image the subsurface morphology of an active sinkhole in Greene County, Missouri. Yassin et al. (2013) used the ERT technique to map karst features and estimate the depth to bedrock at a location in Peninsula Malaysia, while Stepišnik (2008) used the ERT technique to investigate collapse doline floors located in Divača, Slovenia.

Due to the unique and complex nature of karst terrain, anthropogenic activities occurring in karst terrain have increasingly become a major concern to many people and governments around the world, partly due to potential for sinkhole development, structural collapse, and groundwater contamination. As a result, there is increasing demand to more effectively control or manage anthropogenic activities in karst terrain. The U.S. EPA and several states (including Kentucky, Indiana, Georgia, and Pennsylvania), for example, have specific requirements or prohibit certain activities, including waste disposal, in karst terrain. Further, in April 2015, the U.S. EPA finalized

regulations for the disposal of coal combustion residuals (CCR), commonly known as coal ash, from coal-fired power plants in landfills and surface impoundments. The regulations, "Hazardous and Solid Waste Management System: Disposal of Coal Combustion Residuals from Electric Utilities; Final Rule (40 CFR Parts 257 and 261)," prohibit CCR landfills in karst terrain unless it is demonstrated that the integrity of the CCR unit will not be disrupted.

The state of Missouri, for example, depends on coal energy. According to the U.S. Energy Information Administration, "Coal fuelled 83% of Missouri's net electricity generation in 2014, 78% in 2015, and 77% in 2016." Hence, coal continues to be a significant contributor to the energy supply in Missouri. The production of energy from coal-fired power plants results in coal combustion residual that is typically disposed of in landfills or surface impoundments. In Missouri, however, the bedrock is carbonaceous, making the ground susceptible to karstification. Missouri is a karst state (Epstein et al., 2002) and has several different karst features, including sinkholes and pinnacles. According to the Missouri Department of Natural Resources, 59% of Missouri contains thick, carbonate bedrock that hosts a wide variety of karst features, including more than 6,000 caves and 3,000 springs, at least 9,500 sinkholes, and hundreds of miles of losing streams. Thus, constructing landfills or impoundments in Missouri or karst states requires proper and adequate ground/subsurface investigations to prevent or control potential risk to surrounding ecosystems.

Therefore, the goal of this research is essentially to conduct subsurface environmental and engineering investigations in karst terrain using both conventional and geophysical techniques, identify the factors that contribute to karst development, and

propose strategies to mitigate karst features. To achieve the goal for the research, a 200-acre site in southwestern Missouri was selected for an experimental study. Geophysical techniques—electrical resistivity tomography (ERT) and active multichannel analysis of surface waves (MASW)—were used to acquire electrical resistivity and shear-wave velocity data, respectively, to explore the utility of the two geophysical techniques and to map variations in engineering properties of soil/rock and depth to top of rock. While site inspections provided useful insights about the conditions of the experimental site and ground surface phenomena, borehole control was used to verify and constrain the geophysical interpretations. The research also determined the factors that drive karst processes and provided strategies to mitigate karst features for the protection of the health and safety of people and the environment.

1.2. RESEARCH OBJECTIVES

This research aims to use geophysical techniques to map subsurface conditions or potential karst features, determine the factors that induce or increase karst processes, and propose karst mitigation strategies to minimize karst processes. The specific objectives of the research are as follows:

i. Use the ERT and active MASW techniques to map and characterize subsurface lithologic conditions in karst terrain.
ii. Map variations in the engineering properties of soil/rock in karst terrain.
iii. Map variable depth to top of rock.
iv. Explore the utility of the ERT and active MASW techniques in karst terrain.

v. Determine the factors that contribute to karst development.

vi. Propose karst mitigation strategies.

1.3. RESEARCH METHODS

As previously stated, different methods are used to investigate karst terrain. In this research, both conventional and geophysical methods were used. The methods adopted include the following:

i. Site selection for experimental work.

ii. Visual inspections of experimental site and surrounding environment.

iii. Acquisition of historical images from the Missouri Department of Natural Resources and Google Earth to determine historical activities of the experimental site.

iv. ERT and active MASW surveys for the acquisition of electrical resistivity and shear-wave velocity data, respectively.

v. Acquisition of borehole control to verify geophysical interpretations.

vi. Surface terrain modeling to determine the nature (topography) of the ground surface of the experimental site.

1.4. SCIENTIFIC CONTRIBUTIONS

This research makes significant contribution to the existing body of literature. The research shows that active MASW shear-wave velocity data corroborate ERT data to depth of at least 20 ft in karst terrain. In addition, the top of karsted bedrock in southwestern Missouri is a function of the surface topography; that is, the karsted

bedrock depicts the surface topography or topographic expression. Further, active MASW and ERT data complement each other and are consistent with borehole control; active MASW depth to top of bedrock is consistent with ERT depth to top of bedrock to depths of at least 20 ft. Finally, anthropogenic activities, including road construction and farming, are observed as major drivers of karst processes. The research also provides useful data that could improve the karst inventory of Missouri and the United States as a whole. The candidate aims to derive at least five journal and conference publications that might be of significant interest to a broader readership from the research.

1.5. ORGANIZATION OF DISSERTATION

There are five main sections in this dissertation. Section 1 introduces the research. It contains the problem statement, research objectives, methods adopted for the research, and the scientific contributions of the research. Section 2 reviews existing literature on karst, karst mitigation, and karst investigations. Section 3 provides detailed description of the ERT and MASW techniques and discusses the theories and principles underpinning both techniques. Section 4 contains the experimental work. It describes the experimental design, geological setting, data acquisition, data processing and interpretation, and data verification. Section 4 also presents results and discusses the results. The final section, Section 5, provides conclusions.

2. OVERVIEW OF KARST

2.1. KARST

Karst is formed from the dissolution of carbonate rock (limestone or dolomite) as well as other highly soluble rocks, including gypsum and salt. The process begins when carbon dioxide dissolves in rainwater to form weak carbonic acid which infiltrates geologic discontinuities (such as joints, bedding planes, and fractures) within the carbonate bedrock (soluble bedrock) and in the process, dissolves the soluble bedrock. Over many years, a karst landform may be formed and characterized by caves, caverns, sinkholes, closed depressions, subsidence, subterranean drainage, sinking streams, suffusion processes, and fissures (Martínez-Moreno et al., 2014; Pueyo-Anchuela et al., 2010). In some instances, the dissolved bedrock may be overlain by non-soluble rock strata, and therefore, a distinctive karst landform might not be present on the ground surface. According to Palmer (1999), major surface karst features originate from internal drainage, subsidence, and collapse triggered by underlying caves.

Karst is a geologic hazard and can pose significant threat to safety, property, and groundwater. Karst hazards can be gradual, rapid, or catastrophic. Andreychouk and Tyc (2013) classify karst hazards into gravidynamic (hazards posed by gravitational processes) and hydrodynamic (hazards posed by movement of water) and also argue that karst terrain is a vulnerable environment. Figure 2.1 shows karst hazard classification by Andreychouk and Tyc (2013).

Among the karst features, sinkholes have gained more attention due to their potential devastating effects, including fatalities, injuries, costly damage, loss of property,

increased insurance claims, huge repair and maintenance cost, and water pollution (Andreychouk & Tyc, 2013; Currens et al. 2012; Dobecki & Upchurch, 2006; Weary, 2015). Weary (2015), for example, gathered 15 years of karst-related damages and estimated that an average of at least $300 million is spent yearly on sinkhole collapse and subsidence issues in the United States.

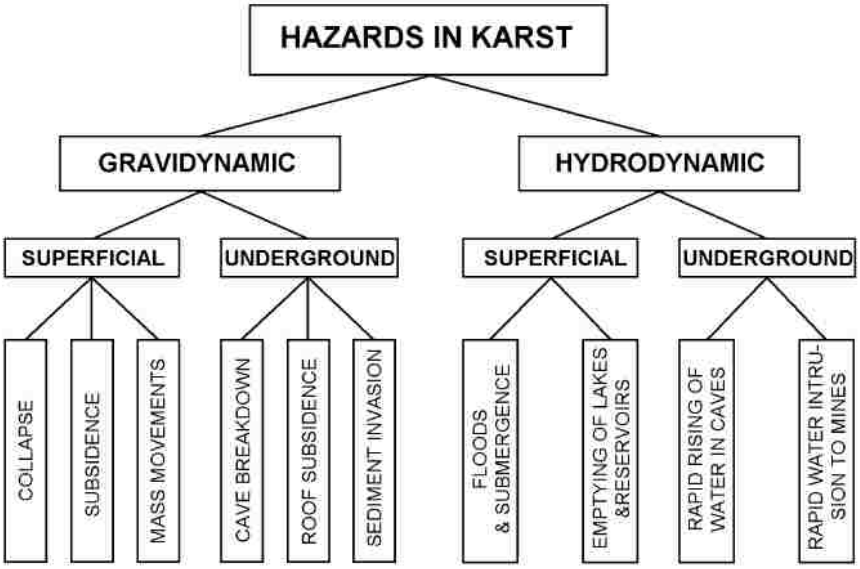

Figure 2.1. Karst Hazard Classification (Andreychouk and Tyc, 2013)

The U.S. Geological Survey (2016) indicate that most damage from sinkholes in the United States has occurred in Florida, Texas, Alabama, Missouri, Kentucky, Tennessee, and Pennsylvania. For example, in November 2013 at Dunedin in Florida, a sinkhole, at least 70 ft in width and 50 ft in depth, collapsed; injured one person, damaged two houses and a swimming pool, and swallowed a boat. And in November 2015, a massive sinkhole, about 600–ft long, 50–ft wide, and 30–ft deep, collapsed at a parking lot in Meridian, Mississippi, sinking at least a dozen vehicles (Figure 2.2). Many

similar sinkhole issues have been reported in many other countries, including Slovenia, China, Italy, and Malaysia (Del Prete et al., 2010; Chen, 1998; Stepišnik, 2008; Šušteršič, 2002; Yassin, et al., 2013; Zhou, 1997). Andrejchuk (2002) studied the causes of the largest sinkhole collapse that occurred above the largest Potash mine in Ural, Russia, in June 1986. He found that a karstic cavity induced the collapse.

Figure 2.2. Sinkhole Collapse at Parking Lot in Meridian, Mississippi (CNN, 2015)

2.1.1. Karst Classification. Karst can be classified as juvenile karst (kI), youthful karst (kII), mature karst (kIII), complex karst (kIV), or extreme karst (kV) (Waltham & Fookes, 2003). Juvenile karst has fissures widespread in the few feet nearest the surface, is characterized by minimal permeability, and does not commonly have sinkholes.

Youthful karst is often characterized by presence of small suffusion and small caves. Mature karst has large dissolution sinkholes, small collapse, buried sinkholes, and caves. Complex karst is characterized by extensive large dissolution openings, many caves, and subsidence sinkholes. Extreme karst has abundant and complex dissolution cavities, very large sinkholes, and arches.

2.1.2. Karst Mitigation. Karst mitigation is conducted to minimize potential risk or damage to the environment as a result of geologic hazards, including ground collapse, flooding, and groundwater contamination. According to Zhou and Beck (2008), mitigation strategy should be informed by the characteristics of the karst feature and anticipated use of the karst site. Karst features that relate water events can be mitigated by controlling the water sources to eliminate or significantly minimize or the solution and erosion processes. Gutiérrez et al. (2008, p.1019) outlined certain measures aimed to mitigate the activity of karst processes. The measures are: "preventing water withdrawal and the decline of water table; lining of canals and ditches; using flexible pipes with telescopic joints; controlling irrigation; making the surface impermeable with geomembranes or geotextiles; using efficient drainage systems and diverting surface runoff; remediating sinkholes and clogging swallow holes; and improving the ground by compaction or injection grouting to increase the strength and bearing capacity of the soils."

According to Gutiérrez et al. (2008, p.1018), the "safest mitigation strategy is avoidance of subsidence features and areas most susceptible to sinkholes," and this could be achieved through land use regulations (Richardson, 2003). However, in areas where developments have taken place, there are procedures to repair sinkholes and stabilize void and prevent future reactivation of the sinkhole. For example, the Missouri Department of Natural Resources recommend the excavation of soil materials to bedrock surface and filling the void with size-graded gravel (graded filter) as shown in Figure 2.3.

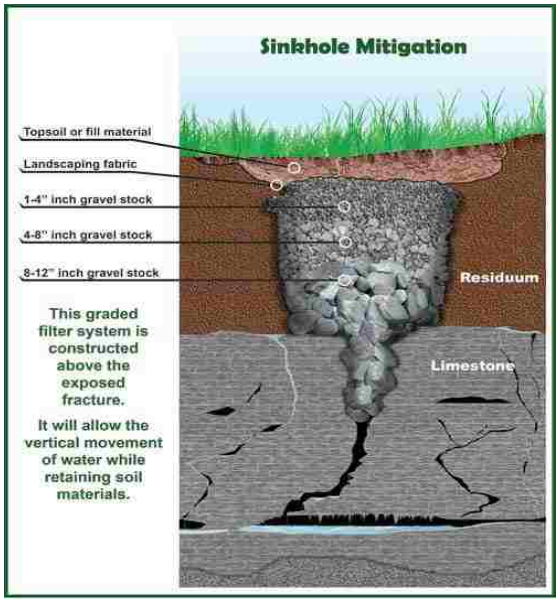

Figure 2.3. Schematic of Sinkhole Mitigation (Missouri Department of Natural Resources, n.d.)

Sowers (1996) suggested grouting for filling cavities. In grout plugging, the sinkhole throat is plugged with concrete, such that the concrete bonds with the rock at the soil-rock interface. Cooper (1998) indicated that filling cavities with grout could lead to focused dissolution because the grout can block underground flow conduits in the soil/rock.

Engineering methods, including (i) excavating and throat plugging or fracture filling and (ii) compaction grouting and cap grouting are described by Zhou and Beck (2008). Compaction grouting plugs the throat of a sinkhole located at depth of at least 10 m and is usually conducted in the overburden or shallow rock. The method involves drilling grouting holes into the sinkhole and its vicinity and grouting with the aim to improve the soil or rock within the sinkhole. According to Zhou and Beck (2008), compaction grouting can lead to focused dissolution, may be less effective in pinnacle rock, and induce additional fractures due to hydrofracturing, when poorly designed. Cap

grouting is usually for treating an extensive area with small but distinct fractures located at the surface of the bedrock. It involves pumping cement at low grout pressure at the bedrock surface to seal solution cavities and to prevent piping of soil. Cap grouting consumes less grout than compaction grouting (Zhou & Beck, 2008). Siegel et al. (1999), graphically present compaction and cap grouting in Figure 2.4.

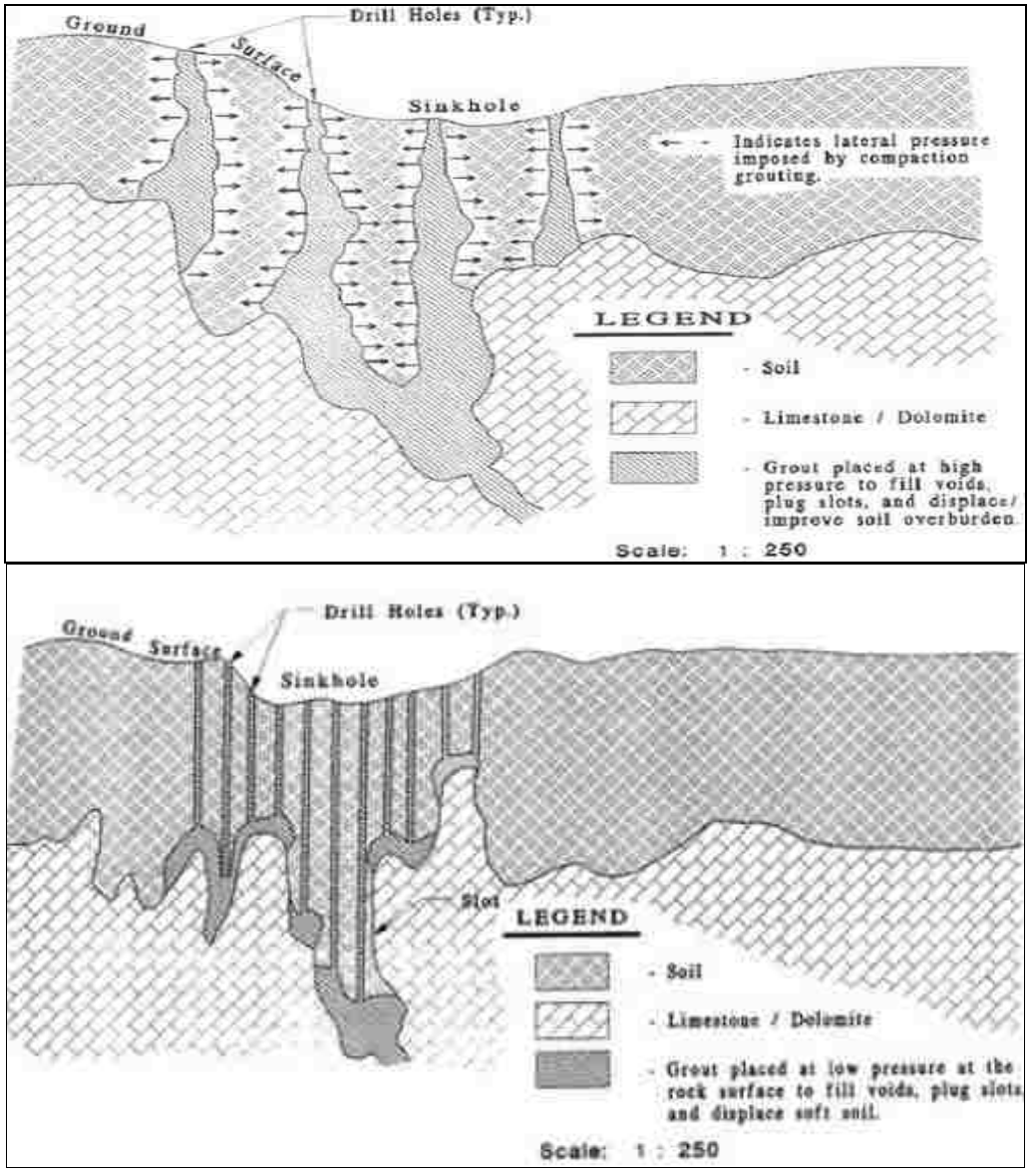

Figure 2.4. Sinkhole Grouting; Top: Compaction Grouting; Bottom: Cap Grouting

2.2. GEOPHYSICAL TECHNIQUES FOR INVESTIGATING KARST TERRAIN

Geophysical techniques have been applied successfully to image subsurface lithologic conditions in karstic environment. Chalikakis et al. (2011) provide an overview of the contribution of geophysical techniques to karst exploration and indicate that geophysical techniques can provide valuable information in karstic environments. Geophysical techniques adopt noninvasive procedures to detect or characterize the physical properties of the subsurface. Physical phenomena that are measured by geophysical techniques may include gravity, elastic waves, potential difference, magnetism, and electromagnetic waves. These physical phenomena may be sensitive to subsurface physical properties, including density, resistivity, magnetic susceptibility, seismic wave velocity, permittivity, and conductance. Geophysical surveys carried out prior to construction activities in karst terrain have high probability to mitigate void risks and optimize intrusive investigations such as drilling. Geophysical exploration can be used to estimate hazard, explore groundwater, or assess vulnerabilities in karst terrain (Ballard et al., 1983; Bernard et al., 2006).

Geophysical techniques that have been used to map the subsurface in previous research include electrical resistivity tomography (Kruse et al., 2006; Nouioua et al., 2013; Obi, 2012; Stepišnik, 2008;Yassin et al., 2013), ground penetrating radar (Kruse et al., 2006; Munroe et al., 2007; Nouioua et al., 2013; Webb et al., 2002), gravity method (Hoover, 2003; Kamal et al., 2013), electromagnetic survey (Hoover, 2003), and seismic surveys (De Giorgi and Leucci, 2014; Hoover, 2003; Kidanu et al., 2016). The choice of any of the geophysical technique for an exploration depends on the physical characteristics of the target. It has been observed that the greater the contrast, the higher

the probability of detecting the geophysical target (Dobecki, 1990). Moreover, each of the geophysical techniques has its strengths and weaknesses, which depend on factors such as the geology of the subsurface, size and depth of the feature of interest, desired image resolution, presence of water, etc.

2.2.1. Electrical Resistivity Tomography. The electrical resistivity tomography (ERT) method determines resistivity distribution by using electrodes. The technique involves the injection of electric current into the ground between one pair of electrode and voltage is measured on another pair. An image of the ground in terms of resistivity is then created. ERT is capable of mapping vertical and lateral variations in apparent resistivity, and has the ability to approximate the shape, size, and depth of air-filled voids (Obi, 2012).

2.2.2. Ground Penetrating Radar. Ground penetrating radar (GPR) uses electromagnetic waves to map the subsurface. The GPR tool has a shielded transmitter antenna which emits electromagnetic pulse at regular intervals as it traverses the ground surface. As the pulse encounters a change in lithologic properties, parts of the pulsed energy is reflected back to the receiver of the GPR. The GPR receiver records the magnitude and arrival times of the reflected pulsed energy. The velocity of a GPR pulse is inversely proportional to the square root of dielectric permittivity of the material through which it propagates.

The GPR technique can be used to locate buried facilities, detect voids/cavities, and map bedrock depth fractures. It has also been used extensively in geotechnical foundation investigations, as well as archaeological, environmental, and hydrogeological studies (Huisman et al., 2003; Kruse et al., 2006; Munroe et al., 2007; Nouioua et al.,

2013; Saarenketo & Scullion, 2000; Webb et al., 2002). For example, Grandjean et al. (2000) used the GPR technique to evaluate a test site for civil engineering applications. GPR signals are attenuated very rapidly in clay medium, as clay is a high conductive material and capable of absorbing the GPR signal. It therefore becomes difficult to image areas containing substantial amount of clay using the GPR technique.

2.2.3. Gravity Method. The gravity method is used to measure differences in gravitational field at specific locations on the ground surface. It can be used to locate karst features, covered stream basins, and determine soil (layer) thickness. The principle is based on contrasting densities of the subsurface materials. Different earth materials have different densities which give rise to varying gravitational field. The variations in gravitational field are then used to estimate the depth and geometry of buried features. The gravity method however, has a set of drawbacks including topographic changes, earth tides, and rotation, which must be corrected before proceeding with modeling and interpretation of data (Obi, 2012).

2.2.4. Electromagnetic Survey. Electromagnetic surveys use electromagnetic induction to determine ground conductivity. The tool for electromagnetic (EM) survey consists of a transmitter and a receiver which are spaced at a fixed configuration. The transmitter generates primary electromagnetic field to induce secondary magnetic field which is detected by the receiver. The magnitude of the secondary magnetic field detected by the receiver is a function of the ground conductivity; different subsurface materials have different conductivity.

In the field, EM data is typically collected in a grid; the size of the target determines the spacing of the grid-lines and recording stations. For smaller targets, closer

survey lines and denser spaced readings are used. Electromagnetic survey adopts different frequencies to image the subsurface. Low frequencies are capable of imaging large underground cavities, while high frequencies are used to detect smaller targets at shallow depth. Obi (2012) indicated that air-filled voids or fractures are transparent to electromagnetic signal and are difficult to detect. Another limitation is the difficulty in isolating changes in depth to bedrock from lateral changes in electrical conductivity.

2.2.5. Seismic Surveys. Seismic surveys utilize acoustic waves generated by impact or explosive source to image the subsurface. Applications of this technology may include, but not limited to depth-to-bedrock, layers of overburden, voids, and faults. Seismic survey methods used in imaging karst terrains include multichannel analysis of surface waves (MASW), seismic refraction and seismic reflection techniques. The MASW tool consists of a seismic source (e.g sledge hammer) and receiver arrays (geophones), typically used for exploring to depths of about 100 ft (30 m). The MASW measures surface waves generated by the seismic source, analyzes the velocities of the surfaces waves, and generates a shear-wave velocity profile of the subsurface. The shear-wave velocity is a measure of material stiffness; the higher the shear-wave velocity, the stiffer the material.

The seismic refraction technique utilizes refraction of seismic waves from geologic interfaces to characterize subsurface geologic structures and conditions. The technique is governed by Snell's Law and principally consists of an array of geophones and a seismic source. The seismic refraction technique operates on the principle that different materials have different characteristics, and therefore will exhibit varying seismic wave velocities. Seismic waves travel through the ground when the seismic

energy source is triggered. As the waves encounter a change in lithologic properties, some of the seismic energy is refracted back to the surface, while the remainder propagates further downwards at a refracted angle. Geophones located on the ground surface record the arrival times of the refracted seismic energy. Based on the travel time data, a velocity model of the subsurface can be generated, and available borehole records could further be used to calibrate the model to establish the levels of subsurface layers with much confidence.

Seismic reflection technique is similar to the seismic refraction method. The seismic reflection technique images the lithologic interfaces between materials with contrasting acoustic velocities. The contrasting acoustic velocities translate to differences in the elastic properties of the material and density. Seismic energy is generated at the surface by an impact or an explosion. This causes the propagation of seismic waves through the subsurface, where they get reflected at interfaces of contrasting seismic velocities. Geophones along the survey line on the ground surface record the magnitude and arrival times of the reflected acoustic energy. Seismic reflection identifies variations in material type with depth and horizontal position. The technique is capable of providing detailed information about “geometry of sedimentary sequences, structural faults, igneous intrusions and evaporite deposits” (RSK Geophysics, n.d., p.25). Seismic reflection can be used for stratigraphic mapping, geological mapping, and to determine depth-to-bedrock.

3. ERT AND MASW TECHNIQUES

3.1. ERT TECHNIQUE

The concepts and theories underpinning the ERT technique are described in the following sections.

3.1.1. Brief Introduction to ERT. The ERT technique is a noninvasive geophysical method that is used to determine electrical resistivity distribution of the subsurface. It is based on the principle that subsurface materials have unique electrical characteristics, and thus, the technique utilizes contrasting electrical properties to map and characterize the subsurface. In the field, electric current is transmitted into the ground through a pair of electrodes, resulting in a potential difference measured by another pair of electrodes. ERT can map lateral and vertical variations in apparent resistivity of geologic materials and can approximate the size, shape, and depth of water or air-filled cavities. The ERT technique depends on certain concepts discussed in the following subsections.

3.1.2. Resistivity Theory. Resistivity logging is based on important equations that relate the resistivity of the subsurface to the resistivity of saturating fluids, porosity, and fractional degree of saturation of each fluid. Fundamentally, the resistivity equations have been derived from Ohm's law, which states that the current flowing through a conductor from point A to point B is directly proportional to the potential difference between the two points. Hence,

$$I = c\Delta V \tag{3.1}$$

where I is the current measured in amperes (A), ΔV is the potential difference in volts (V), and c is a constant of proportionality called conductance measured in siemens (S). But electrical resistance (R) is the inverse of conductance. Therefore, Equation 3.1 becomes

$$R = \frac{\Delta V}{I}. \tag{3.2}$$

Resistance is a function of material properties (resistivity) and the shape of the material through which the current flows. Considering a cylindrical rock sample of length L and cross-sectional area A (Figure 3.1), the resistance to current flow is given by Equation 3.3:

$$R = \rho \frac{L}{A}. \tag{3.3}$$

Thus, $\rho = R\frac{L}{A}$ (3.4)

where ρ is the resistivity of the rock sample.

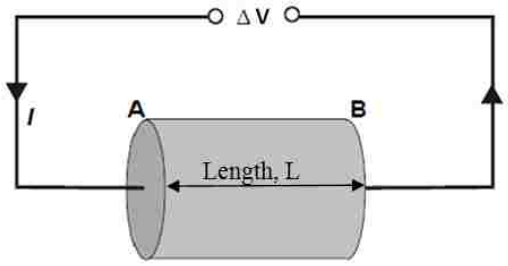

Figure 3.1. Ohm's Law for Cylindrical Rock Sample

In practice, resistivity measurements are done using a pair of current-inducing electrodes and potential difference measured at two other electrodes. In Figure 3.2

(typical array), A and B are the current electrodes, and C and D are the potential electrodes.

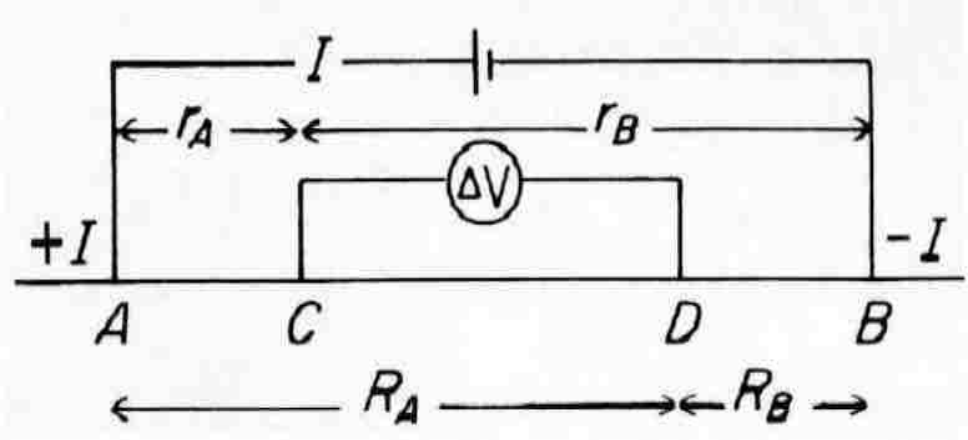

Figure 3.2. Arrangement of Current and Potential Electrodes

Assuming a uniform earth, resistivity can be calculated from Equation 3.5:

$$\rho = RK = \frac{\Delta V}{I} K \tag{3.5}$$

where K is a geometric factor given by

$$K = \frac{1}{\left(\frac{1}{2\pi r_A} - \frac{1}{2\pi r_B}\right) - \left(\frac{1}{2\pi R_A} - \frac{1}{2\pi R_B}\right)}. \tag{3.6}$$

For a Wenner array (Figure 3.3),

$$r_A = R_B = a \,(\text{constant}) \text{and } \mathrm{r_B} = R_A = 2a$$

Hence, $K = 2\pi a$. (3.7)

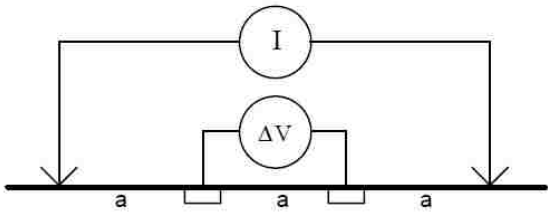

Figure 3.3. Wenner Array

3.1.3. Electrode Arrays. Electrode arrays that are commonly used for electrical resistivity measurements include the Wenner, Schlumberger, dipole-dipole, and pole-dipole arrays (Figure 3.4). The choice of a particular array depends upon the characteristics of the target feature, sensitivity of the resistivity system, and background noise. Loke (2011) mentions investigation depth, array sensitivity, horizontal data coverage, and signal strength as characteristics that should be considered for the choice of an array for a field survey and further discusses the advantages and disadvantages of each electrode array. For example, he states that the Wenner array is appropriate for a noisy environment and has good vertical resolution, but is poor in detecting horizontal changes.

3.1.4. Geology and Resistivity. The flow of electric current in earth materials at shallow depths is by electronic and electrolytic conduction. Electronic conduction involves the flow of current through free electrons, while electrolytic conduction is due to the flow of ions. Electrolytic conduction is a common mechanism in environmental and engineering surveys. According to Cardimona (2002), resistivity is a function of saturation, salinity, and porosity and increases with the decreasing number of water-filled fractures. Hence, compaction of soils or rock units will result in increasing resistivity.

Variations in the resistivity distribution of the subsurface are therefore controlled by the characteristics and nature of the subsurface lithologic units. Figure 3.4 shows the

resistivity of some rocks, soils, and chemicals. The resistivity of igneous and metamorphic rocks mainly depends on the extent of fracturing and moisture content. Depending on the degree of wetness or dryness, the resistivity of these rocks may vary from 1,000 to over 10 million Ω·m. Sedimentary rocks are typically more porous and therefore have a higher water content, resulting in low resistivity that may range from 10 to 10,000 Ω·m.

Unconsolidated sediments (e.g., alluvial deposits) have low resistivity values ranging from 10 to less than 1000 Ω·m due to their degree of saturation. Unconsolidated sediments have a higher porosity and a high clay content. Clay is very conductive and has lower resistivity than sand. As previously stated, porosity, degree of saturation, and salinity can alter the resistivity of subsurface materials and cause an overlap of resistivity for such rock types. Therefore, direct sampling, geophysical, or geotechnical information may be required to ascertain subsurface lithologic units. Cardimona (2002) summarized some typical resistivity values as shown in Table 3.1. Resistivity of groundwater ranges from 1 to 100 Ω·m with a typical value of 5 Ω·m, while seawater has a very low resistivity of about 0.2 Ω·m due to its high salt content.

Table 3.1. Typical Resistivity of Earth Materials

Common Resistivities (ohm-m)		
Material	Resistivity range	Typical Value
Igneous & Metamporphic rocks	10^2 - 10^8	10^4 10^3
Sedimentary rocks	10 - 10^8	10^3
Unconsolidated	10^{-1} - 10^4	10^3
Groundwater	1 - 10	5
Pure water		10^3

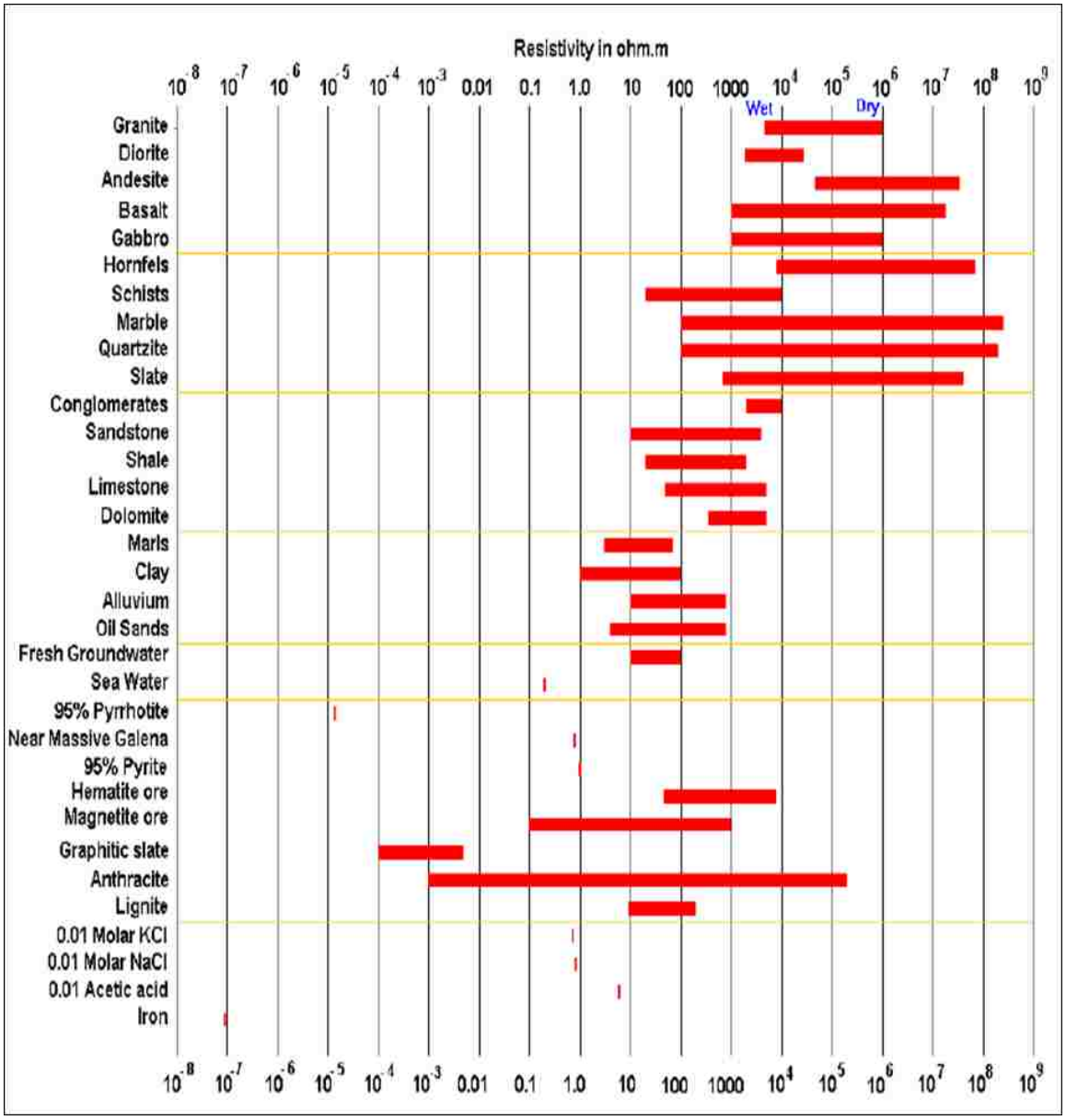

Figure 3.4. Resistivity of Earth Materials (Daniels and Alberty, 1966; Keller and Frischknecht, 1966; Telford et al., 1990)

Electrical conduction through rocks composed of nonconductive minerals and saturated with water is governed by Archie's law, given by

$$\rho = a\rho_w\phi^{-m} \tag{3.8}$$

where ρ is resistivity of the rock, ρ_w is resistivity of the fluid, ϕ is the fraction of the rock filled with the fluid, and *a* and *m* are empirical parameters. For most rocks, *a* is about 1, while *m* is about 2.

3.1.5. Inversion Theory. Resistance measurements are normally reduced to apparent resistivity values after the field survey. Computer software (e.g. RES2DINV/RES3DINV) is usually used to convert the suite of apparent resistivity values into a resistivity model section used for geological interpretation. The conversion process is described by Loke (2011, 2004, 2000).

In dealing with resistivity data, it is important to remove bad data points (outliers) to obtain representative results to boost interpretation. These bad data points can result from systematic or random noise. Systematic noise is shown as unusually high or low values and can be caused by breaks in the cable, weak electrode contact with the ground, a disengaged clip and electrode connection, or wrong cable connection.

Random noise can result from effects such as telluric currents and is more common with dipole-dipole and pole-pole arrays. It is impractical to manually remove random, bad data points since such noisy data points are not obvious. Figure 3.5 shows field data with bad data points.

3.1.6. Considerations and Limitations of the ERT Technique. The automated multi-electrode ERT technique is an effective method for characterizing subsurface lithologic and morphologic conditions. The deliverable is a 2-D ERT image of the subsurface with superposed geologic interpretations.

It is assumed that variations in the resistivity at a specific location reflect changes in soil/rock lithology and moisture content. Interpretations are generally reliable,

especially if borehole control is available to constrain or verify interpretations. One-dimensional (1-D) and 3-D ERT data can be acquired. In water, ERT data can be acquired in using specialized marine cables. Interpretations, especially when constrained, are reliable (less so in stratigraphically/structurally complex areas). Further, there is limited potential for equipment error as instrument is self-testing. However, reliability of interpretations decreases as the lateral and vertical heterogeneity of soil/rock increases.

The choice of the ERT technique for the acquisition of geophysical data depends on certain factors and considerations which are summarized in Table 3.2 (N. Anderson, personal communication, August 17, 2015). Such factors and considerations include utility, reliability, and reproducibility of typical deliverables.

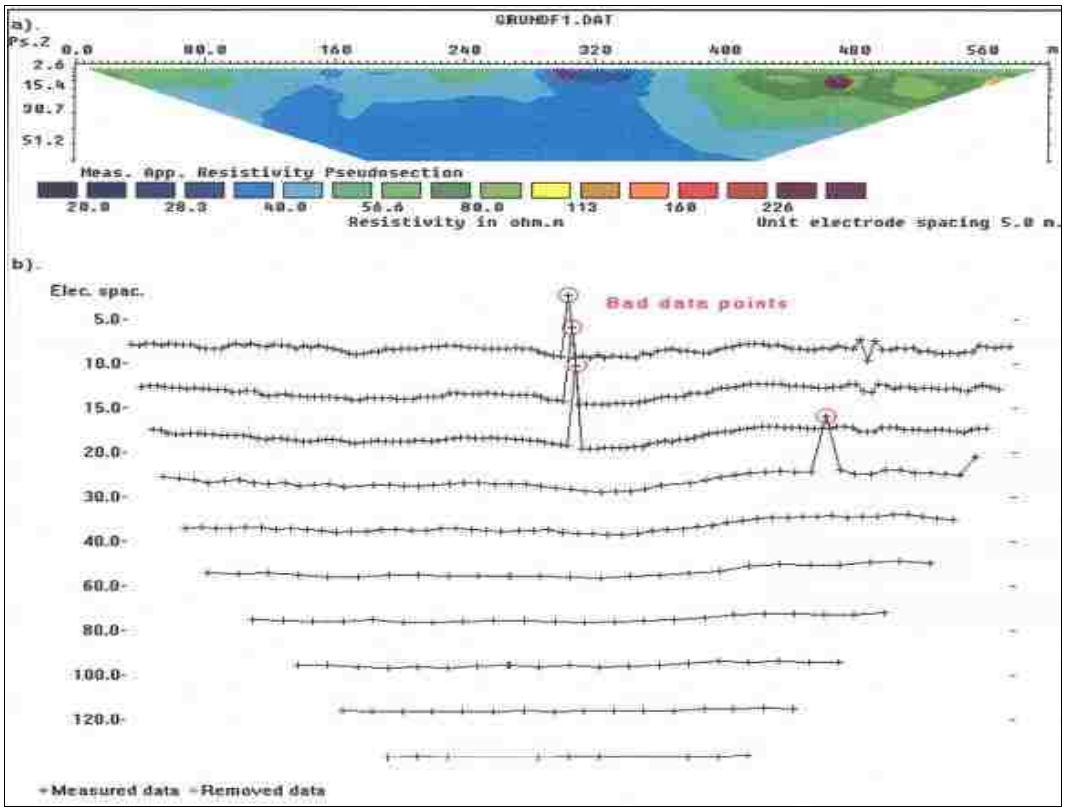

Figure 3.5. Bad Data Points shown on the Pseudosection and Profile (Loke, 2011)

Table 3.2. Considerations and Limitations of ERT

Utility of typical deliverable	ERT interpretations can be used for mapping/identifying: • variations in rock quality and lithology; • depth to top of rock; • pattern, placement ,and density of solution-widened cavities; • pattern, placement, density and offset of faults; • air-filled voids and water- or clay-filled cavities; • depth to top of water table; • distribution of moist soil, dry soil, moist rock, and dry rock; • distribution of soil types (e.g. silty or clayey soil); • groundwater flow pathways.
Reliability of typical deliverable	**Output of data processing:** An uninterpreted ERT profile (output of automated processing) will be reliable if the field data are good quality and if the 3-D subsurface through which the current flows can be reasonably well represented by a 2-D ERT profile. This assumption is usually less valid in more structurally/stratigraphically complex areas. The inversion software generates an error estimate for each output uninterpreted ERT profile. **Deliverable:** An interpreted ERT profile is reliable if it accurately depicts resistivity variations in the subsurface and if ground truth is used to constrain and verify the interpretation.

Table 3.2. Considerations and Limitations of ERT (cont.)

Reproducibility of typical deliverable	The electrical resistivity of soil and rock varies with the moisture content of the subsurface, which causes corresponding changes in the resistivity values displayed on acquired ERT data. However, the resultant geologic interpretation of the output ERT profile does not change significantly in most cases. Experienced interpreters can produce similar 2-D geologic interpretations if good quality ERT data are acquired and if ground truth is available.
Data collection method (automated, semi-automated, manual)	ERT data can generally be acquired (start to finish) along a 395 ft traverse (using 80 electrodes spaced at intervals of 5 ft) in about 3-4 hours. Data collection is slowed because electrodes (stainless steel spikes, typically 18 in. in length) need to be manually inserted into the ground at multiple locations along the length of the traverse and connected to the resistivity meter via cable. However, the recording of the ERT field data is fully automatic. Depth of an investigation can be increased by increasing the length of the array; resolution can be increased by decreasing the electrode spacing.
Network-level investigations	Not applicable to network-level investigations.

Table 3.2. Considerations and Limitations of ERT (cont.)

Applicability for project-level investigations	Very applicable to project-level investigations where detailed stratigraphic and/or structural information about the subsurface is required.
Advantages	• ERT data are in relatively high resolution (compared to other geophysical methods capable of imaging the subsurface to depths in excess of 50 ft). • Resolution can be increased by decreasing electrode spacing. • Depth of an investigation can be increased by increasing array length. • The subsurface can be imaged to depths in excess of 100 ft unless site access is limited. • ERT data can, with some degree of difficulty, be acquired across paved roadways. • Limited potential for human error. • Tool is noninvasive, except for insertion of metal electrodes. • Data collection is relatively rapid and automated (except for the insertion of electrodes and the coupling of cables). • The processing of field data is automated (user input is required when data are noisy). • Data can be processed and interpreted (preliminarily) on-site. • Field data are reproducible except in “noisy” areas.

Table 3.2. Considerations and Limitations of ERT (cont.)

Disadvantages	• Ground truth is required to accurately constrain geologic/hydrologic interpretations. • Resolution and reliability of data decrease with increasing depth. • Reliability decreases as heterogeneity of soil/rock increases. • The array of electrodes must be ~5x the desired maximum depth of investigation. • Full depth coverage is achieved only beneath the central third of the array. • ERT data are not normally acquired while it is raining since moisture can damage non-waterproof cable electrode connections. • Rain, high humidity, and high temperatures can damage the resistivity meter. • It can be very difficult to couple electrodes to frozen ground. • Crew productivity decreases in adverse weather conditions. • ERT field data quality can be adversely affected if traverses are located in close proximity to utilities or parallel to grounded fences or guard rails. • Elevation control along ERT traverses is required, if the elevation differences exceed 1 ft.

Table 3.2. Considerations and Limitations of ERT (cont.)

Recommendations	The acquisition of 2-D ERT data is recommended at any location where detailed geologic control is required. The ERT tool is normally a great tool for imaging the subsurface between and beneath boreholes. If possible, the ERT array should be oriented perpendicular to the strike of linear features of interest.

3.2. THE MASW TECHNIQUE

The MASW technique, which is the second geophysical technique employed for the acquisition of subsurface data is described in the following sections. The theories and governing equations of the MASW technique are discussed.

3.2.1. Brief Introduction to MASW. The MASW technique was first introduced by Park et al. (1999) and is used to evaluate the elastic conditions of soil or rock. The MASW technique measures surface waves from acoustic sources and analyzes the propagation velocities of the surface waves to generate shear-wave velocity variations at the surveyed location.

The shear-wave velocity is an elastic constant, which is closely related to Young's modulus, and is a measure of stiffness. The MASW survey yields shear-wave velocity information that can be presented in 1-D, 2-D, or 3-D formats. The concepts and procedure governing the MASW technique are discussed in the following thematic sections.

3.2.2. Overview of Waves. Body waves (compressional and shear waves) and surface waves (Rayleigh and Love waves) are generated by discharging an acoustic source on the surface. While body waves propagate deeper into the subsurface, surface waves are confined to the shallow subsurface and propagate radially away from the source. Body waves are non-dispersive and travel through a medium with a speed proportional to the density of the medium and its modulus.

The two types of body waves are categorized according to the mode of propagation involving particle movements. The particle motion can be longitudinal (P-waves) or transverse (S-waves or shear waves) to the direction of the traveling wave (Figure 3.6). Compressional waves transfer energy by compressing and dilating particles as the wave passes through a medium and travel at 1.5-8 km/s. Compressional waves travel through the earth's core and shake the ground in the direction of propagation. Shear waves, however, are 1.7 times slower than compressional waves and are second to arrive at a seismic station. Shear waves shake the ground perpendicular to the direction of propagation and do not propagate through liquids.

Surface waves (Rayleigh and Love waves), on the other hand, travel along the surface or along the boundary of dissimilar materials. Surface waves arrive after compressional and shear waves. Rayleigh waves are characterized by retrograde particle motion, while Love waves have particle motion transverse to the direction of propagation, but with no vertical motion (Figure 3.7). The MASW technique employed in this research is based on the Rayleigh waves. Love waves are being currently explored for the acquisition of MASW data. For example, the Kansas Geological Survey more

recently upgraded the MASW data processing software (SurfSeis5) to enable the processing of data acquired with the use of Love waves.

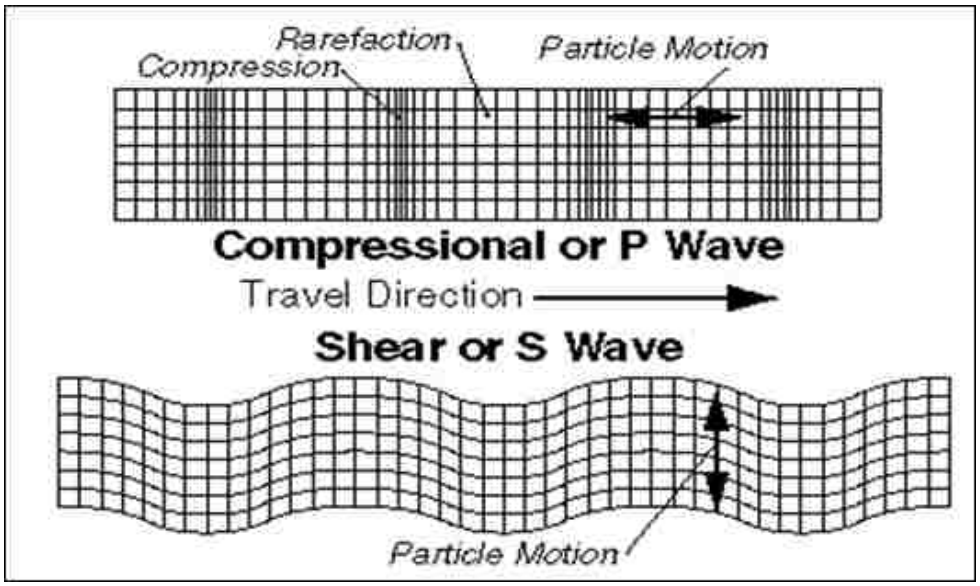

Figure 3.6. Compressional and Shear Waves

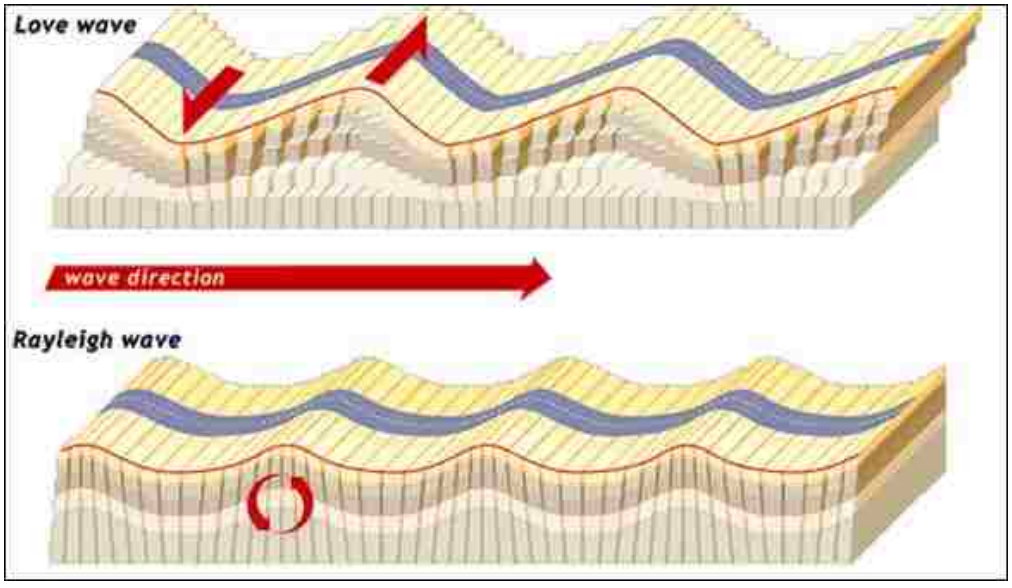

Figure 3.7. Love and Rayleigh Waves

3.2.3. Rayleigh Waves. Rayleigh waves propagate in same manner as ocean waves and get smaller as they propagate deeper in the ground. Rayleigh waves are dispersive since different wave frequencies travel with different phase velocities. Rayleigh wave velocity decreases with increasing depth. The highest Rayleigh wave frequency involves particle motion at shallow depths, intermediate frequencies at intermediate depths, and the lowest frequency at greater depths. Hence, Rayleigh waves are attenuated as depth increases. In order to image the subsurface to a reasonable level of accuracy at depth, Rayleigh wave velocity is approximated to be 0.9 times the corresponding shear-wave velocity. As a result, Rayleigh wave phase velocity versus frequency data can be transformed into depth versus shear wave velocity data.

Rayleigh wave phase velocity in a uniform medium is constant and can be determined using Equation 3.9,

$$V_R^6 - 8\beta^2 V_R^4 + (24 - 16\beta^2/\alpha^2)\beta^4 V_R^2 + 16(\beta^2/\alpha^2 - 1)\beta^6 = 0 \qquad (3.9)$$

where V_R is Rayleigh wave velocity, β is shear-wave velocity, and α compressional wave velocity.

Rayleigh wave velocity is more sensitive to variations in shear-wave (β) velocity than variations in compressional wave velocity (α). Therefore, a value of Poisson's ratio is often assumed such that the Rayleigh wave velocity (V_R) through soil and rock is approximately 90% of the shear-wave velocity. Thus,

$$V_R \approx 0.9\beta. \qquad (3.10)$$

3.2.4. MASW Survey Procedure. The MASW surveys normally involve the following steps (Park et al., 1999).

1. Acquisition of multichannel records.

2. Conducting dispersion analysis.
3. Inverting dispersion curves to obtain 1-D (depth) Vs.
4. Stacking multiple 1-D results into 2-D or 3-D profiles.

The MASW data acquisition method can be categorized into an active or passive method depending on the nature of the seismic source. The active MASW that was employed in this research uses an active seismic source, such as a sledge hammer and a linear receiver array (Figure 3.8).

Data in an active MASW survey is collected in a roll-along manner. The distance of the source is known in the active MASW. The passive MASW method uses surface waves generated from natural or ambient cultural activities (including earthquakes, thunder, traffic from vehicular movements, industrial noise, etc.). The distance of the source in this method is unknown.

The passive MASW can be categorized into passive remote MASW (Park et al., 2007) or passive roadside MASW (Park and Miller, 2008) depending on the receiver configuration. The passive remote MASW utilizes a 2-D receiver array, while the passive roadside MASW uses a horizontal 1-D receiver array. According to the Kansas Geological Survey (2014), optimizing the source distance can improve the quality of dispersion curve imaging and interpretation. The passive method may not be used in areas where naturally or randomly occurring noise is absent.

Dispersion analysis is the first step of data processing in the MASW method. The objective of dispersion analysis is to generate dispersion curves for inversion. The dispersion analysis has traditionally considered the estimation of only the fundamental-mode curve. Curves of higher modes are occasionally estimated in addition to the

fundamental mode in recent times. Inversion is done to generate a 1-D Vs structure from the dispersion curve.

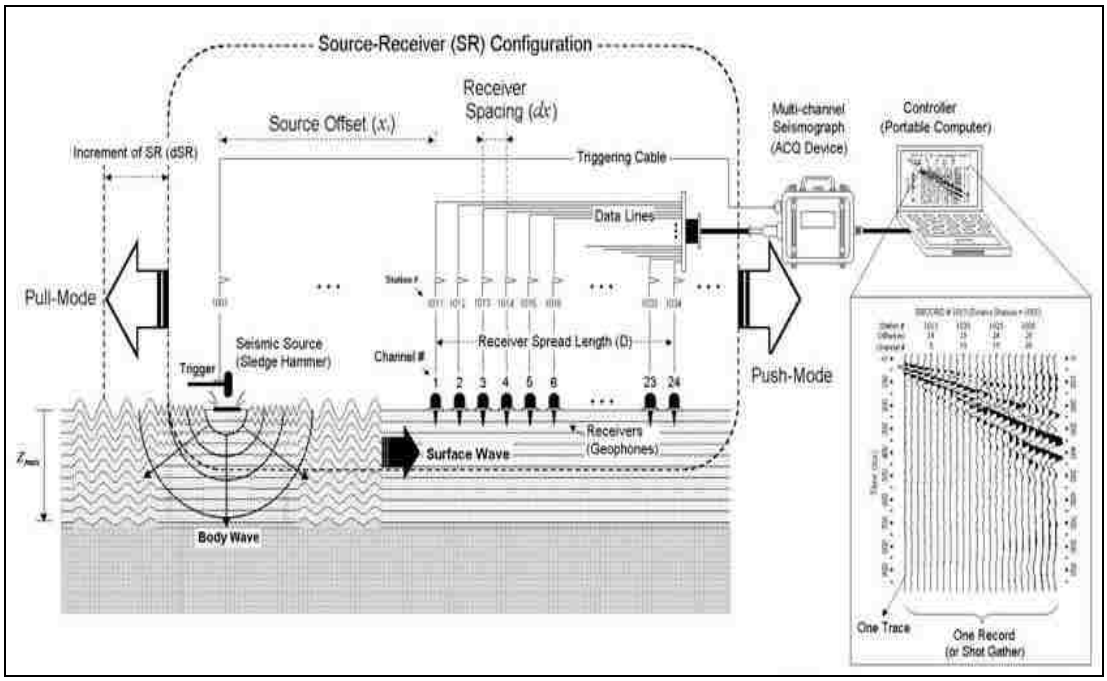

Figure 3.8. Typical Field Setup of the Active MASW Survey (MASW, n.d.)

In the inversion process, a synthetic fundamental mode dispersion curve is matched with a curve picked from the data. A Vs model is constructed automatically or manually, and then a synthetic dispersion Vs curve is generated. Iterative adjustment is done on the initial Vs model to improve the fit between the two Vs curves. Inversion is focused on matching dispersion curves rather than Vs profiles because Vs changes in Rayleigh wave velocity are not directly proportional to changes in Vs (non-linearity) (Reynolds International, 2011). The MASW field data acquisition and processing procedures are summarized by Park et al. (2007) in Figure 3.9.

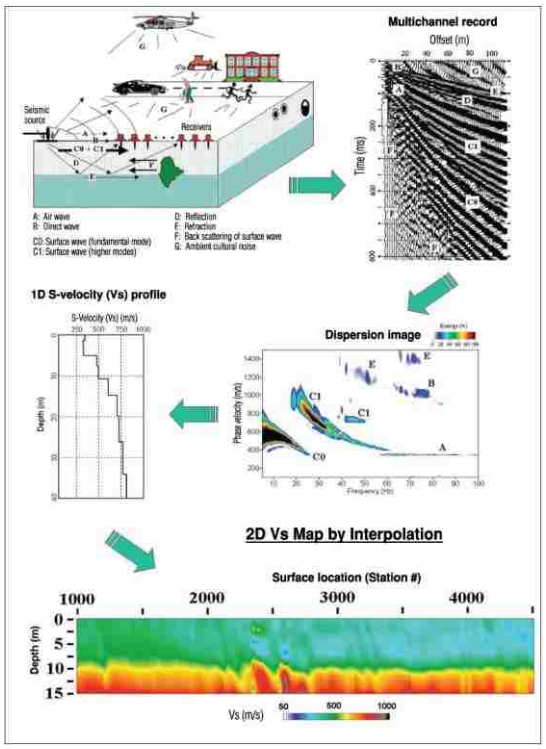

Figure 3.9. Schematic of MASW Data Acquisition and Processing Procedure (Park et al., 2007)

3.2.5. Considerations and Limitations of the MASW Technique. The MASW technique has been used to evaluate ground stiffness for various types of environmental, geotechnical, and engineering projects. The MASW tool is noninvasive and is capable of generating reliable 1-D and 2-D shear-wave velocity profiles of the subsurface in areas where the subsurface is neither stratigraphically nor structurally complex. Additionally, there is limited potential for human error during data acquisition and processing.

However, reliability of data interpretations decreases as vertical and lateral heterogeneity of soil/rock increases. Ground truth is also required to accurately constrain and verify geologic interpretations of MASW data. Table 3.3 provides a summary of the considerations and limitations of the MASW technique (N. Anderson, personal communication, March 17, 2016).

Table 3.3. Considerations and Limitations of the MASW Technique

Description of typical deliverable	The typical deliverable of a MASW survey is a 1-D shear-wave velocity profile of the subsurface often with superposed geologic interpretations. Typically, the subsurface is imaged to a depth of approximately 100 ft or less (if sledge hammer, weight-drop or other relatively small magnitude active sources are employed). If passive surface wave sources are utilized, the 1-D shear-wave velocity profile can be extended to depths of several hundred feet. 2-D shear-wave velocity profiles can be created by acquiring MASW field records at multiple locations along a traverse. The 1-D shear-wave velocity profiles generated for each location can be appropriately placed side by side and contoured, thereby generating a 2-D shear-wave velocity profile.
Utility of typical deliverable	The output 1-D shear-wave velocity profile can be useful in highway construction and/or maintenance. For example, a shear-wave velocity profile that extends to depths of 100 ft can be used for earthquake site classification purposes. Although the interfaces between adjacent velocity layers on a 1-D shear-wave velocity profile may not correlate to specific geologic contacts, the velocity assigned to each layer may be indicative of the dominant lithology of that layer (e.g., sand, clay, limestone).

Table 3.3. Considerations and Limitations of the MASW Technique (cont.)

Utility of typical deliverable	Furthermore, the depth to the interface between an overlying layer with a shear-wave velocity consistent with that of soil and an underlying layer with a velocity consistent with rock can be indicative of the depth to top of rock. 2-D shear-wave velocity profiles can also be of significant utility. Variable depth to the top of rock, low velocity zones, lateral and vertical changes in lithology, etc., can often be inferred on the basis of the interpretation of the 2-D shear-wave velocity profiles.
Reliability of typical deliverable	If high quality MASW field data are recorded, and if the subsurface can be reasonably well-represented by a layered velocity model (this assumption is usually less valid in more structurally/stratigraphically complex areas), the output 1-D and/or 2-D shear-wave velocity profiles can be very reliable. If ground truth is available, the superposed geologic interpretations can also be highly reliable.
Reproducibility of typical deliverable	If the subsurface is stratigraphically and/or structurally complex, the output 1-D shear-wave velocity profile generated for a specific observation location can vary if the length and/or orientation of the geophone array are changed.

Table 3.3. Considerations and Limitations of the MASW Technique (cont.)

Reproducibility of typical deliverable	However, if good quality field data are acquired, if the subsurface can be well-represented by a layered-velocity model, and if ground truth is available, experienced interpreters will produce very similar 1-D or 2-D shear-wave velocity profiles and comparable superposed geologic interpretations.
Data collection method (automated, semi-automated, manual)	An array of geophones (typically 24) are placed on the ground surface at uniform intervals and connected to an engineering seismograph. The length of the array should be approximately equal to the desired maximum depth of investigation. If active MASW data are desired, an acoustic source is discharged off the end of the array (typically ~20 ft depending on the length of the array) and the generated surface wave signal is recorded as it passes through the geophone array. Active data are normally used to generate relatively high-resolution 1-D shear-wave velocity images of the upper 100 ft. If high-resolution images of the shallow subsurface (to depths significantly less than 100 ft) are required, shorter geophone arrays and lower magnitude acoustic sources can be employed. If passive MASW data (only) are desired, a field source is not employed.

Table 3.3. Considerations and Limitations of the MASW Technique (cont.)

Data collection method (automated, semi-automated, manual)	Rather, the user simply places a linear or symmetric array of geophones on the surface and records passive surface wave signal generated by non-active sources (includes traffic, distal earthquakes, quarry blasts, etc.). Passive MASW data are normally used to generate lower-resolution 1-D shear-wave velocity images extending to depths of multiple hundreds of feet. Combination active/passive MASW data can be acquired.
Applicability for network-level investigations	Not applicable to network-level investigations as data acquisition is relatively slow.
Applicability for project-level investigations	Applicable to project-level investigations. Tool can often be used to generate reliable 1-D and/or 2-D shear-wave velocity profiles of the subsurface. It is usually relatively easy to acquire high quality active MASW data even in acoustically noisy areas and across paved, rocky, frozen, muddied, graveled, or sandy surfaces. Passive ReMi data are usually easy to acquire in a DOT ROW because traffic is a great source of passive surface wave energy.
Advantages	• If ground control is available, reliable geologic models can be generated.

Table 3.3. Considerations and Limitations of the MASW Technique (cont.)

Advantages	• Depth of investigation is typically on the order of 30 ft when active sources are employed, but much greater if passive sources are utilized. • Average shear moduli can be assigned to each "velocity layer" imaged. • Data can be acquired while it is raining as long as the recording instrument is protected. • Data can be processed in the field. • Data processing is semi-automated and relatively fast. • Superposed geologic interpretations, especially when constrained, are reliable (less so in stratigraphically/structurally complex areas). High quality data can often be acquired even in acoustically noisy areas and across paved, rocky, frozen, muddied, graveled or sandy surfaces.
Disadvantages	• Ground truth is required to accurately constrain geologic interpretations. • Crew productivity decreases in adverse weather conditions. • A suitable source of passive surface wave energy may not be present at the survey site during data acquisition.

Table 3.3. Considerations and Limitations of the MASW Technique (cont.)

Disadvantages	• Reliability of interpretations decreases with depth and as the lateral and vertical heterogeneity of soil/rock increases.
Recommendations	The acquisition of active MASW data is recommended at any location where general information about stratigraphy/structure/elastic moduli of shallow (depths < 30 ft) soils and/or rock is required. If high-resolution images of the shallow subsurface (to depths significantly less than 100 ft) are required, shorter geophone arrays and lower magnitude acoustic sources can be employed. If greater depths of investigation are required, the acquisition of combination active/passive MASW control is recommended.

4. EXPERIMENTAL WORK

4.1. OVERVIEW

An experimental study was conducted to address the objectives of the research. As stated in Section 1 of this dissertation, the specific goals of the research are to (i) use the ERT and active MASW techniques to map and characterize the subsurface in karst terrain; (ii) map variations in the engineering properties of soil/rock in karst terrain; (iii) map variable depth to top of rock; (iv) explore the utility of the ERT and active MASW techniques in karst terrain; (v) determine the factors that contribute to karst development; and (vi) propose karst mitigation strategies.

To address the goals of the research, a potential karst terrain was chosen for the experimental study. Desk study was conducted and a plan for the execution of the research was developed together with the determination and assignment of logistics prior to the field work. Modifications to the plan were made based on site conditions during data acquisition. Both geophysical and conventional data, including 2-D ERT data, 1-D MASW data, and borehole control, were part of major data acquired from the experimental site.

This section therefore describes the methods adopted in this research and informs the reader about the experimental site (study area), geological setting, and data acquisition, processing, interpretation, and verification procedures. A description of the study area, research approach, and techniques employed for the research are provided in this section to help the reader appreciate the subject matter. To address the objectives of the research, three thematic topics are used: (a) mapping subsurface and acoustic

properties of soil/rock in karst terrain; (b) imaging subsurface in karst terrain using 2-D ERT and 1-D MASW techniques; and (c) determining drivers of karst processes and mitigation. The reason for the choice of the experimental site and the rationale for each of the thematic topics have been discussed. The following subsections describe the study area, data acquisition and processing techniques, provide the results of the study, and discuss the results.

4.2. STUDY AREA DESCRIPTION

The study area is located near the city of Springfield in southwest Missouri in the United States (Figure 4.1). Springfield is found in Greene County and is the county's seat. The state of Missouri borders eight different states, on the north by Iowa; on the south by Arkansas; on the east by Illinois, Kentucky, and Tennessee; and on the west by Oklahoma, Kansas, and Nebraska. Vandyke (1993) documented the geologic and stratigraphic units in Greene County (Table 4.1).

Bedrock comprises Mississippian limestones and cherty limestones, which are underlain by Ordovician and Cambrian rocks. These three sedimentary rock systems (Cambrian, Ordovician, and Mississippian) were deposited on a crystalline rock of the Precambrian System. The Cambrian System is overlain by the Ordovician System, comprising the Gasconade Formation, Roubidoux Formation, Jeffersion-City Formation, and Cotter Formation. The Gasconade Formation, which is the basal unit in the Ordovician System, is composed of Gunter Sandstone, Lower Gasconade Dolomite, and Upper Gasconade Dolomite. The Gasconade Formation has total thickness 375 ft, the Roubidoux Formation has thickness 150 ft, and the Jefferson-City and Cotter Formations

together are 600 ft thick. The Cambrian System consists of the Lamotte Formation, Bonneterre Formation, Davis Formation, Derby-Doerun Formation, Potosi Formation, and Eminence Formation. The Cambrian System has a total thickness of about 1000 ft: Lamotte Formation (150 ft); Bonneterre Formation (200 ft); Davis Formation (150 ft); and Derby-Doerun Formation, Potosi Formation, and Eminence Formation (500 ft).

The Mississippian System, which has thickness of at least 425 ft, is made up of six formations: Compton, Northview, Pierson, Reeds-Spring, Elsey, and the Burlington-Keokuk Formation. The Mississippian System starts with the Compton Formation with a thickness 30 ft. The Compton Formation is overlain by the Northview Formation with thickness up to 80 ft. The Pierson, Reeds-Spring, and Elsey Formations have total thickness of more than 240 ft and overly the Northview Formation. The youngest formation in the Mississippian System, the Burlington-Keokuk Formation has a thickness of 150 – 270 ft.

The Mississippian Burlington-Keokuk Limestone, which is exposed in some places, is pervasively fractured and extensively karsted. The karsted limestone bedrock is susceptible to dissolution by slightly acidic percolating waters. In the Mississippian Burlington-Keokuk Limestone, layers of limestone are interbedded with thin layers of chert. Bedrock is highly and unevenly dissolved, resulting in an irregular bedrock-overburden interface. Surface topography is undulating with surface flow commonly intercepted by roadways. Soils at the study area are mainly residual soils compacted or eroded in some places. Farming activities are commonly observed at the study area. Kidanu et al. (2016) and Muchaidze (2008) further describe the geology and stratigraphy

of the study area and Greene County in general. These authors describe the genesis and composition of the various rock formations.

Table 4.1. Geology and Stratigraphy of Greene County (Vandyke, 1993)

System	Series	Group	Formation		Thickness (ft)
Mississipian	Osagean		Burlington-Keokuk Formation		150-270
			Elsey Formation		25-75
			Reeds-Spring Formation		125
			Pierson Formation		90
	Kinkerhookian	Chouteau	Northview Formation		5-80
			Compton Formation		30
Ordovician	Canadian		Cotter Formation		600
			Jefferson-City Formation		
			Roubidoux Formation		150
			Gasconade Formation	Upper Gasconade Dolomite	350
				Lower Gasconade Dolomite	
				Gunter Sandstone Member	25
Cambrian	Upper		Eminence Formation		500
			Potosi Formation		
		Elvins	Derby-Doerun Formation		
			Davis Formation		150
			Bonneterre Formation		200
			Lamotte Formation		150
Precambrian	Crystalline rock				

The study was conducted on a 200 acre site proposed for the disposal of industrial solid waste. Industrial solid waste may contain toxic heavy metals such as arsenic, mercury, and lead that can pollute groundwater and threaten the health of consumers. Therefore, the disposal of industrial solid waste in karst terrain must be given critical

consideration because inadequate environmental and engineering investigations of the subsurface could lead to significant environmental and safety issues when the waste is deposited. Accordingly, the proposed industrial solid waste site offered an area of significant choice for this study. This is because this study involves detailed subsurface investigations and employs advanced and state-of-the-art techniques to obtain unique and complex information for environmental, geological, and geotechnical purposes.

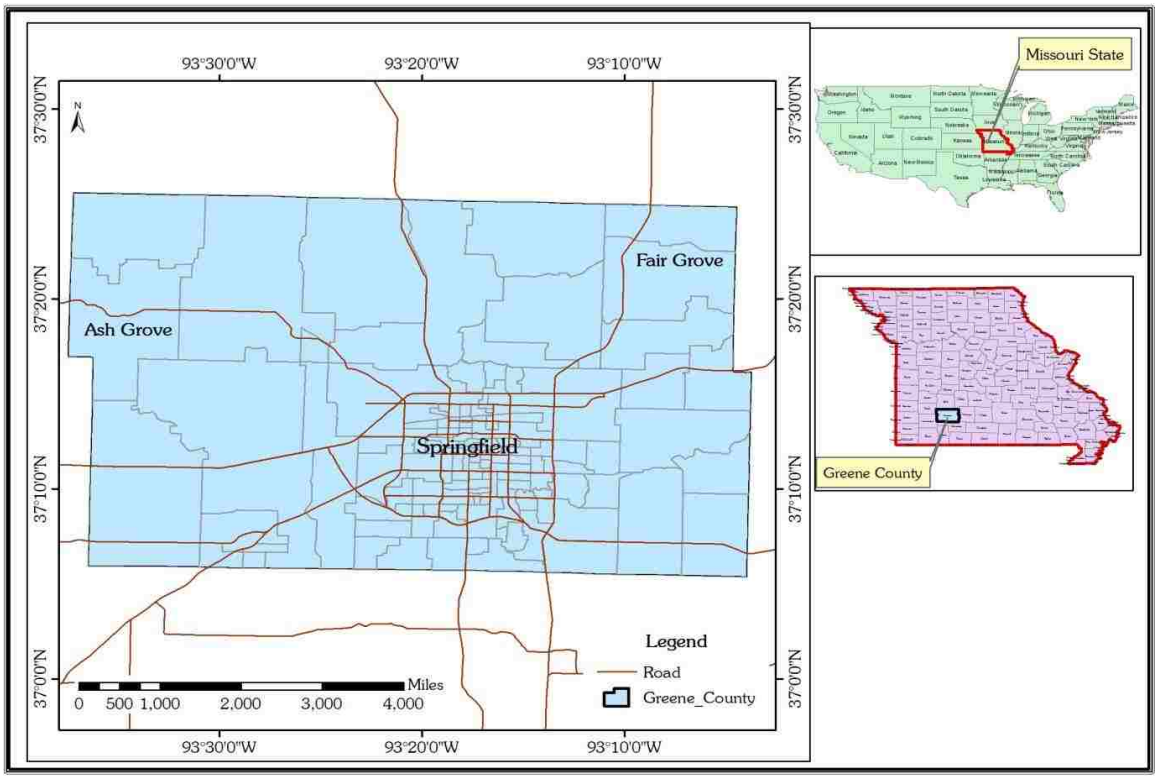

Figure 4.1. Study Area

4.3. EXPERIMENTAL DESIGN

Geophysical and conventional techniques were employed in the acquisition of data for this research. Geophysical techniques used included the ERT and MASW techniques, while conventional techniques mainly comprised site inspections and

acquisition of ground truth (borehole control). Additional methods employed included digital terrain modeling and acquisition of historic data.

4.3.1. ERT Technique. The ERT technique employed a multi-electrode resistivity system powered by a 12-volt deep cycle marine battery, 5 ft electrode spacing, and a dipole-dipole array configuration with the intent to map the subsurface to a depth of at least 100 ft. The resistivity meter used in this study is the SuperStingR8 developed by the Advanced Geosciences Inc. (Figure 4.2). The resistivity measurements employed 168 electrodes mounted on a coaxial cable. In the field, a measuring tape is typically placed horizontally on the ground surface across the orientation of the subsurface feature to be imaged. The purpose of the measuring tape is to ensure the accuracy of the electrode spacing. The electrodes are ground-coupled using metal stakes and then connected to the SuperStingR8 resistivity meter. The field setup is checked and corrected for setbacks such as improperly connected cable, weak electrode contact, or wrong cable connection and the appropriate data acquisition settings applied. A test run is conducted on the setup and any detected anomaly is corrected before the actual data acquisition. Data is automatically stored in the resistivity system.

Data acquisition times vary depending on site conditions or the acquisition settings applied. For example, an icy or a muddy ground can delay the setting up of the resistivity system and increase the data acquisition time. Furthermore, a resistivity system that is set to re-acquire data if the initial data acquired were noisy might take a longer time to complete the data acquisition process. A three-member crew would typically acquire 800 ft to 1200 ft of data in a single working day if 5 ft electrode spacing is employed and if crew movement is not impeded.

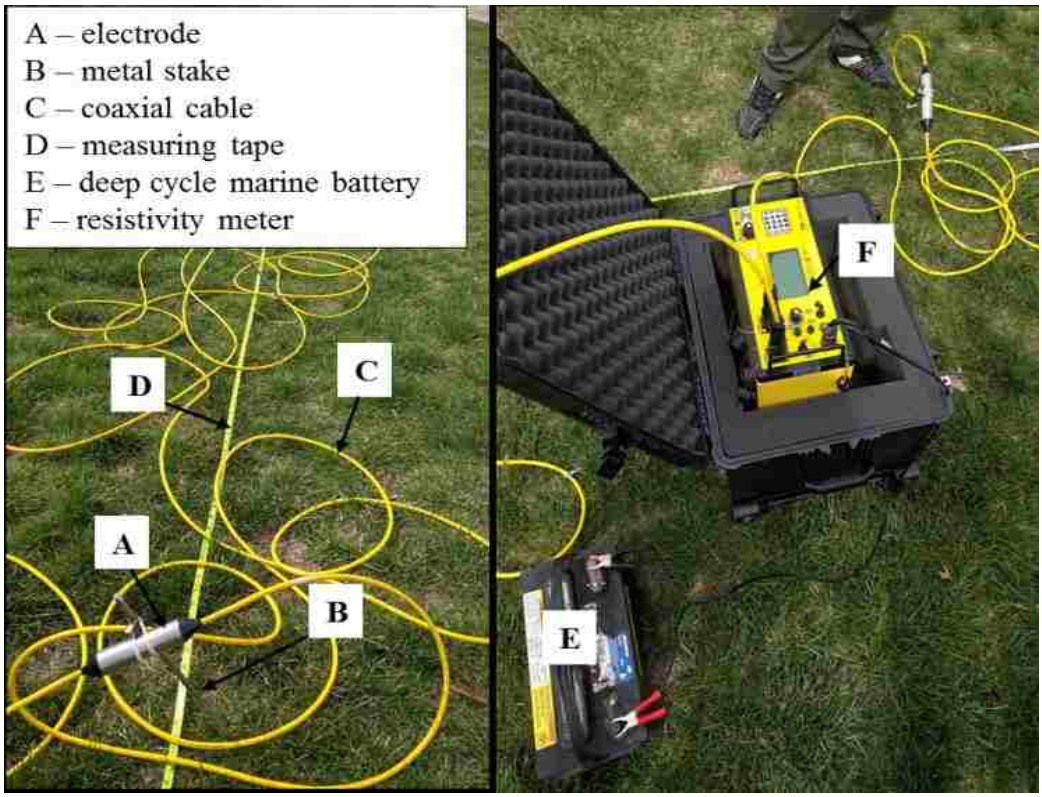

Figure 4.2. ERT Setup

The resistivity measurements stored in the resistivity system are downloaded onto a laptop computer following data acquisition in the field. The resistivity data can quickly be processed in the field to check the quality of the data before the equipment and its accessories are disassembled and the crew departs the field. The actual data processing or inversion is completed post-field in a laboratory using inversion software such as RES2DINV. During the inversion process, an apparent resistivity model is compared with a synthetic model through seven iterations. The number of iterations can be varied by the software user. However, the manufacturer's recommendation of seven iterations is commonly adopted. Topographic corrections can be applied during data processing such that the final two-dimensional output displays the nature of the surface terrain. Multiple

parallel profiles of the same traverse length can be lined up to give a three-dimensional view of the subsurface or the target of interest.

4.3.2. MASW Technique. Surface wave data for the MASW technique were acquired using an engineering seismograph powered by a 12-volt deep cycle marine battery. Geophone spacing of 2.5 ft and 5 ft were adopted with source offset of 10 ft. Geophone frequency of 4.5 Hz and a 20-pound sledge hammer as an acoustic source were used with the goal to image the subsurface to a depth of at least 50 ft. The MASW data were processed using the SurfSeis4 software produced by the Kansas Geological Survey.

The engineering seismograph used for this study is the Seistronix Ras-24 seismograph (Figure 4.3). In the field, a measuring tape is placed along the survey traverse to ensure reliable and consistent geophone spacing. The geophones mounted on a coaxial cable are coupled to the ground using metal stakes. The geophone assembly and the deep cycle marine battery are connected to the seismograph and then connected to a laptop computer. Any detected anomaly in the setup is corrected, and the setup is tested to ensure readiness for data acquisition. Surface waves generated by striking the 20-pound sledge hammer on the impact plate are automatically received by the geophones and transmitted to the seismograph for storage. The field record (multichannel record) is displayed on the laptop computer, which is connected to the seismograph. If the multichannel record displayed on the laptop computer is noisy or is of low quality, the cause of the noise or the source of the low quality data is checked and corrected. One way to improve the quality of the multichannel records is the acquisition of multiple records at the same source location. That is, at every record location, the impact plate is struck

multiple times with the sledge hammer to obtain multiple records that can be stacked in order to mute unwanted noise and to improve data quality, enhance resolution, and to boost data interpretation.

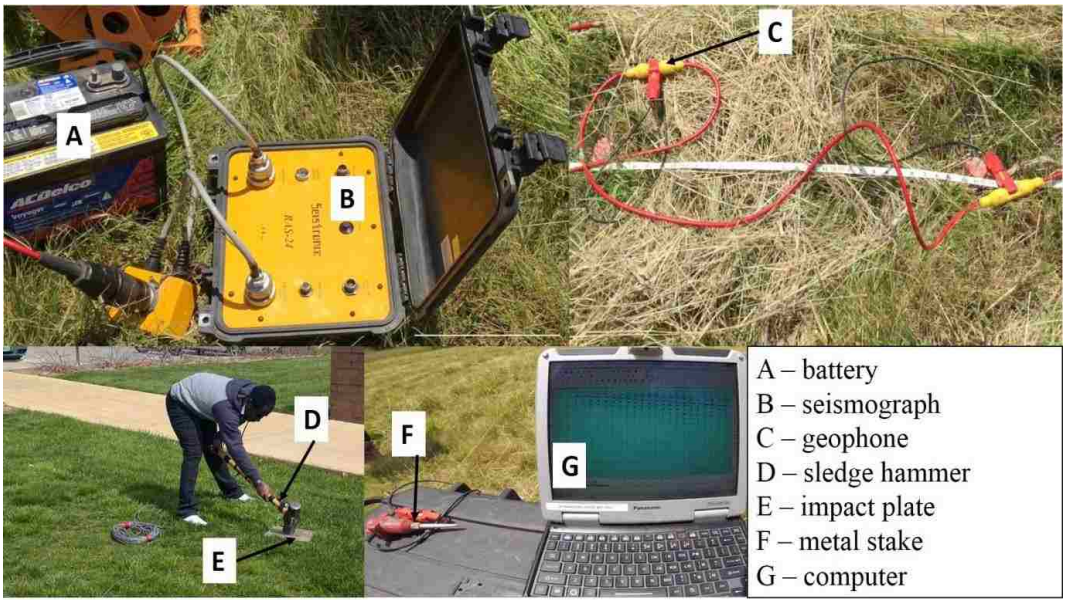

Figure 4.3. MASW Setup

4.3.3. Conventional Techniques. Conventional techniques such as drilling, pitting, or trenching are typically used to provide complementary data to verify geophysical data or interpretations.

In this study, site inspections and acquisition of ground truth (borehole control) were used to provide additional data to support the geophysical investigations. Site inspections were conducted by walking over and around the study area for identification and observation of surface features. Photographs and video recordings of features such as ponded water locations were taken using a 14-megapixel camera.

The geographic locations of the observed features were acquired with a handheld GPS. The locations of the features were verified through Google Earth. Borehole control data were acquired using a CME track-mounted drill rig. Soil testing, including in situ moisture content, was conducted on recovered samples. Some of the borehole control (BC) and ponded water (PW) locations at the investigative site are shown in Figure 4.4.

Figure 4.4. Example Ponded Water and Borehole Control Locations

4.3.4. Digital Terrain Modeling. Digital terrain modeling was conducted to develop visual representations of the terrain surface. The digital terrain modeling was done using the Surfer13 software. Some of the models generated included the surface elevation model, top of rock model, and soil thickness/depth to top of rock model. The surface terrain model (Figure 4.5) provides the elevations of the surface topography and gives an impression of the surface flow directions. Surface elevation is up to 1245 ft in the high areas and 1195 ft in the low land areas. The high areas can be found in the north, east, and west. Hence, surface flow directions of north-south, west-east, and east-west are observed. Surface water flows in those directions and eventually drains south.

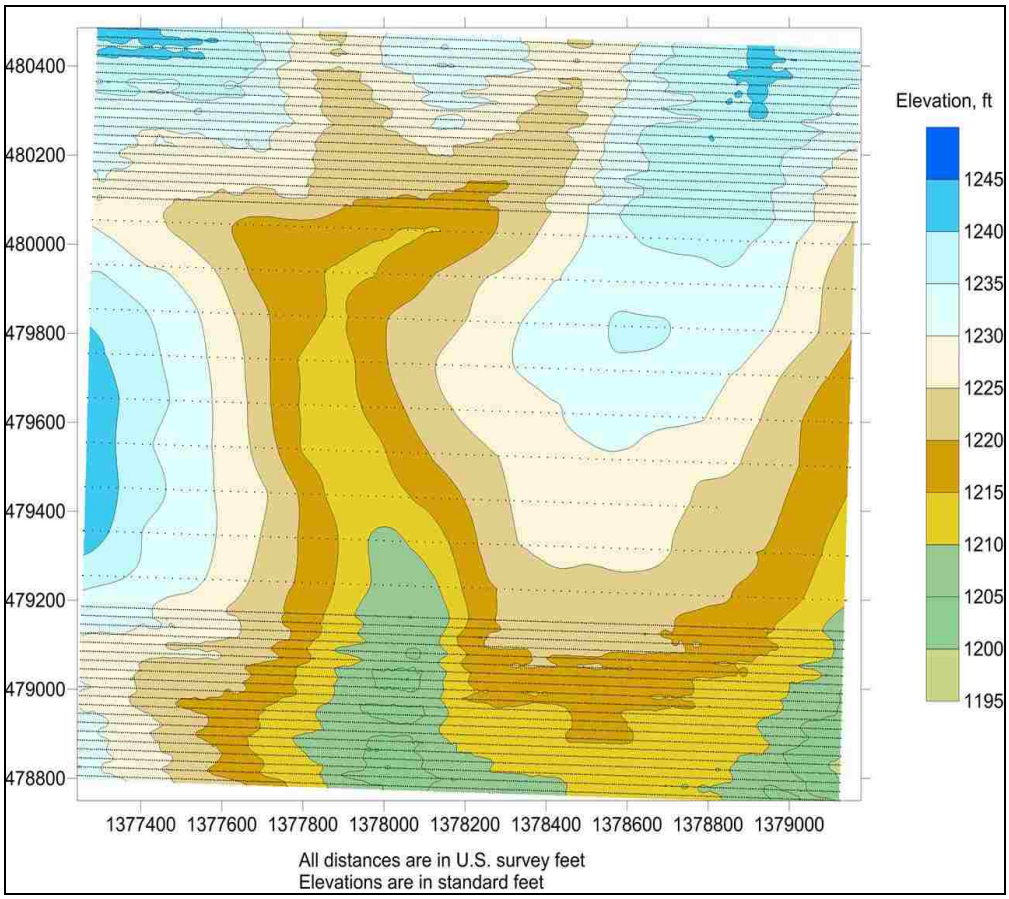

Figure 4.5. Surface Elevation Model

Top of rock elevations are as high as 1235 ft and as low as 1150 ft (Figure 4.6). The top of rock elevations are high in most parts of the north, east, and west. These elevations in the top of rock model depict variations in elevations of the surface terrain model. Groundwater flow direction follows the same direction as the surface flow. Top of rock is highly irregular and is characterized by marked variations in elevations. This top of rock shows characteristics of bedrock that is intensely dissolved or has undergone extensive karstification. Thus, top of rock model partly proves that the study area is a karst terrain.

Soil thickness/depth to top of rock model is shown in Figure 4.7. As previously indicated the bedrock is exposed in some areas and therefore has little or no soil coverings. In areas where the bedrock is covered with soils, mainly residuum, the bedrock is located at shallow depth and the soil thickness is mostly 5 to 20 ft. In some areas, the soils have thickness averaging 70 ft.

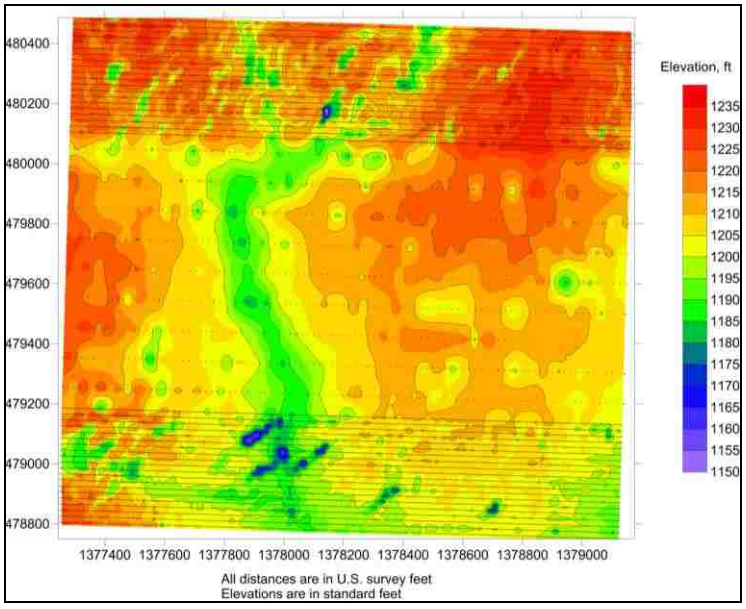

Figure 4.6. Top of Rock Elevation Model

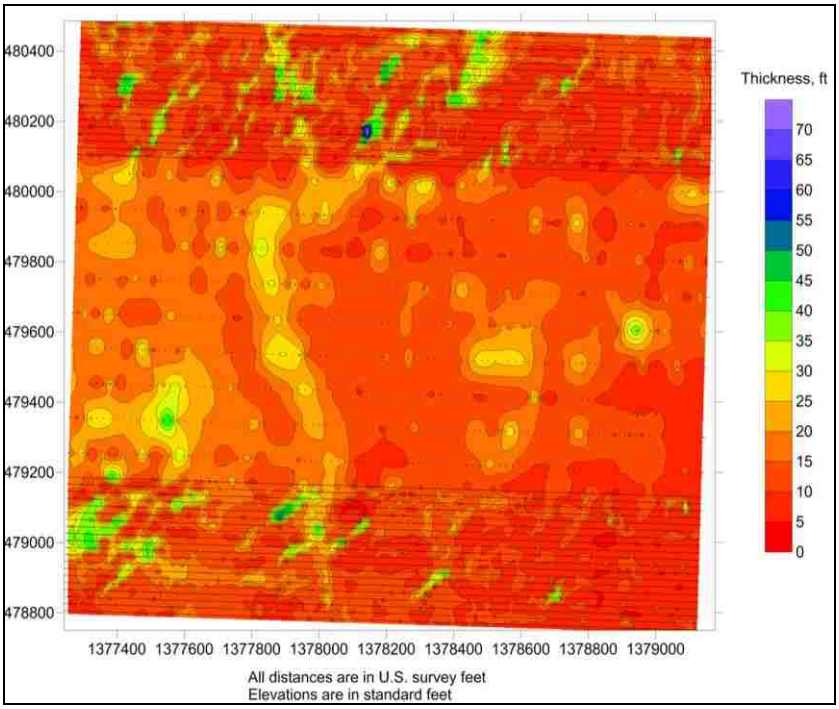

Figure 4.7. Soil Thickness/Depth to Top of Rock Model

4.4. MAPPING SUBSURFACE AND ACCOUSTIC PROPERTIES OF SOIL AND ROCK IN KARST TERRAIN

This section describes how the geophysical and conventional techniques were used to map the subsurface and acoustic properties of soil and rock in the study area.

4.4.1. Brief Introduction. Geophysical techniques, including MASW and ERT are being increasingly used to image the top of bedrock and to determine the acoustic properties of soil/rock karst terrain. To test the utility of the two geophysical techniques in a complex karst terrain, the MASW and ERT tools were deployed to acquire geophysical data in the study area.

The MASW tool was used to acquire shear-wave velocity data, while the ERT tool was used for electrical resistivity measurements. The goal of the study was to

explore the utility of the geophysical techniques in complex karst terrain and to estimate the depth to bedrock and acoustic properties in karst terrain.

The active MASW technique was employed as the main investigative technique to estimate the depth to bedrock and the acoustic properties. The ERT was used as a complementary technique and employed the SuperStingR8 for the acquisition of resistivity measurements. As previously discussed, the active MASW technique uses a seismograph, an active acoustic source (sledge hammer), and an array of receivers (geophones). The tool records acoustic energy produced from the active seismic source and estimates surface wave phase velocities. The phase velocities are analyzed to obtain a 10-layered 1-D shear-wave velocity profile that typically extends to a depth of about 100 ft. The output at each test location is a 1-D shear-wave velocity profile typically used to map variations in the engineering properties of soil and rock and to estimate depth to top of bedrock.

4.4.2. Data Acquisition and Processing. The Seistronix Ras-24 seismograph with 24 geophones (4.5 Hz) and a 20-pound sledge hammer were used for the acquisition of the shear-wave velocity data. The survey employed 2.5 ft geophone spacing and 10 ft acoustic source offset. The aim was to image the subsurface to a depth of at least 50 ft. The source was discharged seven times at each test location; the field data were vertically stacked to attenuate random noise and enhance surface wave signal.

The MASW field data were processed using the SurfSeis4 software. The MASW field records were first imported into the SurfSeis4 software where geometry, including source offset and geophone spacing were assigned. An overtone image was created and a dispersion curve generated. The process was repeated for each test location to produce a

1-D shear-wave velocity profile that is representative of each test location. The data acquisition and processing steps are summarized in Figure 4.8. The process involves field measurements to obtain multichannel records (shot gather), dispersion analysis to generate dispersion curves, and inversion to produce 1-D shear-wave velocity profile (model).

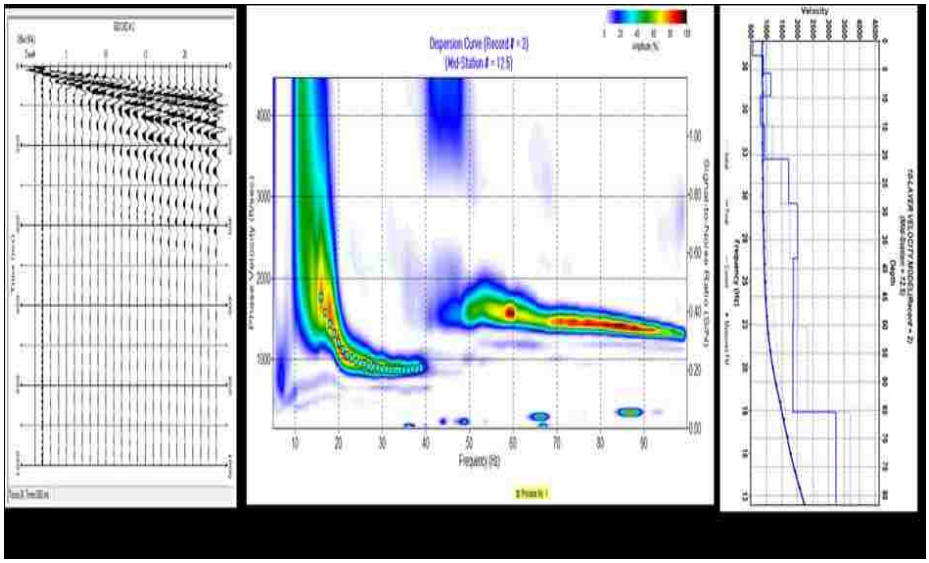

Figure 4.8. Summary of the MASW Data Acquisition and Processing Steps

4.4.3. Data Verification. The interpretations of the 1-D MASW shear-wave velocity profiles were verified and constrained with 2-D ERT data and borehole control. The ERT determined resistivity distribution of the subsurface by utilizing contrasting electrical properties of the subsurface materials.

The 2-D ERT technique involved the injection of electric current (I) into the ground using a linear array of 168 electrodes spaced at 5 ft intervals, the measurement of potential differences (V), the calculation of resistances (V=IR), and the determination of the lateral and vertical variations in the resistivity (ρ) of the subsurface in a vertical plane

containing the electrode array. The deliverable is a 2-D resistivity image of the subsurface with superposed geologic interpretations.

4.4.4. Results and Discussion. Example MASW profiles (Figure 4.9 to Figure 4.13) and ERT profiles (Figure 4.14 to Figure 4.18) acquired from the various test locations are presented. Additional MASW and ERT data are presented in Appendix A. Borehole control data used to verify and constrain the interpretations of the geophysical data are shown in Appendix B. Each of the MASW and ERT profiles is assigned a unique number for identification purposes. The 1-D MASW profiles show the shear-wave velocity (ft/s) with respect to depth (ft) and the corresponding frequency (Hz). On the ERT profile, resistivity is measured in ohm.m, elevation and distance in feet, and iteration absolute error in percent (%). The iteration absolute error is an indication of the quality and reliability of the ERT data; a smaller iteration absolute error suggests high quality and more reliable data.

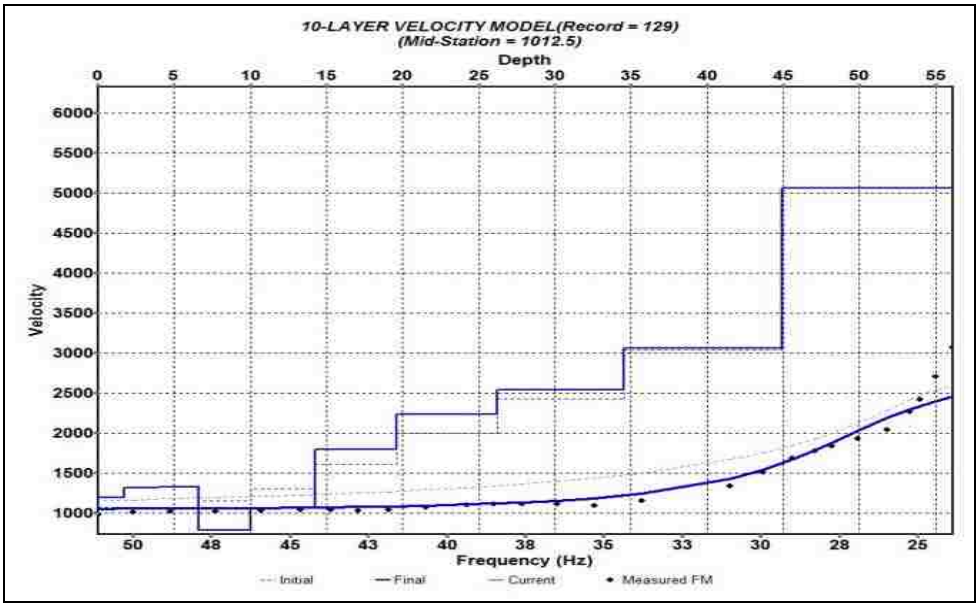

Figure 4.9. 1-D MASW Profile_101

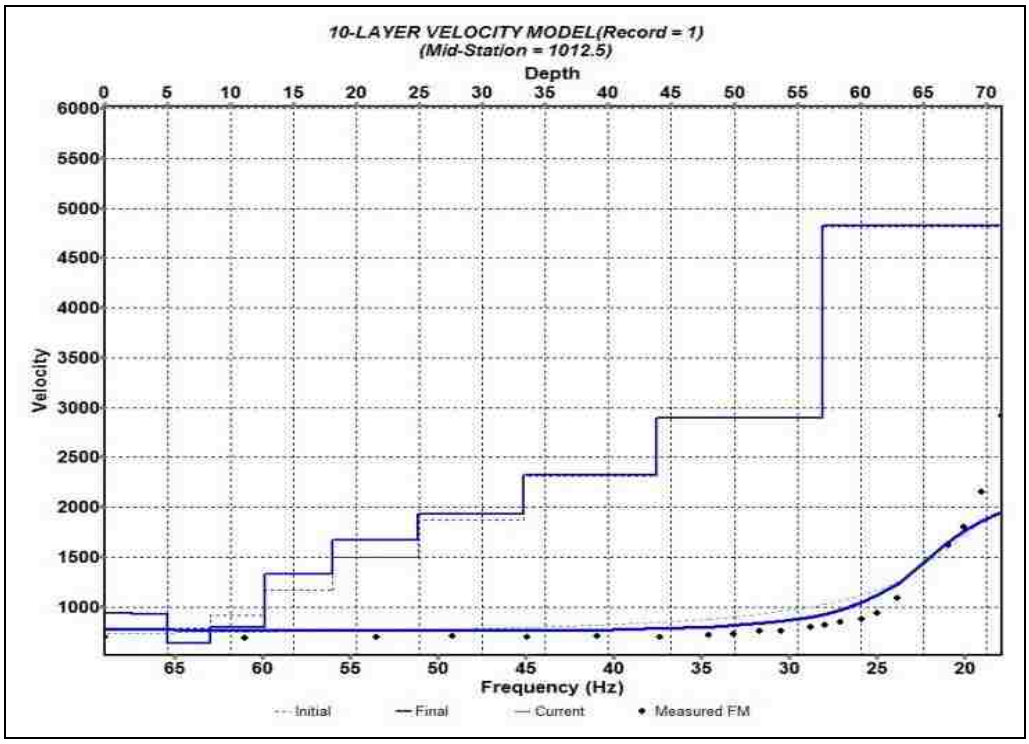

Figure 4.10. 1-D MASW Profile_102

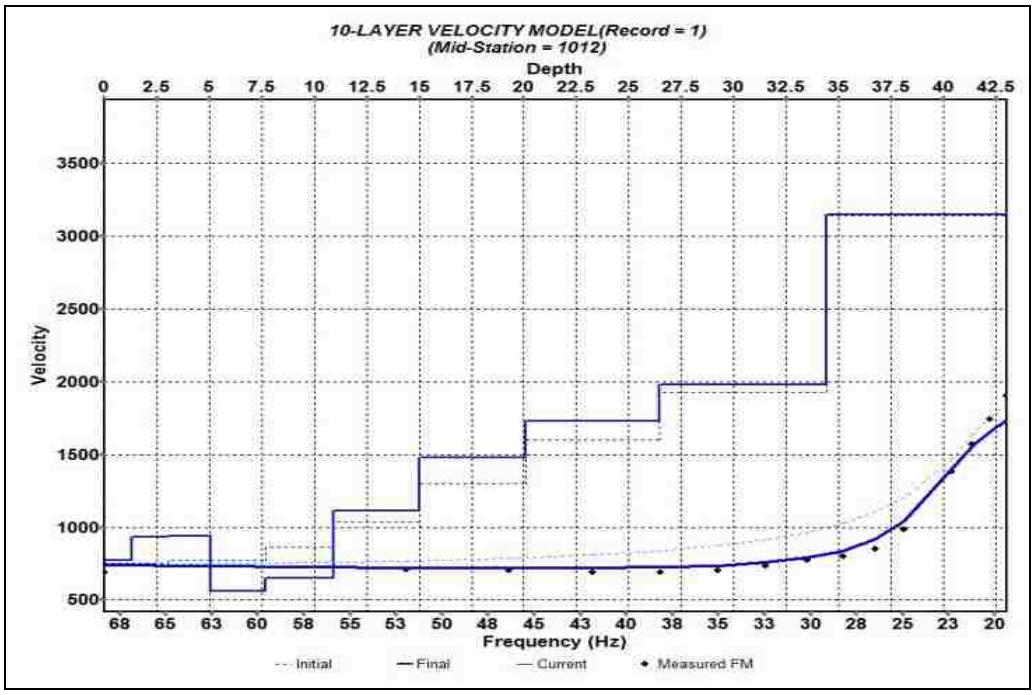

Figure 4.11. 1-D MASW Profile_103

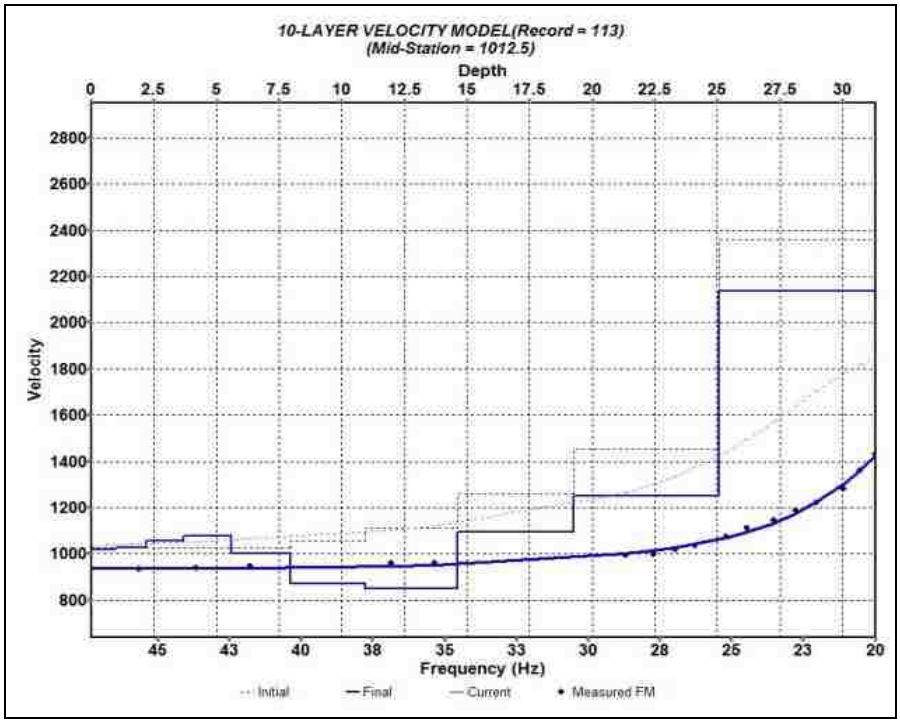

Figure 4.12. 1-D MASW Profile_104

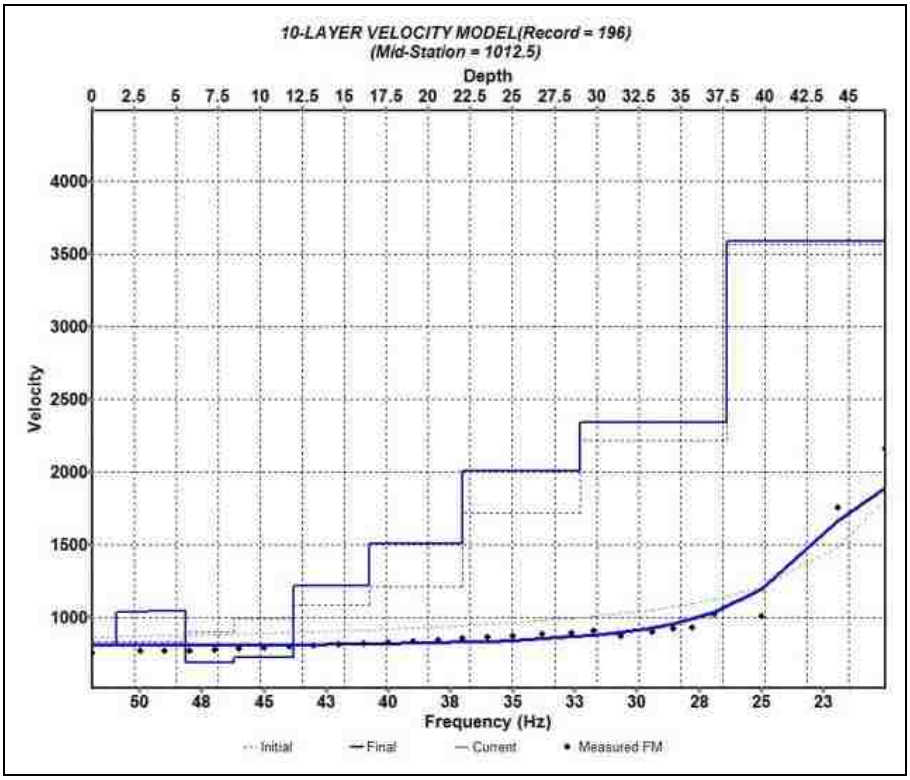

Figure 4.13. 1-D MASW Profile_105

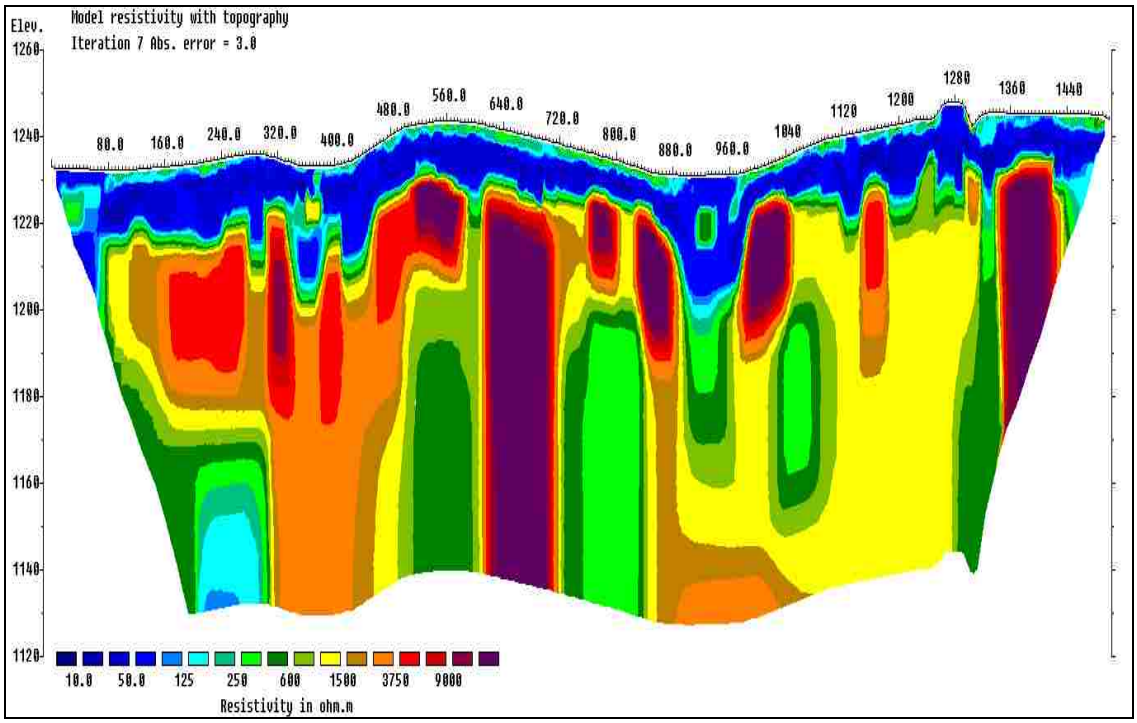

Figure 4.14. 2-D ERT Profile_301

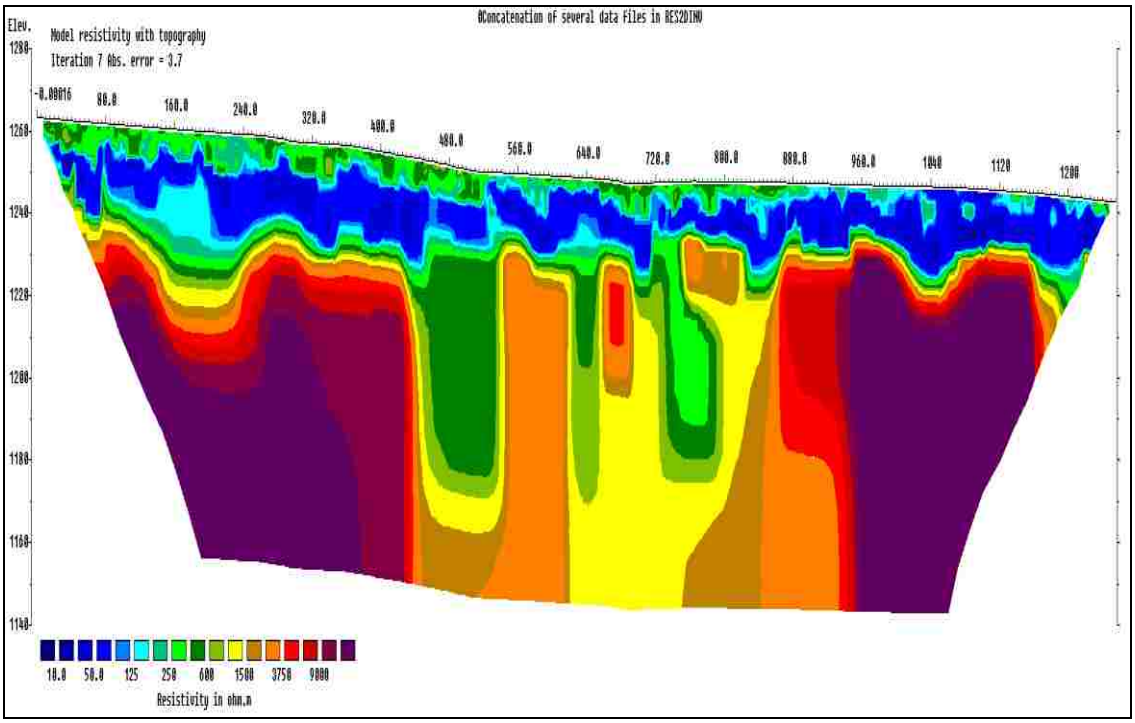

Figure 4.15. 2-D ERT Profile_302

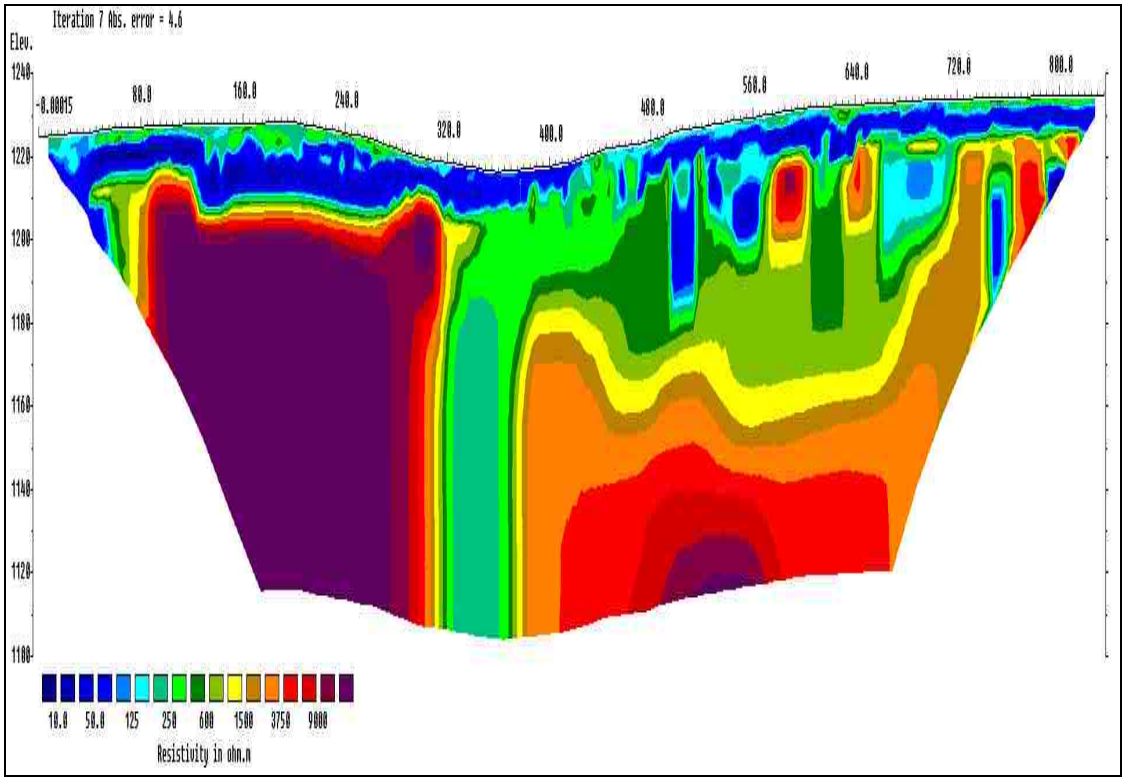

Figure 4.16. 2-D ERT Profile_303

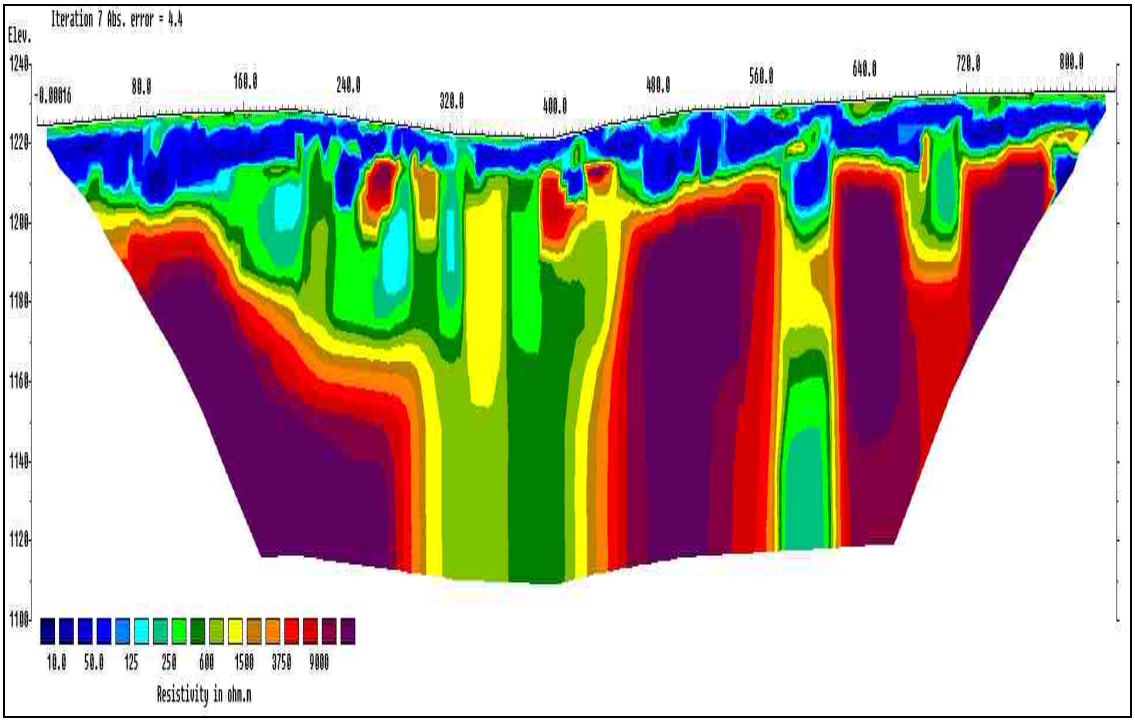

Figure 4.17. 2-D ERT Profile_304

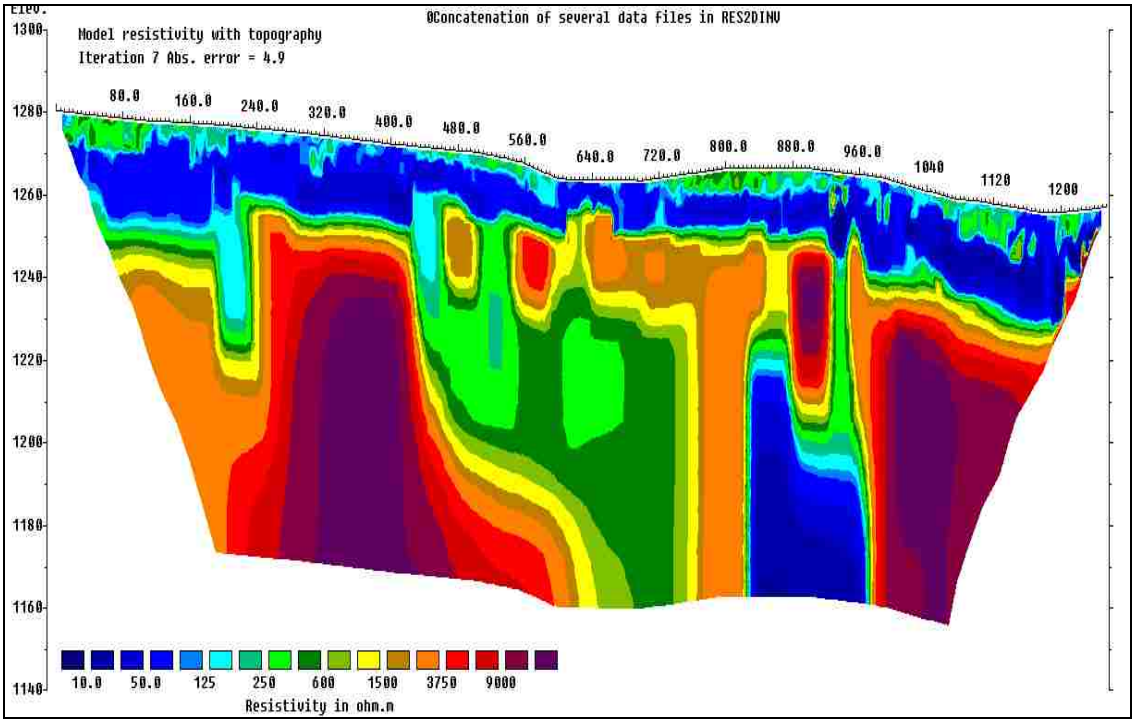

Figure 4.18. 2-D ERT Profile_305

For the purposes of data interpretation, MASW profile obtained from test location 110 is discussed. The MASW field record from the test location 110 is presented in Figure 4.19, and its corresponding dispersion curve is shown in Figure 4.20. An interpreted shear-wave velocity profile produced from the inversion of the dispersion curve is shown in Figure 4.21. As observed in Figure 4.21, the shear-wave velocity of soil generally increases with increasing depth due to compaction by frequent vehicular movements.

Soil/rock classification systems are typically used to classify soils/rocks for environmental or geotechnical purposes. The National Earthquake Hazard Reduction Program (NEHRP) and the International Building Code (IBC) have soil/rock classification systems based on shear-wave velocity. In this research, the NEHRP classification system was adopted. The NEHRP soil/rock classification system based on

the top 100 ft of the soil profile are as follows: hard rock (>5000 ft/s); rock (2500 to 5000 ft/s); very dense soil and soft rock (1200 to 2500 ft/s); stiff soil (600 to 1200 ft/s), and soft soil (<600 ft/s). The interpretations presented in Figure 4.21 are consistent with borehole control and the NEHRP classification system.

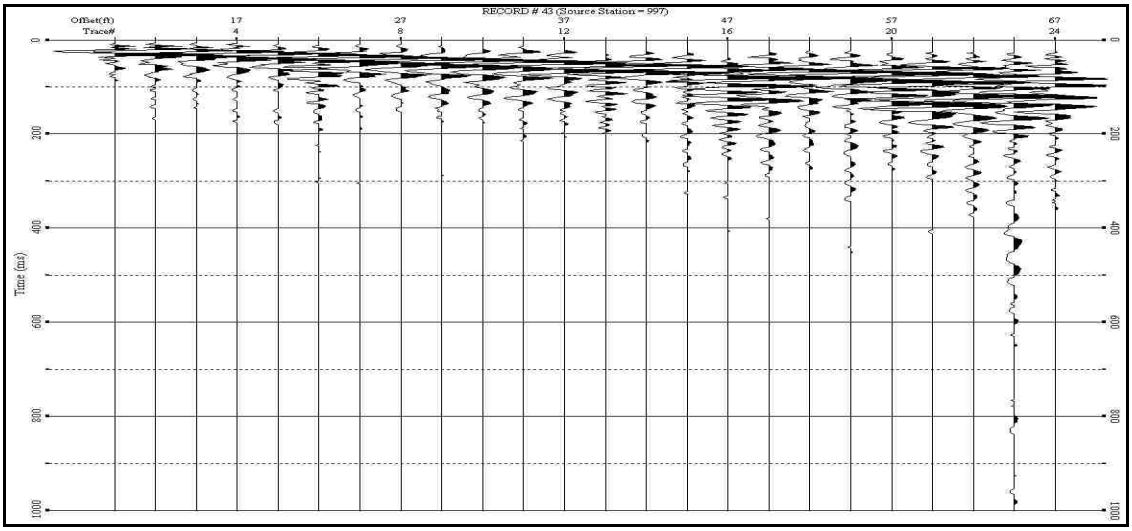

Figure 4.19. An Example Field Record (Short Gather) from Test Location 110

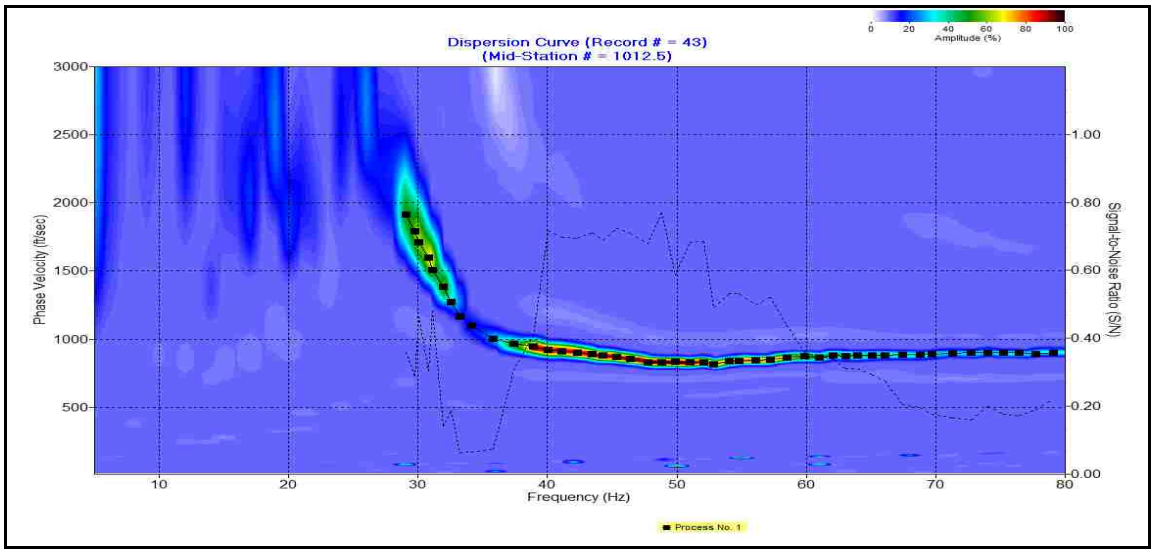

Figure 4.20. Dispersion Curve for Test Location 110

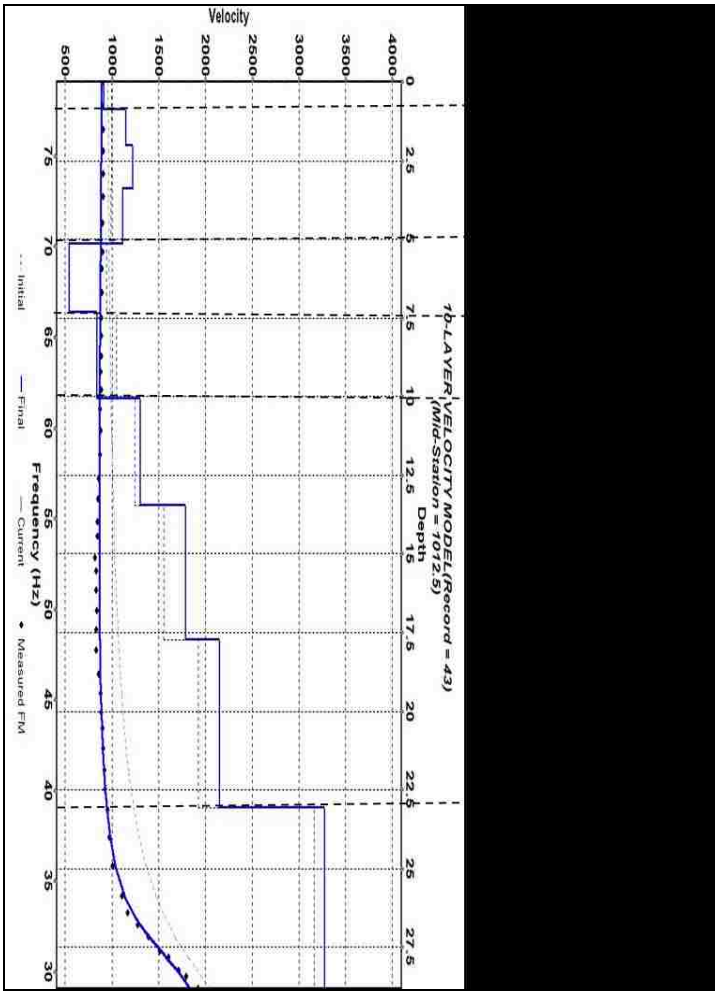

Figure 4.21. A 10-Layer Shear-wave Velocity Profile for Test Location 110 with Superposed Geologic Interpretations

The soil profile at the test location 110 includes stiff soil, very dense soil, soft soil, stiff soil, soft rock, and rock. The stiff soil is underlain by very dense soil, soft soil, stiff soil, soft rock, and rock to depth of 30 ft, as summarized in Table 4.2. Stiff soil has shear-wave velocity of 900 ft/s, very dense soil has shear-wave velocity of 1200 ft/s to 1300 ft/s, and soft soil has shear-wave velocity of about 500 ft/s. Soft rock has shear-wave velocity from 1300 ft/s to 2300 ft/s, and rock has shear-wave velocity of 3300 ft/s.

The denser surficial soils could be attributed to compaction by vehicular movements in the area.

Table 4.2. Estimated Shear-wave Velocity Values at Test Location 110

Depth (feet)	Soil/Rock Description	Shear-wave velocity (ft/s)
0 - 1.5	Stiff soil	900
1.5 - 5	Very dense soil	1200 - 1300
5 – 7.5	Soft soil	500
7.5 - 10	Stiff soil	900
10 - 23	Soft rock	1300 - 2200
23 - 30	Rock	3300

Resistivity of subsurface materials is typically a function of moisture content, salinity, clay content, porosity, and permeability. The resistivity of the subsurface at the test location is typically controlled by moisture content. Thus, moist rock has lower resistivity than dry rock. For quality assurance purposes, ERT profiles (from a karst terrain) with iteration absolute error of 5% are usually considered to be high quality data. The ERT profiles obtained in this research have iteration absolute errors below 5%, demonstrating high quality data and thereby enhancing data interpretation. In Figure 4.22, for example, the ERT profile has iteration absolute error of 2.3%. Therefore, interpretations from the ERT profile can strongly be used to validate the interpretations of the MASW shear-wave velocity data.

Top of rock interpretation based on MASW is observed to be consistent with ERT data. For example, the ERT profile shown in Figure 4.22 corresponds with the 1-D MASW shear-wave velocity profile at the 700 foot mark. Top of rock corresponds to the 125 ohm.m resistivity contour, consistent with what was reported by Kidanu et al. (2016) for southwest Missouri. Top of rock is estimated at 12.5 ft on the ERT profile (Figure 4.22) and 12 ft on the corresponding MASW profile (Figure 4.23). Top of rock on borehole control data is 13 ft. The shear-wave velocity of the top of rock is 1500 ft/s. Top of rock on ERT profile in Figure 4.24 is 16 ft, and the corresponding MASW top of rock is also 16 ft with estimated shear-wave velocity of 1400 ft/s (Figure 4.25). Top of rock on corresponding borehole control is estimated at 16 ft. These top of rock estimates on the ERT profile are consistent with borehole control and estimates provided by Kidanu et al. (2016) within the same geologic domain.

It has been shown that active MASW tool can be used to image the subsurface, provide reliable estimates of depth to top of rock, and map variations in engineering properties of soil and rock in a complex terrain. The active MASW interpretations are consistent with ERT data and borehole control. Further, the active MASW technique complements intrusive geotechnical investigation, reduces data acquisition time, minimizes cost, and eliminates karst hazards posed to field crew. Hence, the active MASW technique is recommended for estimating top of rock and acoustic/engineering properties of soil/rock in karst terrain.

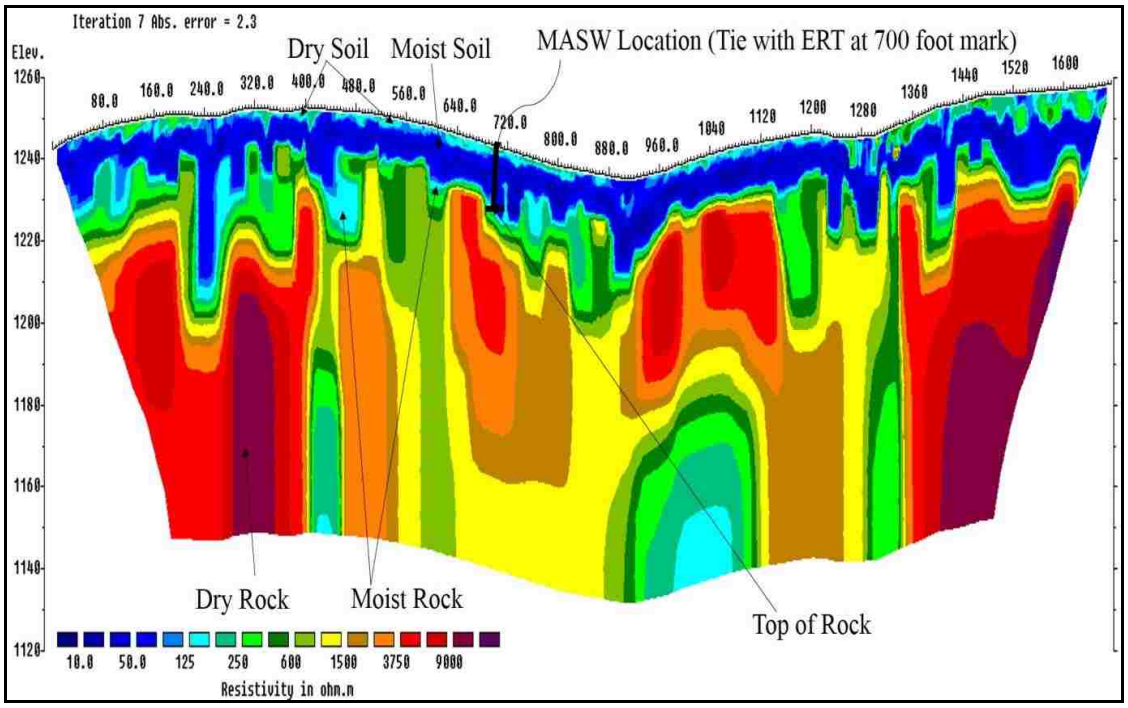

Figure 4.22. Top of Rock at 700 Foot Mark on ERT Profile

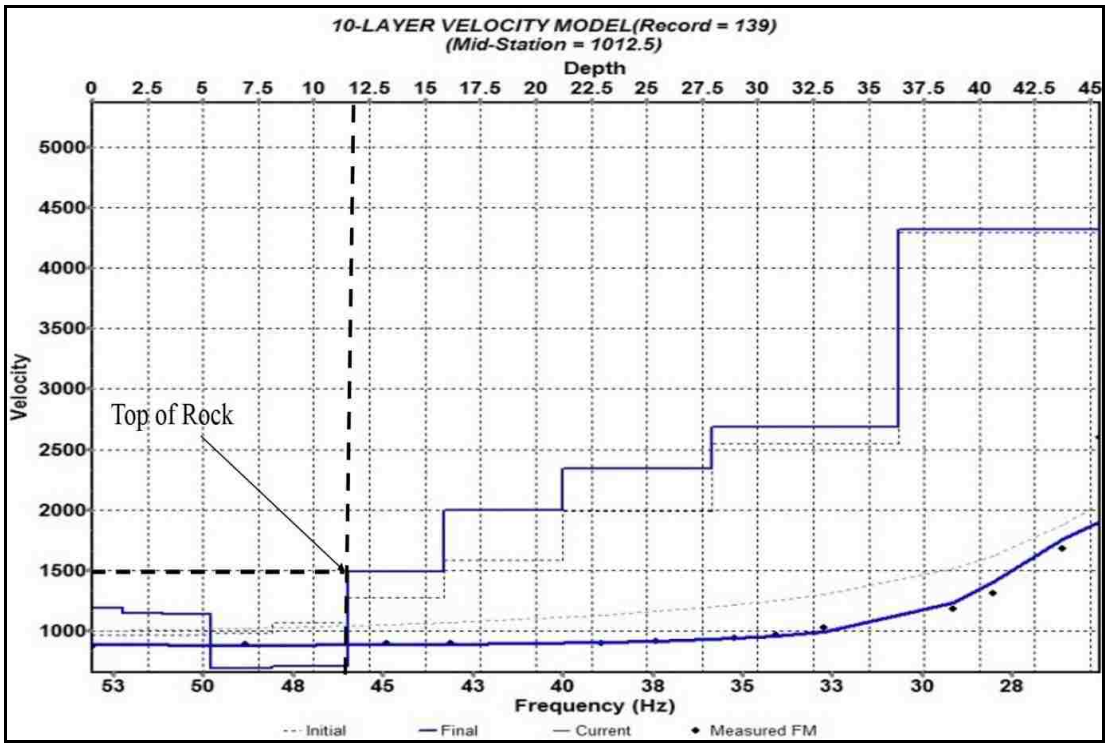

Figure 4.23. Top of Rock on 1-D MASW Profile at 700 Foot Mark

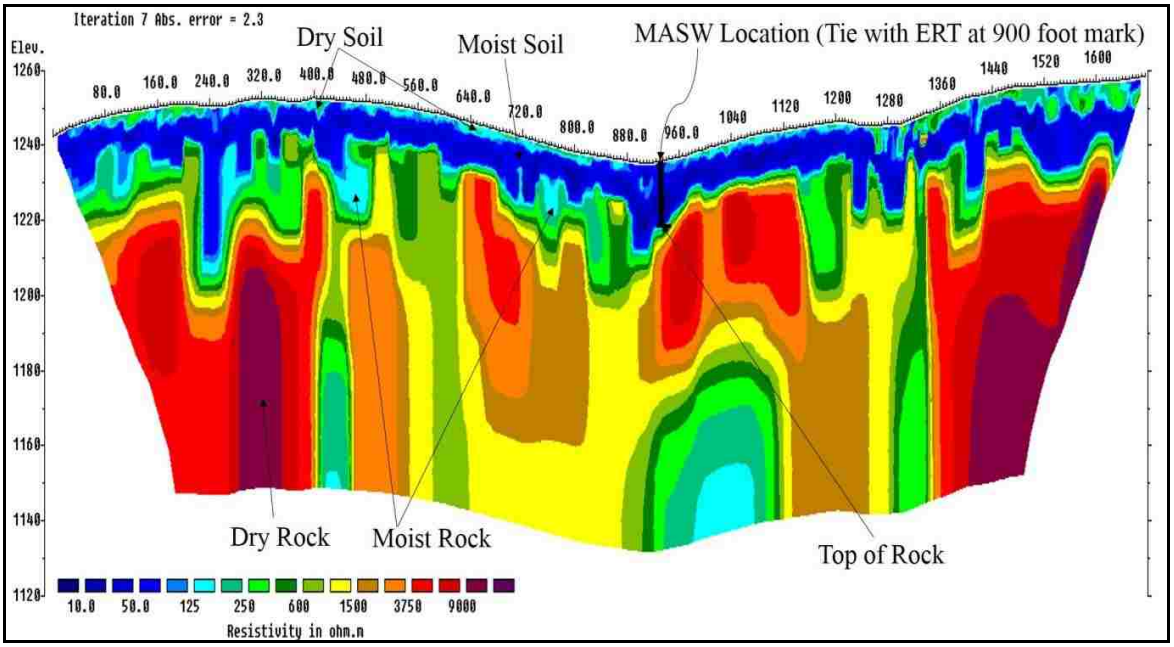

Figure 4.24. Top of Rock at 900 Foot Mark on ERT Profile

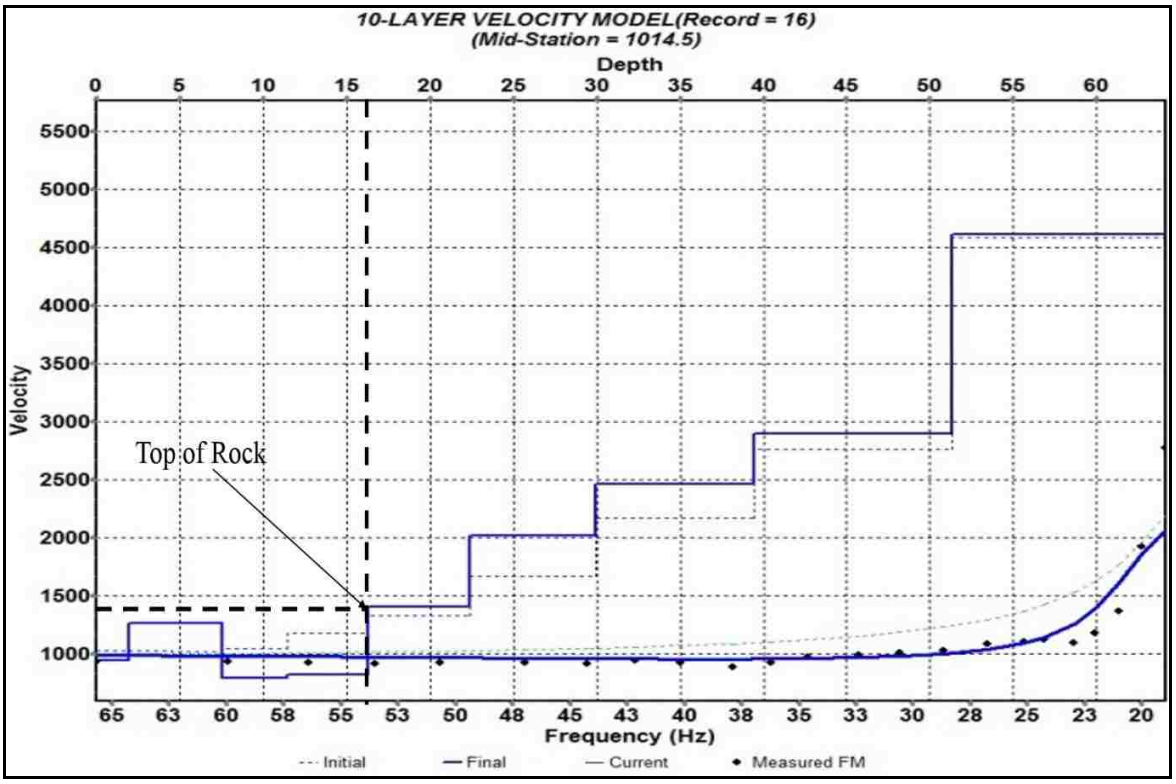

Figure 4.25. Top of Rock on 1-D MASW Profile at 900 Foot Mark

4.5. IMAGING SUBSURFACE IN KARST TERRAIN USING 2-D ERT AND 1-D MASW TECHNIQUES

This section describes how the ERT and MASW techniques were used to image the subsurface and map variable depth to top of rock.

4.5.1. Brief Introduction. Over the years, the ERT and MASW techniques have been used to investigate karst terrain for geotechnical, environmental, or archeological purposes. Some of the applications of these two geophysical techniques include locating buried artifacts, characterizing subsurface materials, and determining groundwater pathways. Conventional techniques such as drilling have been used to perform these subsurface investigations to a high level of accuracy over many years. As previously mentioned, conventional techniques are invasive, more expensive, and more time-consuming. As a result, geophysical techniques are increasingly being used for subsurface investigations (Storz et al., 2000; Sudha et al., 2009; Styles et al., 2005).

Multiple geophysical tools have usually been used as complementary tools to investigate a particular exploratory site. For example, Šumanovac and Weisser (2001) combined electrical and seismic geophysical techniques for hydrogeological mapping in karst terrain. Gibson (2004) located a cave and a large collapse feature beneath glacial surficial sediments using resistivity and magnetometry techniques. Kruse et al. (2006) combined the resistivity and ground penetrating radar to image the structure of a large sinkhole in Florida. Even though the ERT, MASW, and other geophysical techniques have widely been used for imaging the subsurface, the application of those geophysical techniques to map variable depth to top of rock and to characterize the subsurface based on moisture content is as of yet widely to be reported. Therefore, this study aims to use

the 2-D ERT and 1-D MASW techniques to map variable depth to the surface of karsted bedrock and to characterize the subsurface based on moisture content.

4.5.2. Data Acquisition and Processing. The multi-electrode resistivity system (SuperStingR8) with 168 electrodes was used to acquire ERT data along west-east traverses spaced at 100 ft. The dipole-dipole array was used with electrode spacing of 5 ft with the intent to image the subsurface to a depth of at least 100 ft. The resistivity measurements obtained from the field were processed using the RES2DINV software into 2-D ERT profiles. Active MASW data were acquired along north-south traverses as shown in Figure 4.26.

The active MASW data were obtained using the multi-channel seismograph (Seistronix Ras-24) with 24 geophones spaced at 5 ft. Geophone frequency of 4.5 Hz, source offset of 10 ft, and 20 pound sledge hammer as an acoustic source were employed. The active MASW data were processed using the SurfSeis4 software into 1-D MASW shear-wave velocity data for geologic interpretations. The 1-D MASW shear-wave velocity data were used to verify and constrain the 2-D ERT data. Borehole control and soil laboratory testing results were used as additional verification data.

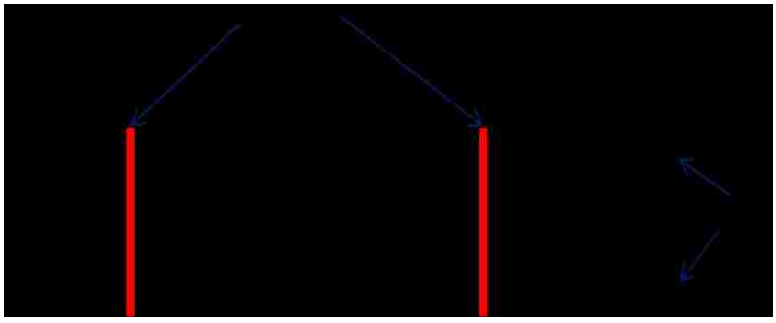

Figure 4.26. Configuration of ERT and MASW for Data Acquisition (Figure not drawn to scale; ERT traverse is 835 ft long; MASW is 115 ft long)

4.5.3. Results and Discussion. Three representative 2-D ERT models acquired from three different test locations in the study area are discussed to address the goals of the study. The 2-D ERT profiles with superposed geologic interpretations are shown in Figure 4.27 to 4.29. Top of rock is the 125 ohm.m contour (dark dotted line). The 2-D ERT profiles show that the rocks are pervasively fractured and are anomalously moist. Resistivity of the test locations is controlled by moisture content. Accordingly, the soils and rocks can be classified into dry soil, moist soil, moist rock, and dry rock.

Dry surficial soil with resistivity 125 ohm.m is underlain by moist soil with resistivity <50 ohm.m. Moist rock has resistivity of at least 125 ohm.m, while dry rock has resistivity more than 1500 ohm.m. Soil testing results of in situ moisture content on recovered samples to a depth of 11 ft are presented in Table 4.3. Moisture content varied from 21% to 49%. Soils at the surface have low moisture content of 21%. Moisture content increases to a depth of about 8 ft and decreases thereafter. The results of the soil laboratory testing corroborate the classification based on moisture content. The results are consistent with the ERT interpretations; dry surficial soil overlying moist soil, and moist soil overlying moist rock and dry rock. The surficial soils are typically dry probably because of evaporation and compaction from vehicular movements.

Table 4.3. Moisture Content of Recovered Samples

Sample Depth (ft)	Moisture Content (%)
1.5 - 3	21
4 – 5.5	46
6.5 - 8	49
9.5 - 11	37

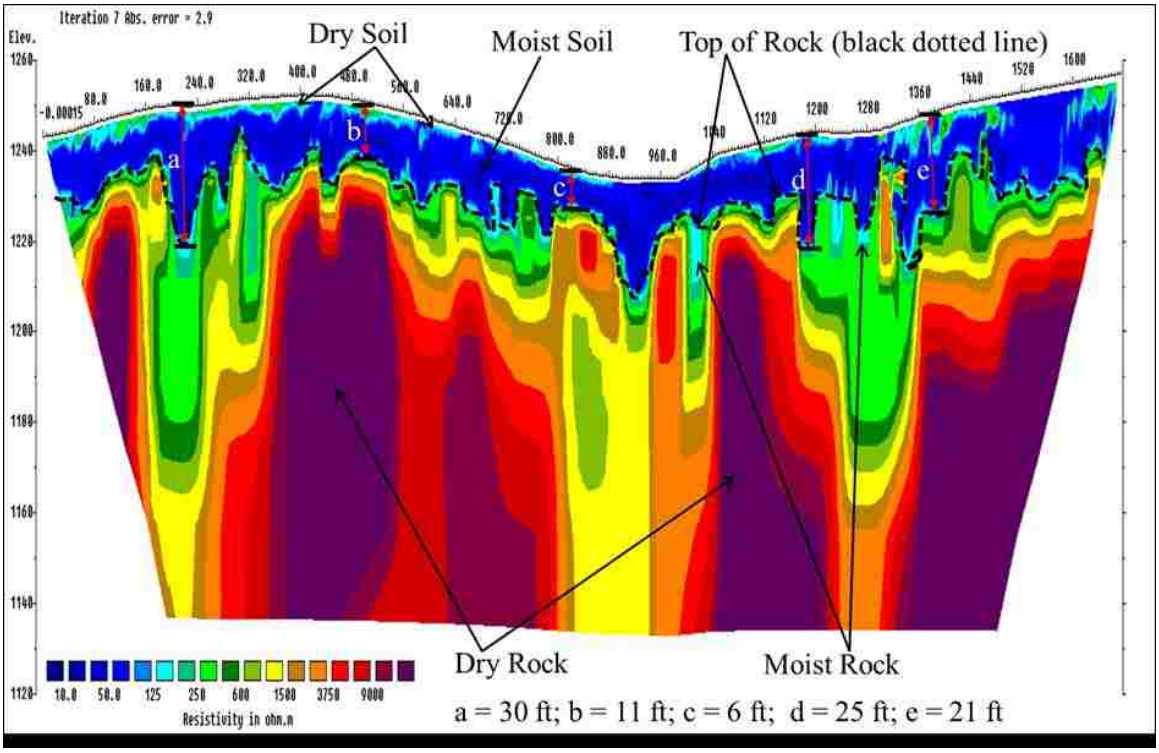

Figure 4.27. 2-D ERT Profile_306

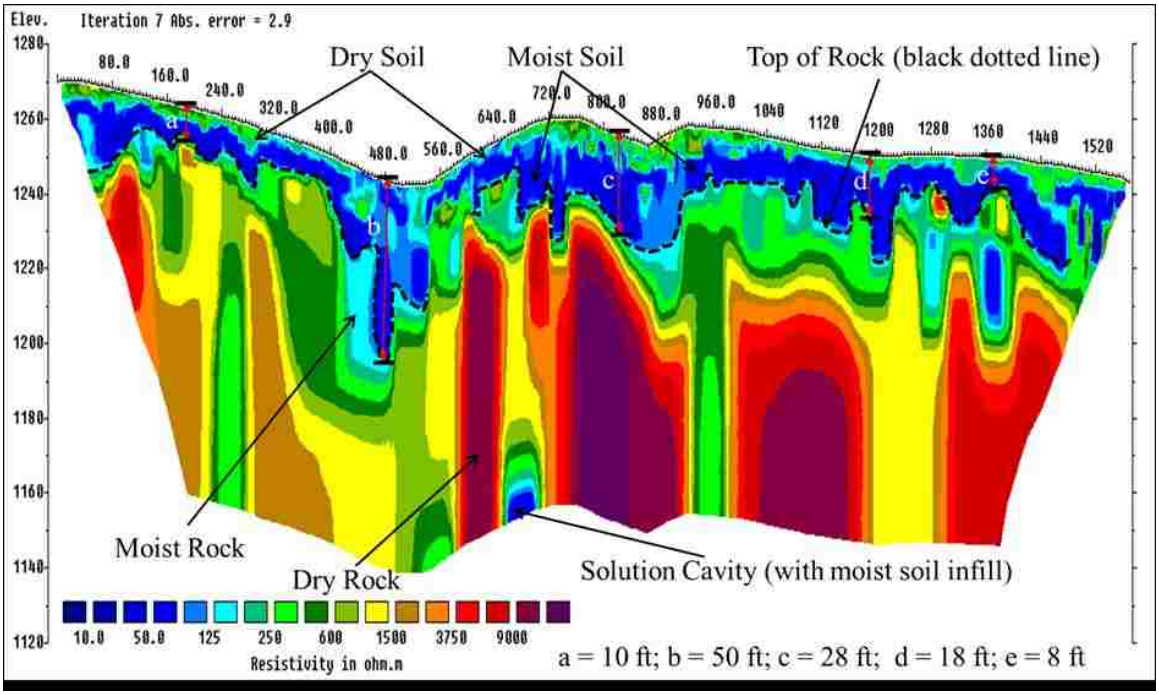

Figure 4.28. 2-D ERT Profile_307

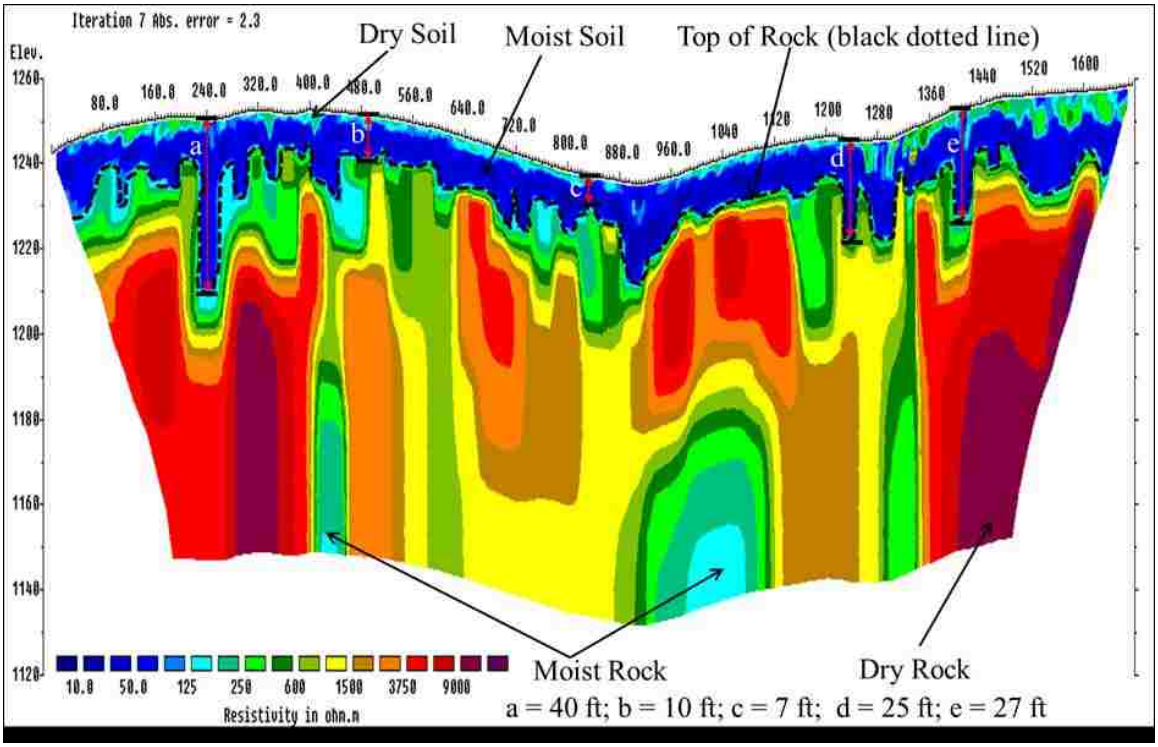

Figure 4.29. 2-D ERT Profile_308

The 2-D ERT profiles (models) show significant variations in depth to top of rock. Top of rock can be located at depths as shallow as 6 ft and as deep as 50 ft. Based on the data, top of rock in the study area is undulating and cannot be defined by a specific depth (Appendix C). Therefore, localized site investigations should be conducted to determine the actual depth of top of rock prior to engineering/construction projects. It is also observed that the topography of top of rock in many instances depicts the surface topography. In many areas, depressions in the top of rock manifest in the surface topography (see also 3-D surface and top of rock elevation models in Appendix C).

Figure 4.30 is a 1-D MASW profile acquired with the goal to verify and constrain the ERT interpretations. The shear-wave velocity of soil/rock on the 1-D MASW profile varies from 600 ft/s to about 4000 ft/s. Based on the NEHRP soil/rock classification

criteria, soil and rock at the test location were classified into stiff soil (700 ft/s to 1050 ft/s), very dense soil (1200 ft/s to 1300 ft/s), soft rock (1800 ft/s to 2300 ft/s), and rock (> 2500 ft/s). Stiff soil on the surface overlies very dense soil, stiff soil, soft rock, and rock. The 1-D MASW profile was superposed on the corresponding 2-D ERT profile (Figure 4.31). At the 100 foot mark, where the 1-D MASW profile ties with the 2-D ERT profile, estimated depth to top of rock on both the 1-D MASW profile and 2-D ERT profile is 13 ft. The MASW data and interpretations corroborate the ERT interpretations. The MASW data reasonably verifies and validates the ERT data, and therefore in the absence of borehole control, active MASW could be a useful technique for verifying and constraining ERT data.

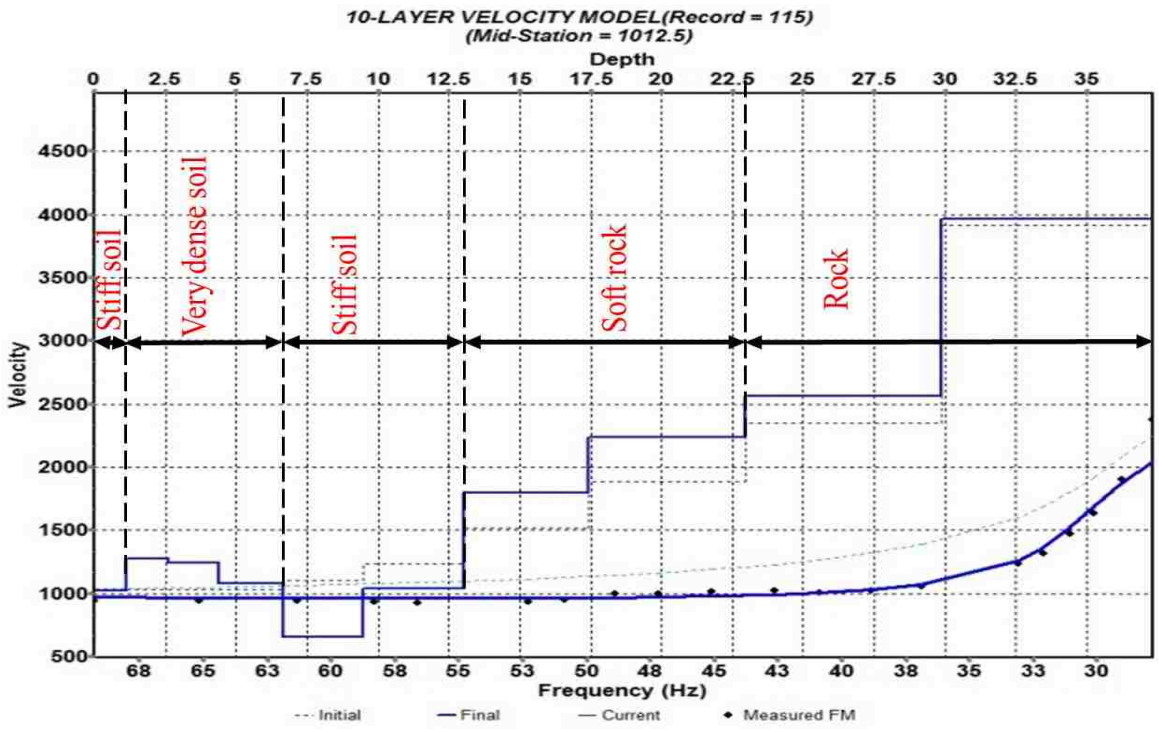

Figure 4.30. 1-D MASW Profile. MASW Data were acquired transversely to ERT Profile_307

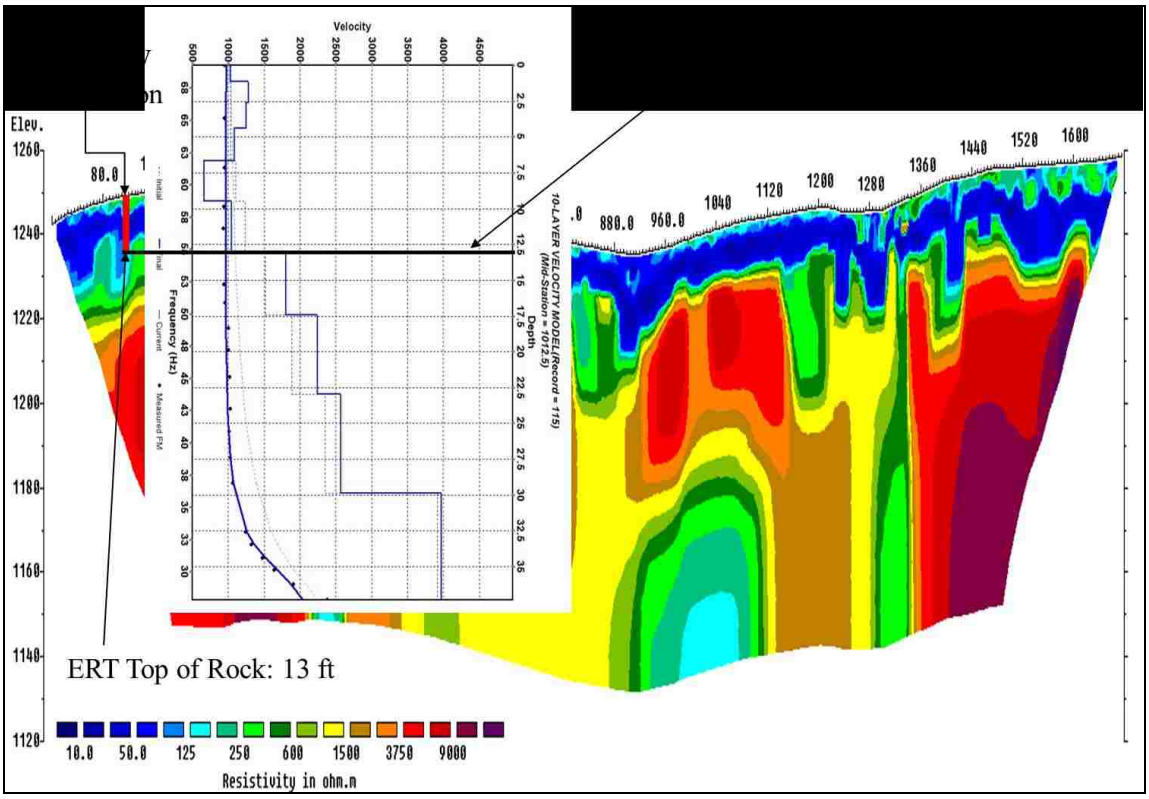

Figure 4.31. 2-D ERT Profile with Superposed Corresponding 1-D MASW Profile

4.6. DETERMINING DRIVERS OF KARST PROCESSES AND MITIGATION

This section discusses the factors that facilitate karst processes and proposes mitigation.

4.6.1. Brief Introduction. It is generally known that karst is formed by the dissolution of carbonate or evaporite bedrocks. Thus, presence of carbonate or evaporite bedrock forms the primary condition for the formation of karst. Other factors that facilitate karst processes and contribute to karst development have not been well documented in the literature.

Proper identification of potential factors that can cause karst processes could help determine appropriate mitigation measures. The focus of this study is to explore the

factors or conditions that drive the development of karst processes and recommend mitigation strategies.

While karst terrain offers an important karst water resource for the supply of drinking water, certain activities that occur during or after the karst development process can negatively affect the water resource. Parise and Gunn (2007) stated that land degradation with intense deforestation and overgrazing exposes the ground surface and causes serious impacts in karst. That is, such activities can facilitate karst processes and at the same time impact karst aquifers. It is important to pay critical attention to the factors that drive karst processes because karst terrain poses significant environmental, health, and financial threat.

Karst features, including sinkholes, have been reported to cause severe problems to people and the environment. The Guardian (2017) compiled at least 90 major sinkhole collapse cases that have occurred since May 2010 around the world. Among the major sinkhole collapse episodes is a sinkhole about the size of a football field that opened up north of Detroit, Michigan, in the United States in January 2017. About two dozen homes were temporarily evacuated and three homes eventually condemned. The sinkhole collapse affected water use by about 400,000 people in surrounding communities and was estimated to cost more than $70 million for repair works and about a year to fix. The sinkhole was attributed to a broken sewer line, but, the exact cause of the sewer collapse was unknown. In June 2010, a sinkhole about 100 ft deep and 66 ft in diameter opened up in Guatemala City and swallowed an entire crossroads and a three-story textile factory. The immediate cause of the sinkhole was unknown; however, an expert from the National

Disaster Management Agency indicated that underground sewage leaks could have been the cause of the sinkhole.

There were many instances where the immediate cause of sinkholes was not known. In the examples mentioned, the costs associated with the sinkhole damage could have been avoided if the factors controlling the karst development were identified earlier. Identifying the drivers of karst and karst processes could significantly reduce the costs associated with karst terrain. Early detection of karst processes and the contributing factors could help mitigate the many significant dangers that are usually attributed to karst. Using southwest Missouri as a case study, this research identifies the factors that contribute to karst processes and suggests measures to minimize the processes.

4.6.2. Data Acquisition and Processing. A site reconnaissance survey and visual assessments of the study area were conducted. Potential sinkhole locations were observed during the reconnaissance survey and visual assessments of the study area. Photographs of the study area and particularly, potential sinkhole locations were taken. Historical images (from 1997 to 2015) of the potential sinkhole locations were obtained from Google Earth to support the visual inspections and analyzed to observe characteristics of the locations over the period. A three-dimensional (3-D) surface terrain model was generated to determine surface flow direction. More than 4,000 data points (geographic positions) in a grid were used to generate 3-D surface terrain model using the Surfer13 software.

To determine if the subsurface is undergoing karst processes, 2-D ERT data were collected and verified with borehole control. The multi-electrode resistivity system with 168 electrodes was used to acquire the 2-D ERT data. The 2-D ERT data were acquired

along traverses across the surface flow path. The dipole-dipole array configuration was employed with electrode spacing of 5 ft with the goal to image the subsurface to a depth of at least 100 ft. The resistivity measurements were inverted using the RES2DINV software.

4.6.3. Results and Discussion. Two potential sinkhole locations are illustrated to demonstrate the activities facilitating karst processes. Historical images of one of the potential sinkhole locations are shown in Figure 4.32. The feature under consideration is observed to have enlarged over the years. A depression in 1997 appears to have accumulated water. Surface terrain model (Figure 4.33) demonstrates natural flow pathways for surface water. The surface flow direction of north–south has been blocked by a roadway without a drainage system, causing water to pond. A still photograph of the ponded water location taken in 2016 is shown in Figure 4.34. Using the double yellow markings at the center of roadway as reference, Side A and Side B are expected to be about the same elevation when the roadway was constructed. However, on October 25, 2016, Side A was observed at lower elevation of several inches than Side B. This change in elevation is usually gradual and takes a longer time to be observed. The settlement in the northern section of the roadway could be attributed to increased effective stress due to piping of fine-grained sediments beneath the roadway and at the ponded water location. This process of settlement would ultimately cause the northern section of the road to fail if the underlying cause is not mitigated.

An example 2-D ERT data (Figure 4.35) acquired south of the ponded water along west-east traverse shows pervasively fractured and anomalously moist bedrock. The network of discontinuities offers pathways for percolating acidic waters which can

dissolve the limestone bedrock and increase karst processes. Again, moist soil is characterized by resistivity lower than 50 ohm.m and surficial dry soils have relatively high resistivity of up to 250 ohm.m. Top of rock is characterized by resistivity 125 ohm.m depicted by the thick black line. Dry rock has resistivity at least 1500 ohm.m. The ponding of water over the pervasively fractured bedrock makes the subsurface very susceptible to karst processes. This is because the water can percolate the subsurface through the fractures and dissolve the bedrock in the process. This view is supported by Kidanu et al. (2016) who argue that sinkholes develop in areas where water is temporarily retained and the water has the ability to percolate into the subsurface. Therefore, the continuous accumulation and seepage of water into the ground over many years would eventually lead to the formation of sinkholes.

The above findings are similar to findings observed with other ponded water locations. For example, Figure 4.36 shows ponded water (PW 6) located south-west of PW 1 and west of a roadway. The pond is located at an elevation of 1200 ft. The pond's elevation is lower than the elevations of the surrounding terrain. The terrain on the west of the pond is several feet above the pond location, while that on the east is a couple of feet above the pond location. The surface flow direction of west–east is obstructed by the road embankment which has no drainage system to drain the pond water. Two-dimensional (2-D) ERT data acquired parallel to the roadway shows pervasively fractured bedrock amenable to karstification (Figure 4.37). The 2-D ERT profile shows very low resistivity value (50 ohm.m) at depths of at least 80 ft. This very low resistivity zone gives an indication that the pond water seeps through the discontinuities and percolates deeper in the subsurface—a process that over many years can lead to the

formation of a pronounced karst feature such as a sinkhole. The subsurface offers suitable conditions for karst processes.

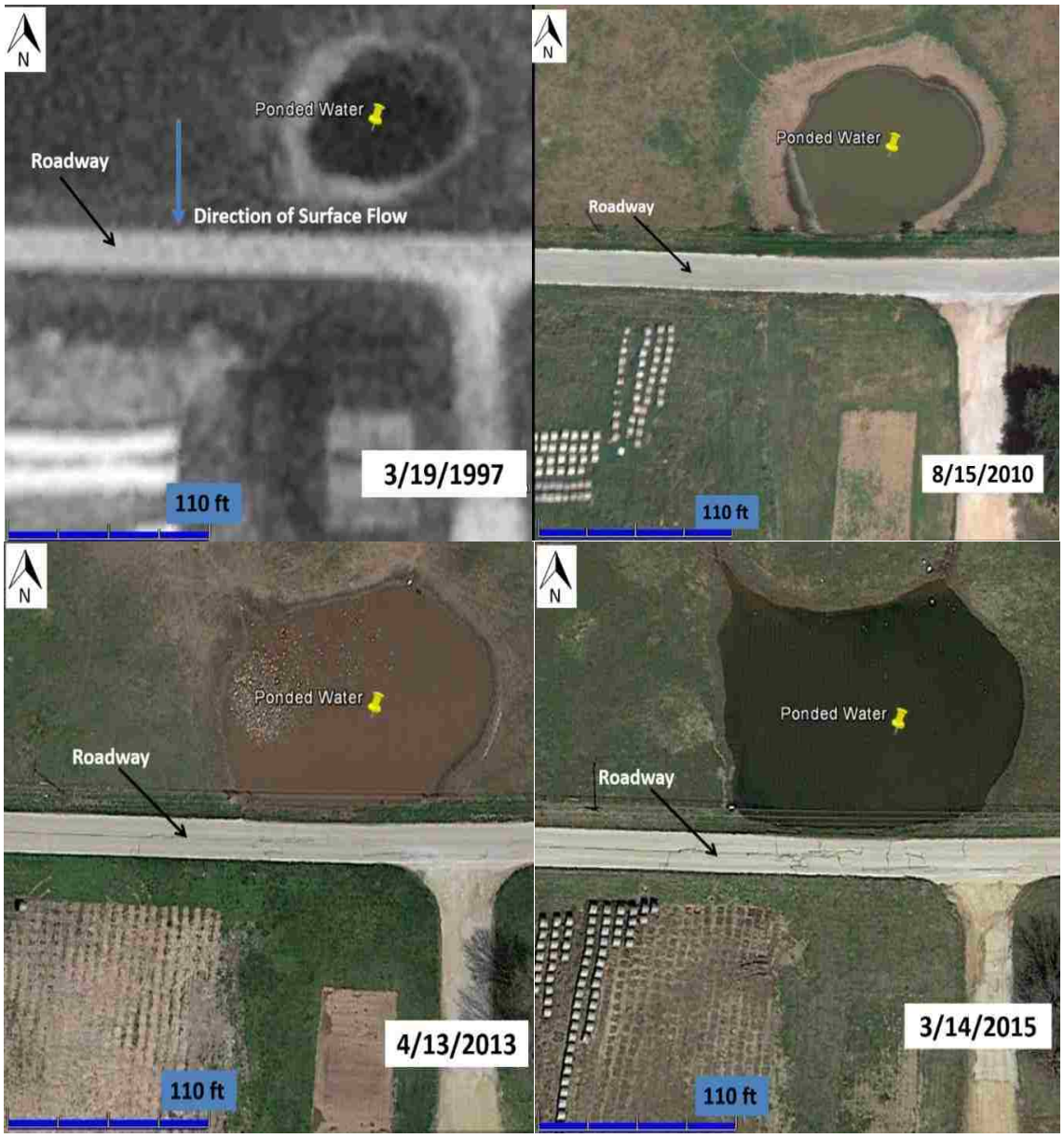

Figure 4.32. Historical Images of Potential Sinkhole Location (PW 1). Data were acquired from Google Earth for the Period of 1997 to 2015

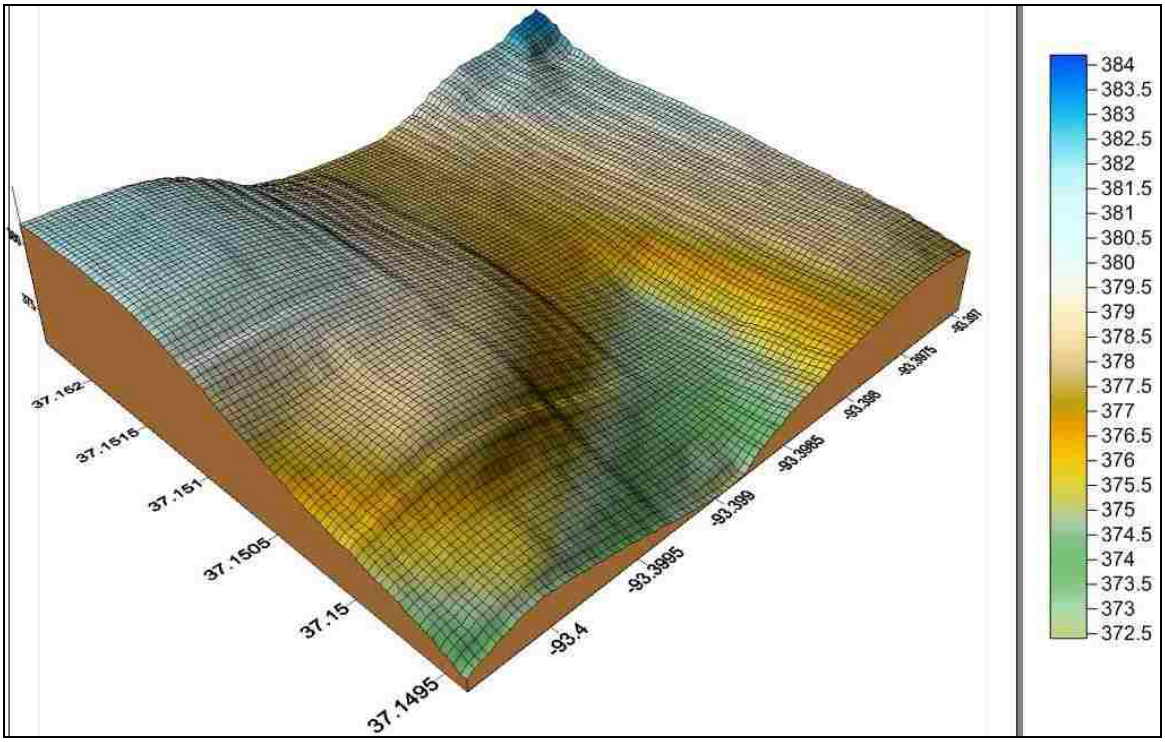

Figure 4.33. Three-dimensional Surface Terrain Model

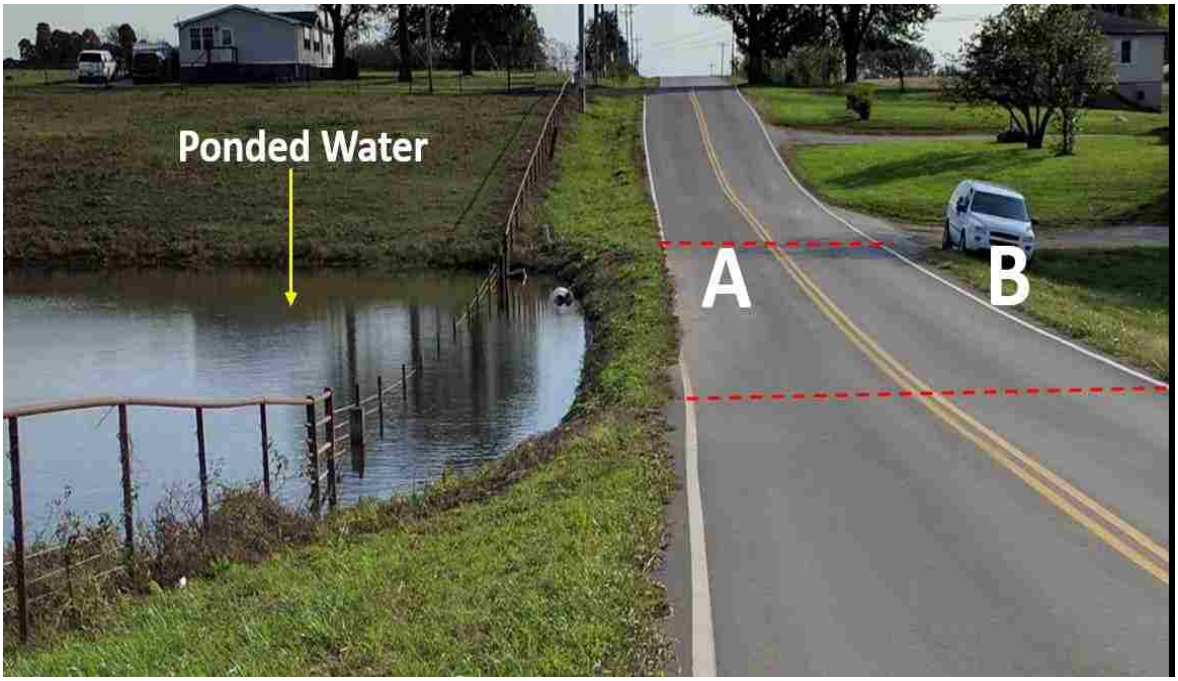

Figure 4.34. Ponded Water Location (PW 1)

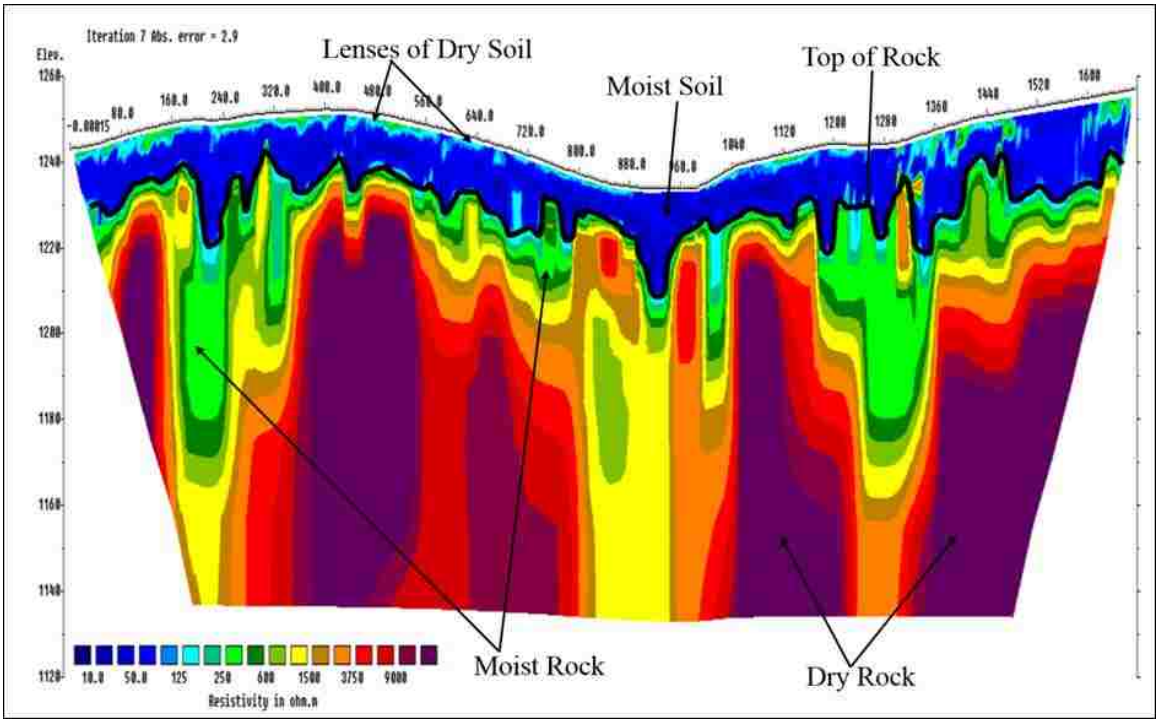

Figure 4.35. Example 2-D ERT Profile (acquired 140 ft south of the pond)

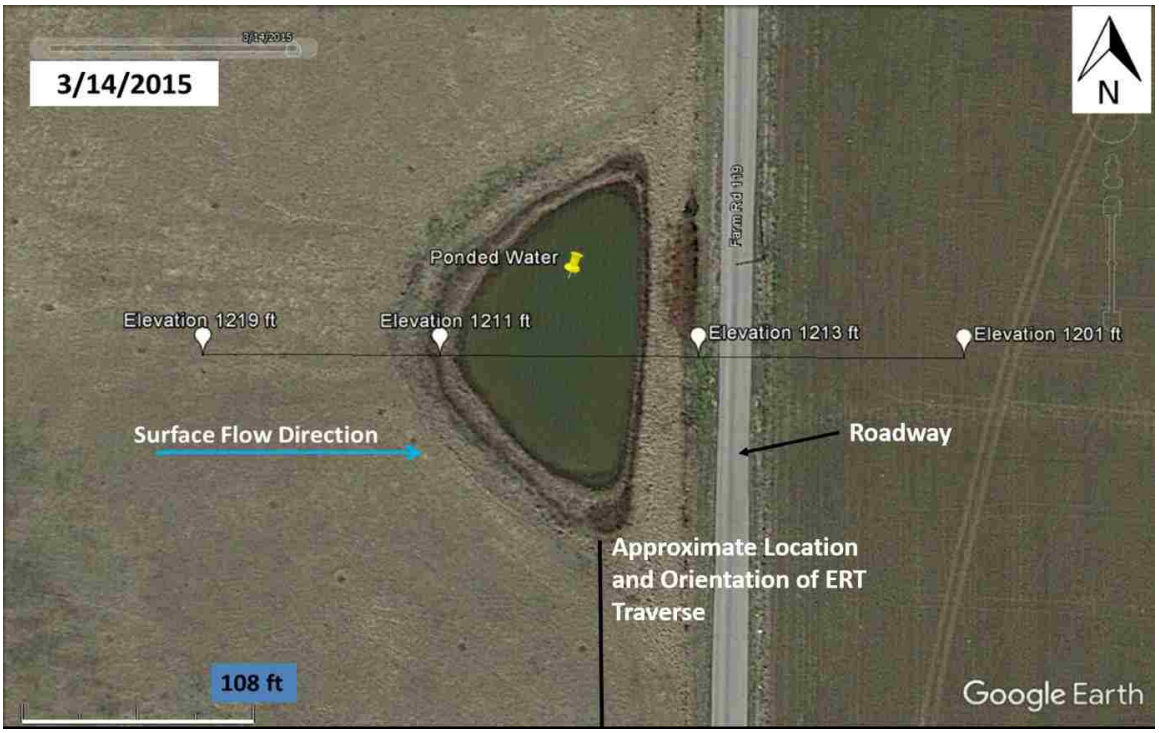

Figure 4.36. Ponded Water (PW 6)

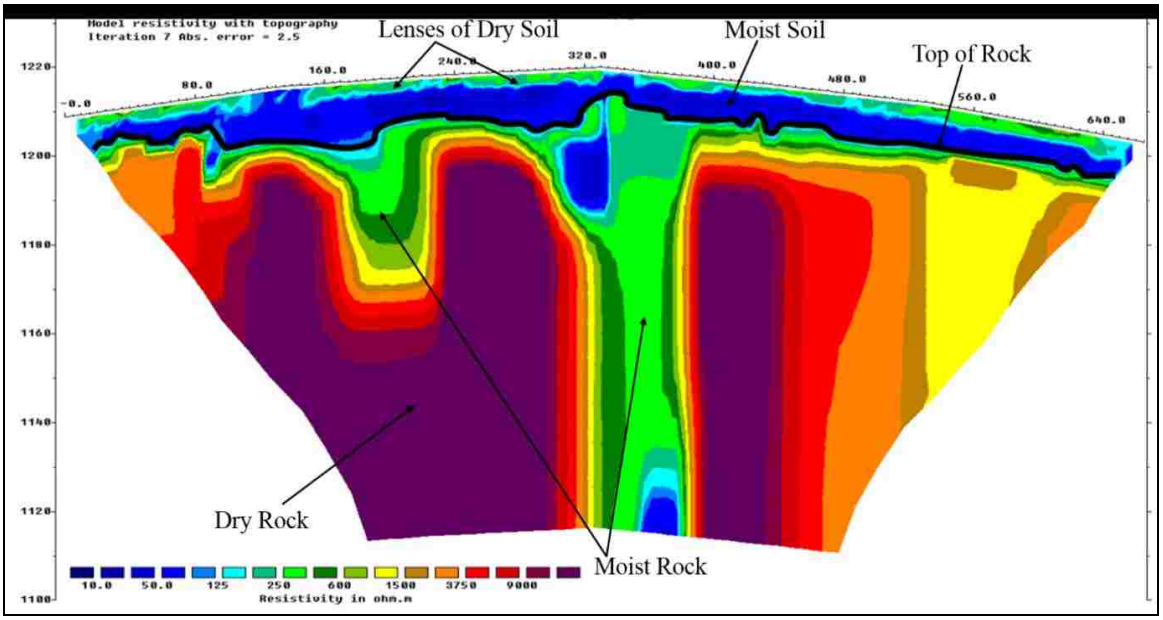

Figure 4.37. ERT Profile Acquired in the Vicinity of PW 6

Karst processes can be natural or induced by anthropogenic activities. In this study, it is clearly observed that anthropogenic activities are the major drivers of karst development in the study area, and by extension, southwest Missouri. In most instances, the karst processes were driven by human activities, including construction of roadways, parking lots, buildings, and farming activities. These activities impede surface flow pathways and cause water to pond. The pond water percolates existing discontinuities and seeps into the subsurface. The continuous percolation of ponded water together with solution-widening of the discontinuities and the piping of fine-grained sediments over many years could eventually lead to formation of karst features.

Planning, education, and legislation and enforcement are required to mitigate karst processes and karst features. Reducing amounts and rate of percolating water in karst-prone areas could reduce karst processes and related features. This could be achieved by developing effective drainage systems before or during construction

activities. Controlled grazing in farming areas can prevent overgrazing, reduce erosion, and minimize destruction of the epikarst. This view is consistent with the view espoused by Parise and Gunn (2007), who suggest that human activities such as land degradation can cause irreparable damage and produce severe impacts in karst terrain. Education should be about basic awareness on the factors that drive karst processes. Educating people who live in potential karst areas about the various activities that facilitate the development of karst landforms could help reduce karst activities. For example, in one of the cases observed at the study area, bales of hay were continuously piled in a waterway. This caused surface water to accumulate at one particular location with the potential to percolate the subsurface and dissolve the bedrock. Perhaps if the farmers knew about the potential consequence of their farming activities in the karst terrain, they would have created a drainage system or piled the hay bales in a manner to allow the surface water to flow freely without impediments. Legislation and enforcement may include enacting appropriate local laws to control activities that could facilitate karst processes. These laws should be written in a way that is accessible and understandable to the people to whom the laws apply. That is, the enactments should be in plain language and authorities should ensure that they are evenly applied and enforced.

In summary, anthropogenic activities are the major factors driving karst processes in southwest Missouri and many states of the United States. Karst processes in overburden materials are usually more rapid than those occurring in underlying limestone bedrock. Karst processes in the bedrock are typically gradual and take a longer time, sometimes several hundreds of years, to manifest. Therefore, controlling karst processes in the epikarst can significantly minimize karstification and its concomitant dangers. This

can be accomplished by mitigating the factors that facilitate the percolation of acidic waters that serve as the major dissolving agent. Strategies to minimize karst processes or activities should involve the removal of water through appropriate and effective drainage or dewatering systems.

5. CONCLUSIONS

This study was conducted in karst terrain with the aim to map and characterize subsurface lithologic conditions, map the variations in engineering properties of soil/rock, map variable depth to top of rock, test the utility of the electrical resistivity (ERT) and multichannel analysis of surface waves (MASW) techniques, determine the drivers of karst processes, and propose mitigation. To achieve these goals, a site in southwest Missouri, known for its pronounced karst landforms and features, was selected for an experimental study. Both conventional and geophysical investigative techniques, including site inspections, boring, digital terrain modeling, ERT imaging, and active MASW surveys, were employed for data acquisition. Data collected included aerial and still photographs, GPS coordinates, borehole control, resistivity, and shear-wave velocity.

Resistivity data were acquired using the ERT technique, which involved the acquisition of subsurface electrical resistivity data with a multi-electrode resistivity system of 168 electrodes. The resistivity data were processed with the RES2DINV software into 2-D ERT profiles for geologic interpretations. Shear-wave velocity data (MASW data) were acquired using a multi-channel engineering seismograph with 24 geophones and a 20-pound sledge hammer as an acoustic source. The MASW data were inverted into 10-layered 1-D shear-wave velocity profiles. Borehole control was obtained with a CME truck-mounted drill rig. Aerial photographs were retrieved from Google Earth, while still photographs were acquired with a digital camera. GPS coordinates were obtained with a handheld GPS.

From the results and analysis of the data, bedrock in the study area is extensively weathered with pervasive and systematic network of discontinuities partially filled with water and moist soils. Solution-widening has occurred (preferentially) where waters have seeped into the underlying rock. Seepage rates have probably been controlled mostly by surface topography, but perhaps also by intensity of fracturing. Even though resistivity is a function of permeability, salinity, moisture content, porosity, and clay content, moisture content was observed as the major controlling parameter of resistivity in the karst terrain. Thus, the subsurface was characterized as moist soil (≤50 ohm.m), dry soil (125 – 250 ohm.m), moist rock (≥125 ohm.m), and dry rock (≥1500 ohm.m). From the shear-wave velocity data, and adopting a soil/rock classification system developed by the National Earthquake Hazard Reduction Program (NEHRP), soil/rock could be classified into stiff soil (<1200 ft/s), soft soil (<600 ft/s), very dense soil (1200 – 1300 ft/s), soft rock (≥1300 ft/s), and rock (≥2500 ft/s). Stiff soil was observed as the surficial soil and had relatively high shear-wave velocity values due to compaction. The ERT and MASW interpretations were observed to be consistent with borehole control.

Digital terrain modeling and geophysical mapping showed undulating surface terrain that mostly depicted the topography of top of rock. Depression in the surface topography followed depression in the bedrock surface. Bedrock was exposed and weathered in some places and could be located at shallow depth (6 ft) in areas where residuum overlies the bedrock. Depth to top of rock varied significantly along the survey traverse. This variation is attributed to the intense dissolution of the limestone bedrock.

ERT and MASW techniques can reliably be used to map and characterize the subsurface, estimate depth to top of rock, and determine variations in engineering

properties of soil and rock in karst terrain. These two geophysical techniques can provide significant data to support intrusive geotechnical assessments and to minimize cost and data acquisition time. Borehole control was consistent with the 2-D ERT and 1-D active MASW data. Therefore, it is argued that 2-D ERT and 1-D active MASW can be used independently to explore karst terrain and produce high quality and very reliable subsurface data for environmental, geological, and geotechnical purposes. However, understanding of local geology and adequate knowledge about the subsurface processes may be required to provide very accurate interpretations of the geophysical data.

An assessment of the factors contributing to karst development found anthropogenic activities such as construction of parking lots, roads, buildings, and farming activities as major drivers of karst processes. These activities, in most instances, intercept surface flow pathways and cause water to pond. The ponding and percolation of water with solution-widening of fractures and the piping of fine-grained sediments over many years can cause the development of prominent karst features. Thus, sinkholes in the study area may not be random, but perhaps induced by human activities.

Planning, education, legislation, and enforcement of enactments can help mitigate the factors that facilitate karst development. Reducing amounts and rate of percolating water in karst-prone areas could reduce karst processes. This can be achieved by developing effective drainage systems before or during construction activities. Education should be about awareness on the factors that drive karst processes. Educating people who live in karst-prone areas about the drivers of karst landforms could help minimize karst activities. Legislation and enforcement should involve enacting appropriate local laws to control activities that could facilitate karst processes. These laws should be

accessible and understandable to the people to whom the laws apply, and authorities should ensure that the laws are evenly applied and enforced.

Most importantly, removing water by adopting appropriate and effective drainage or dewatering systems would significantly minimize karst processes with their concomitant features. This mitigation strategy will reduce the amounts and rate of percolating acidic waters and considerably slow down dissolution processes along the pervasive and systematic vertical and horizontal fractures. In areas where farming occurs, controlled grazing by farm animals could be employed to prevent overgrazing and eliminate or reduce erosion, thus preventing exposure of the epikarst to agents of karst processes.

APPENDIX A.
EXAMPLE MASW AND ERT PROFILES

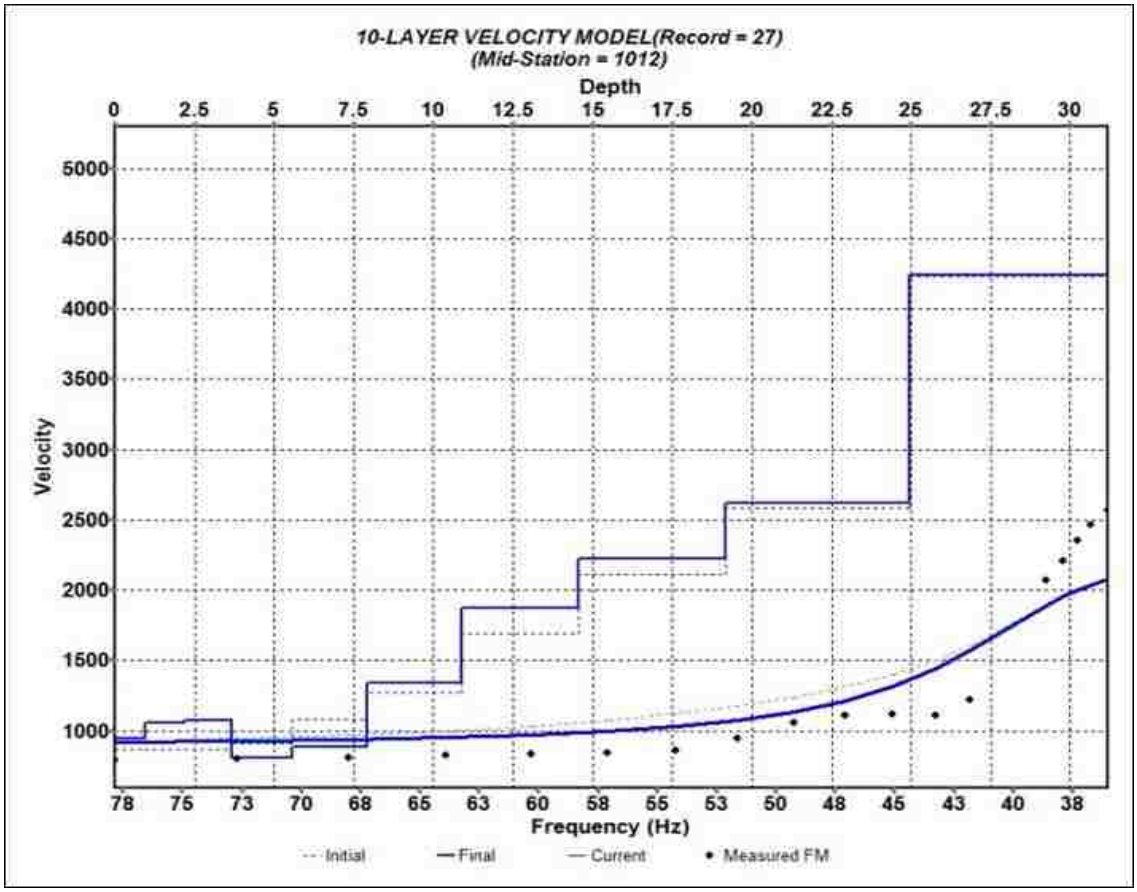

MASW Profile_401

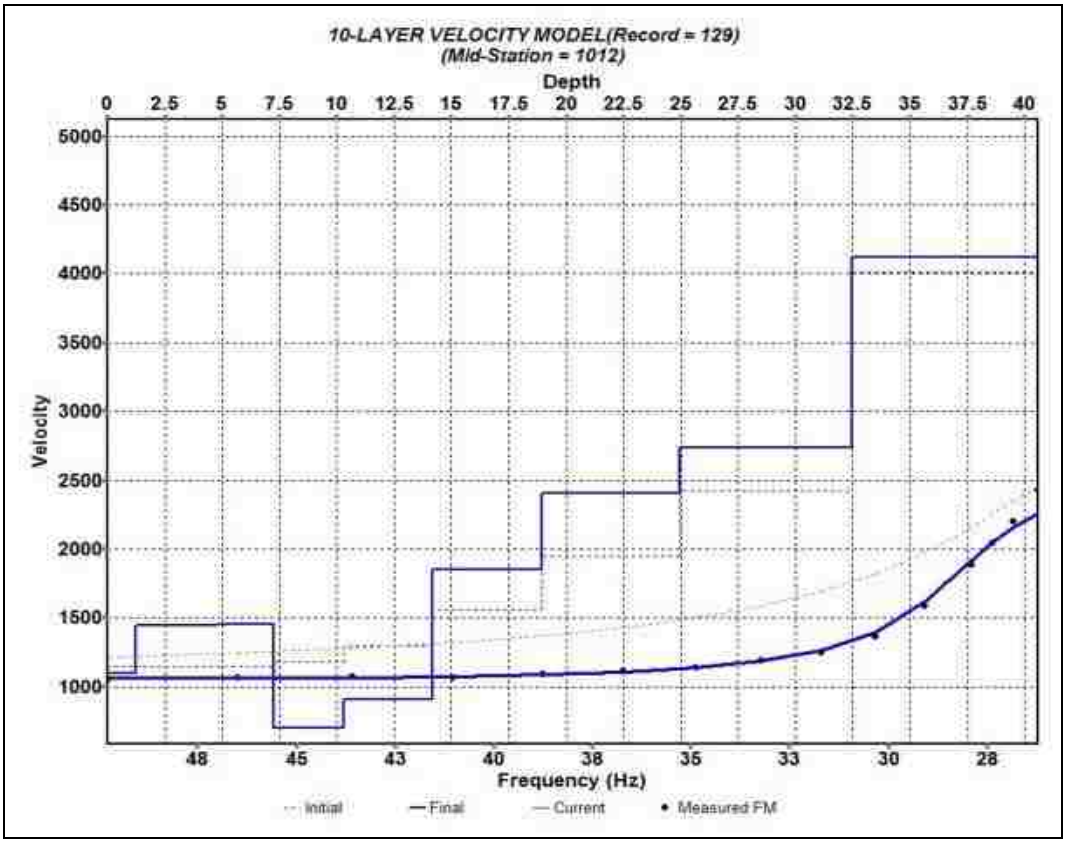

MASW Profile_402

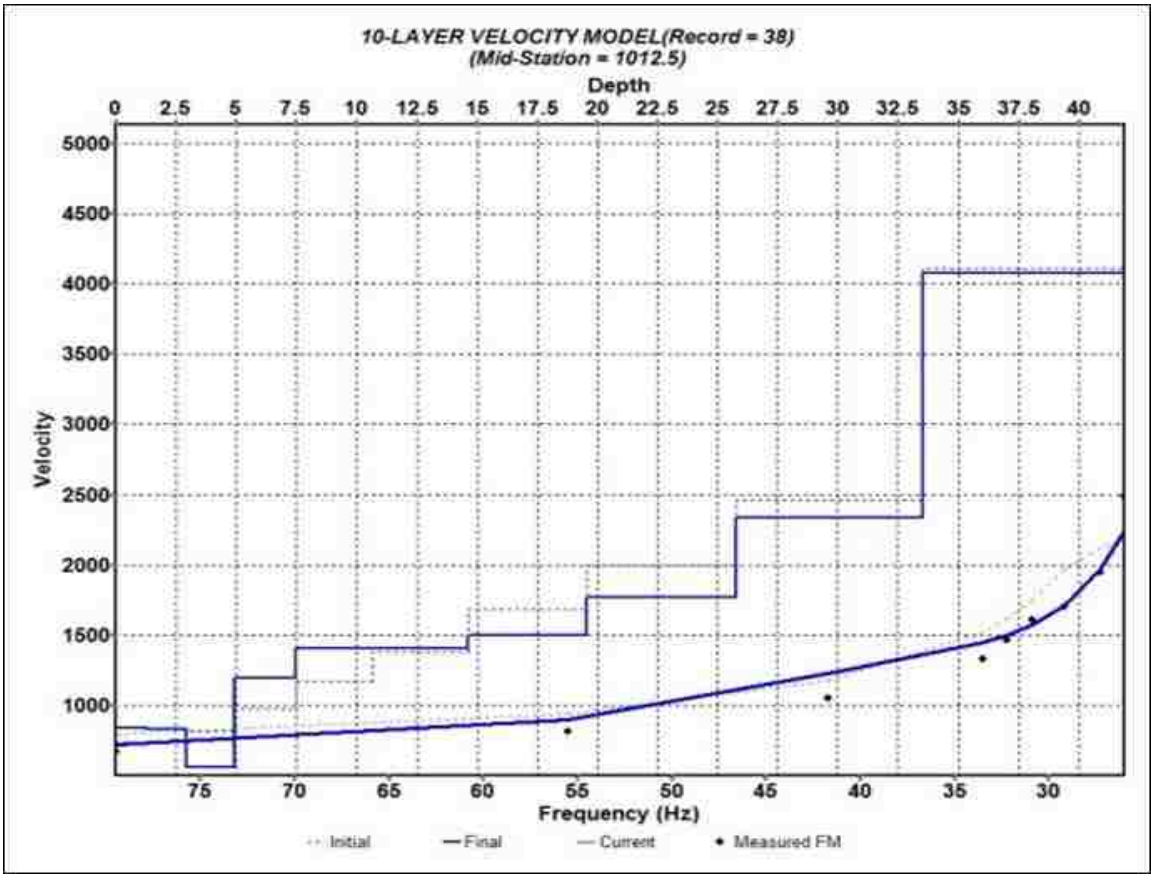

MASW Profile_403

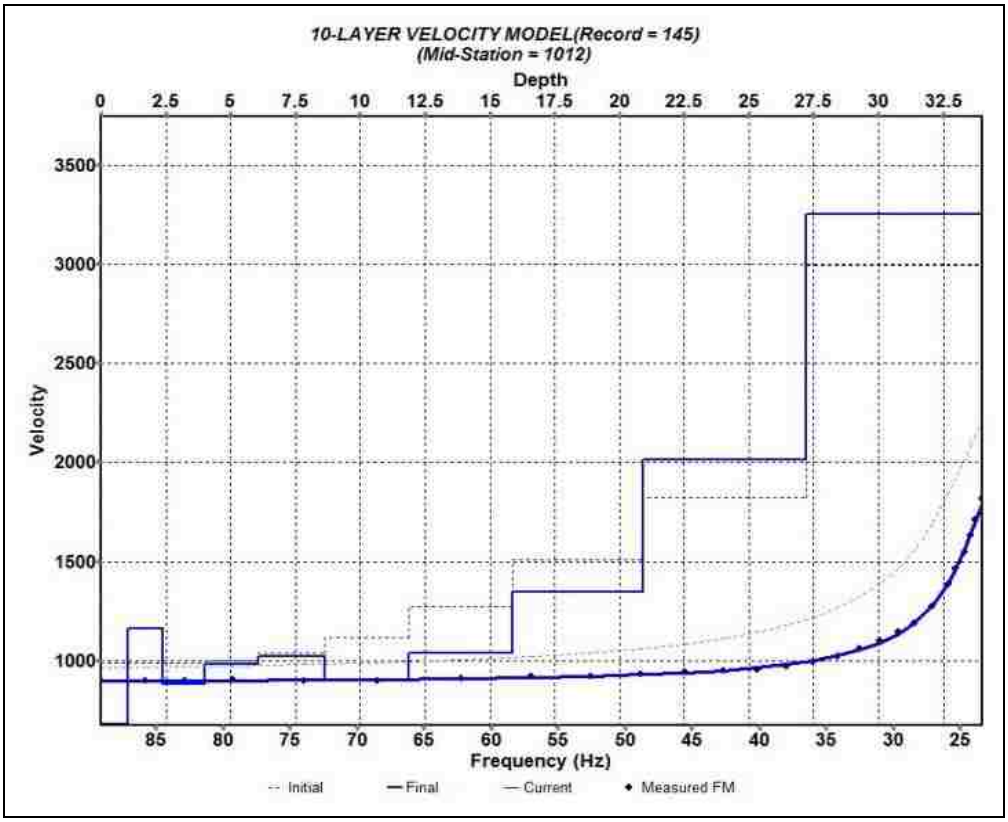

MASW Profile_404

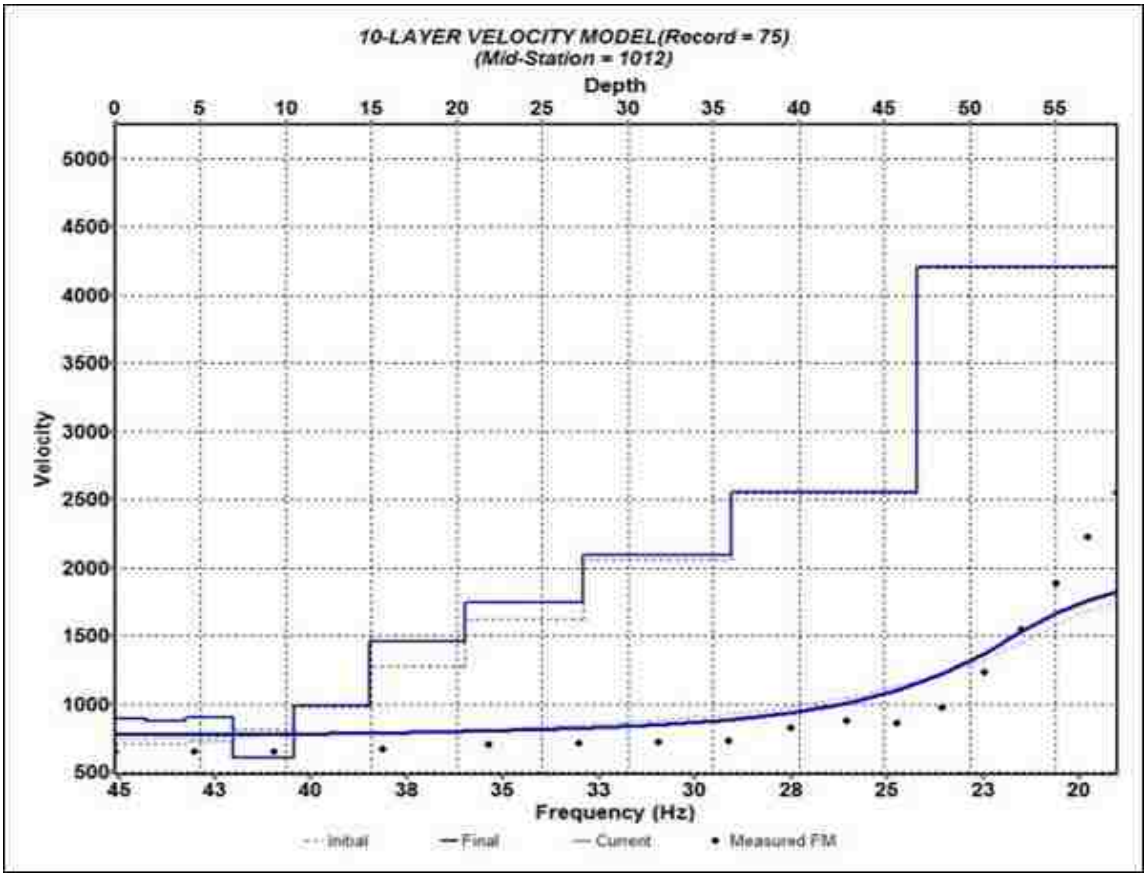

MASW Profile_405

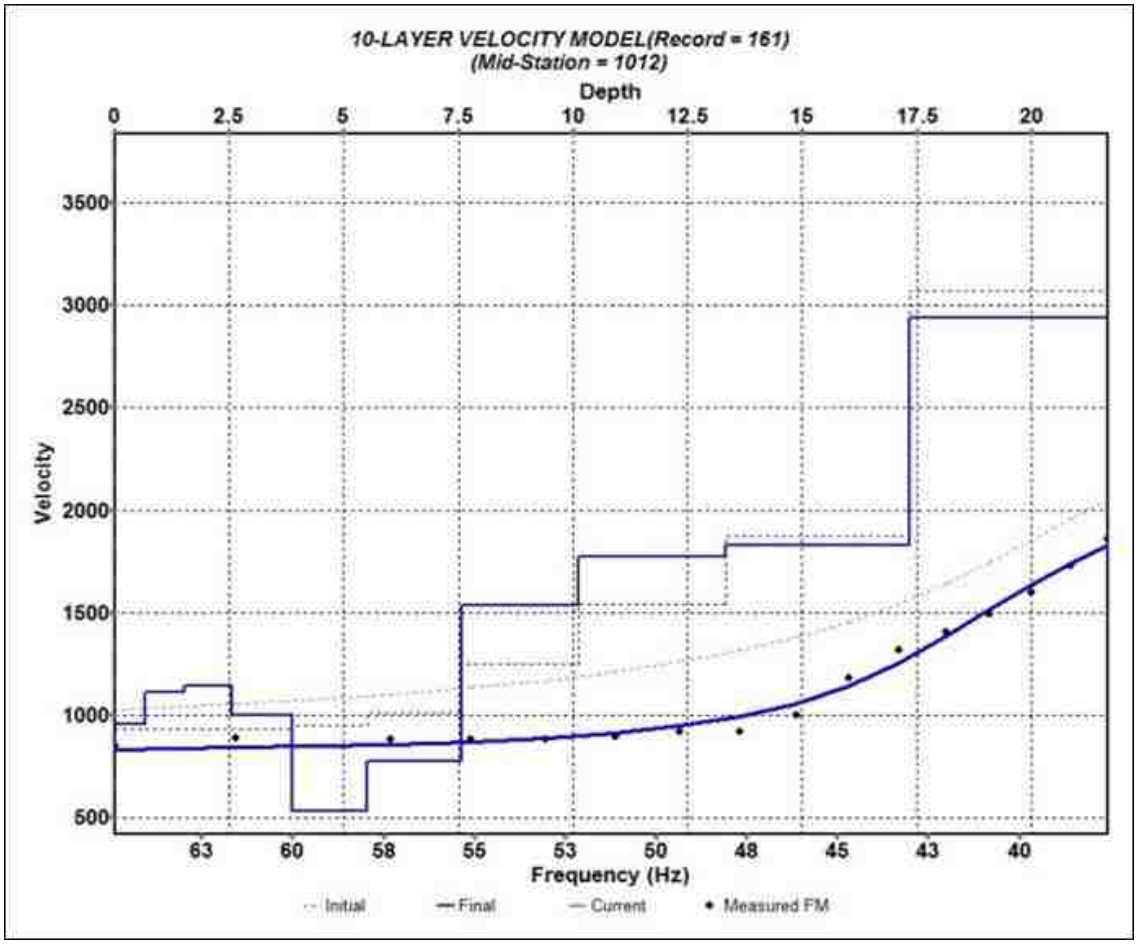

MASW Profile_406

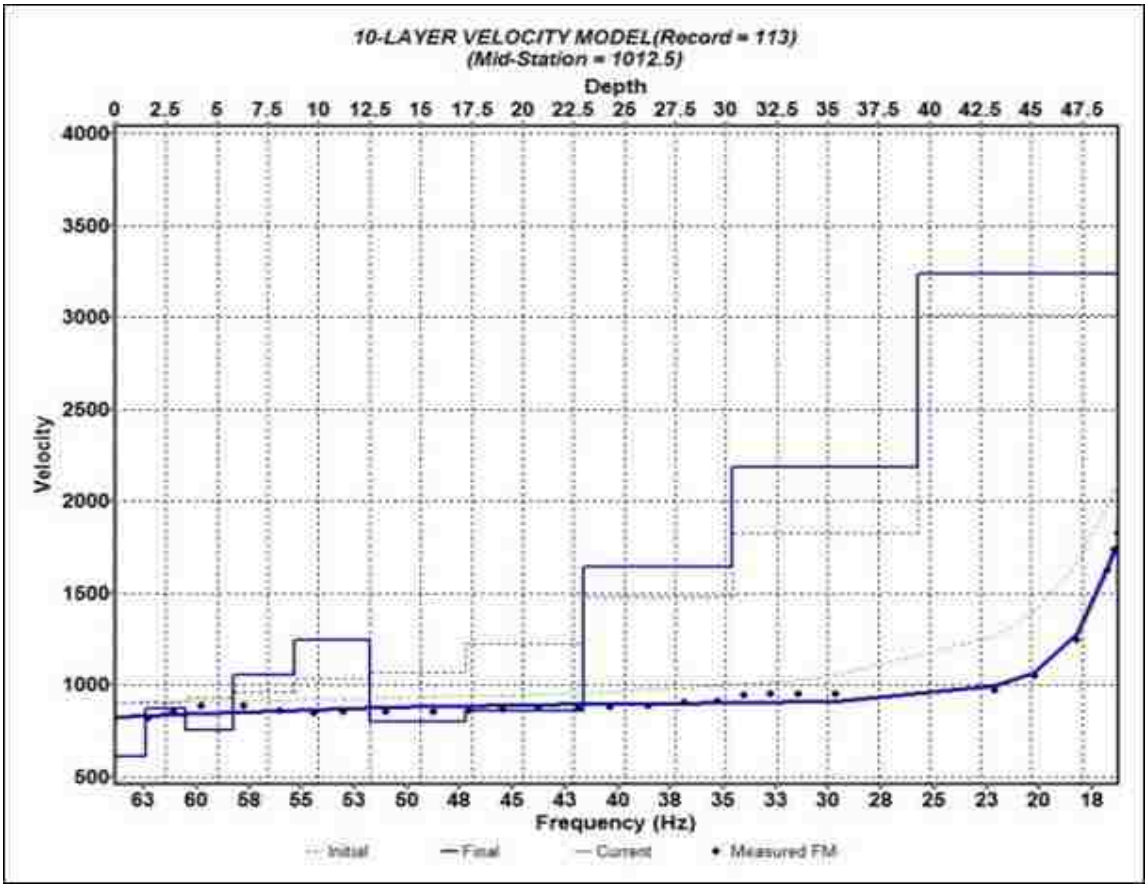

MASW Profile_407

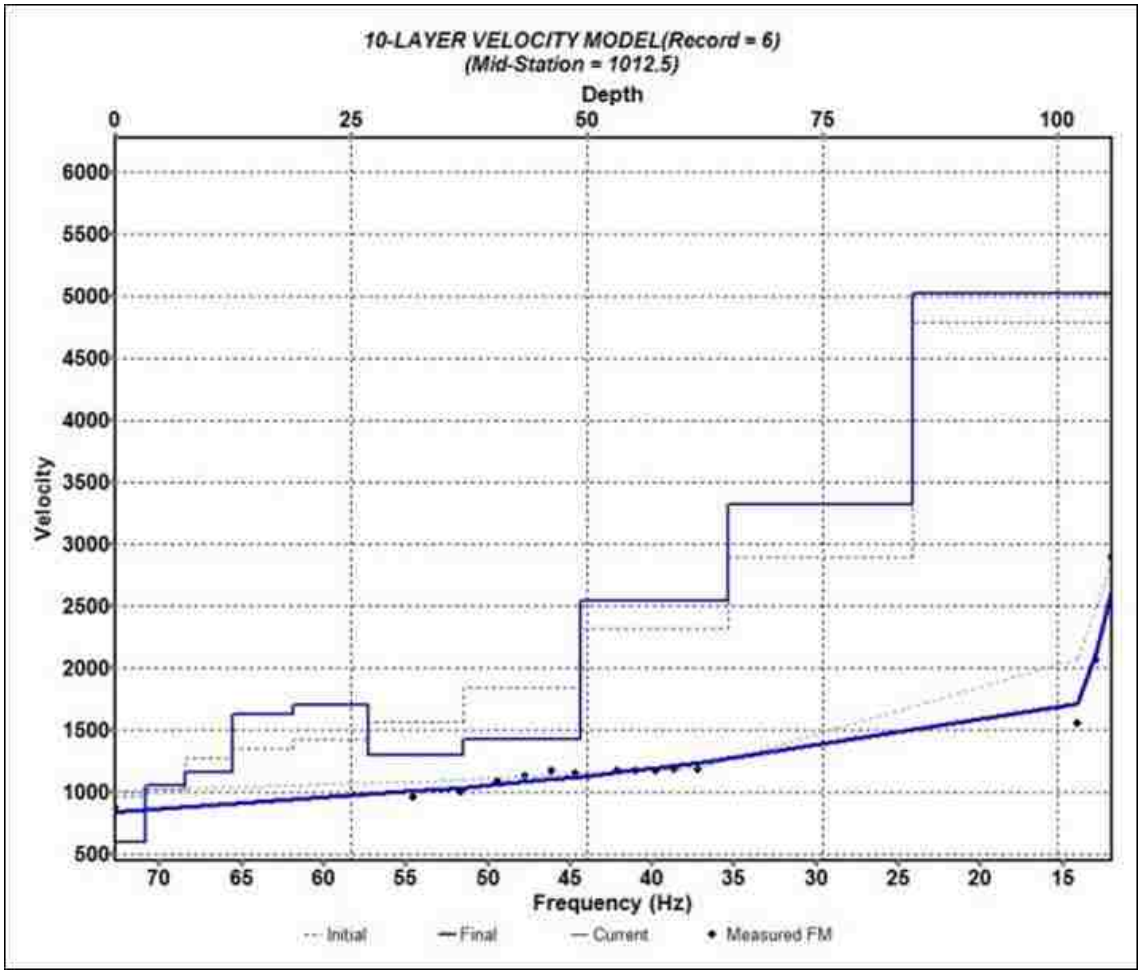

MASW Profile_408

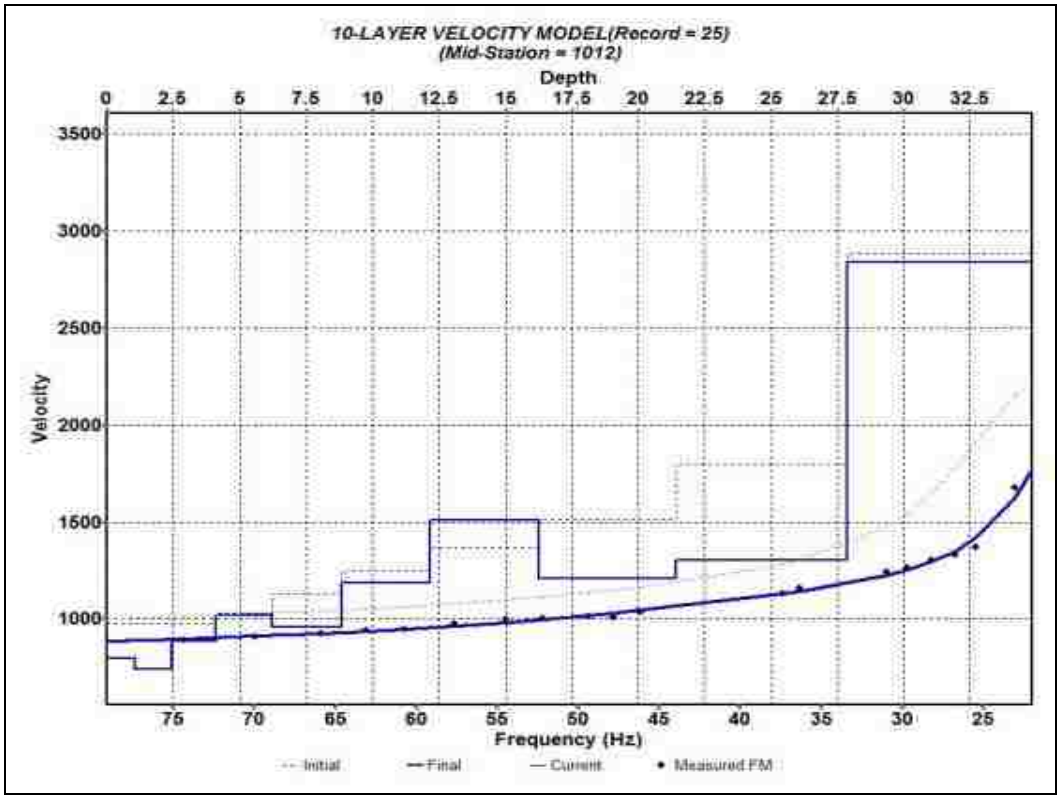

MASW Profile_409

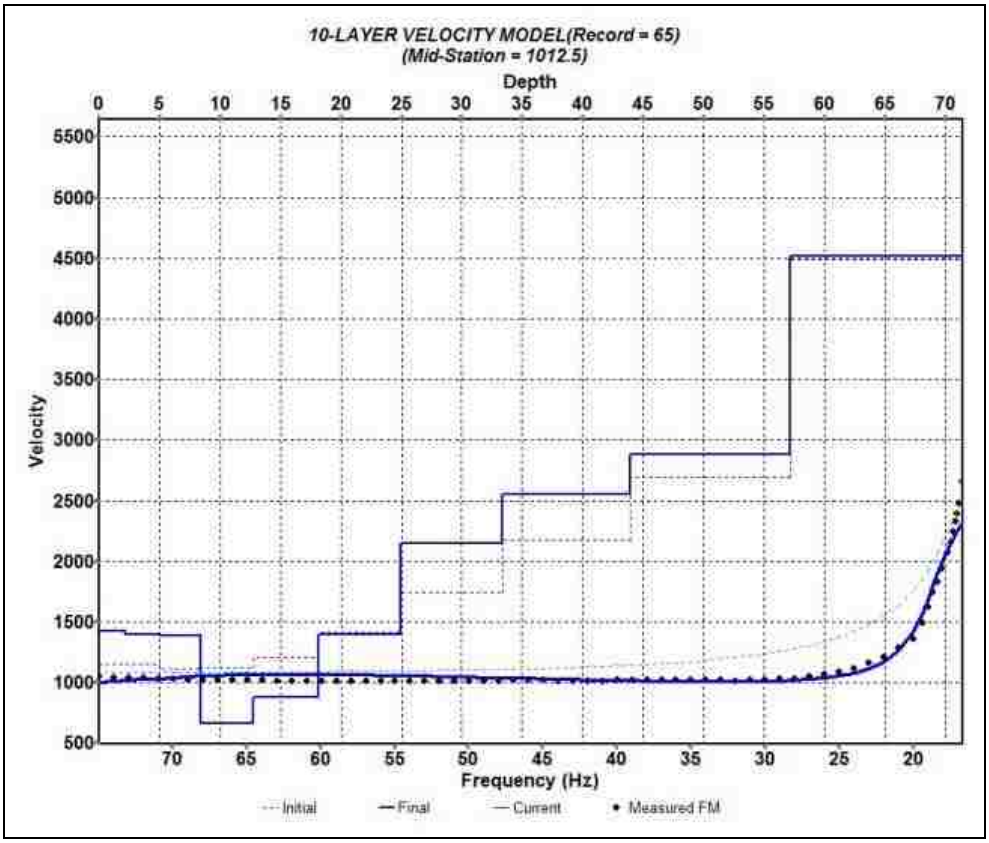

MASW Profile_410

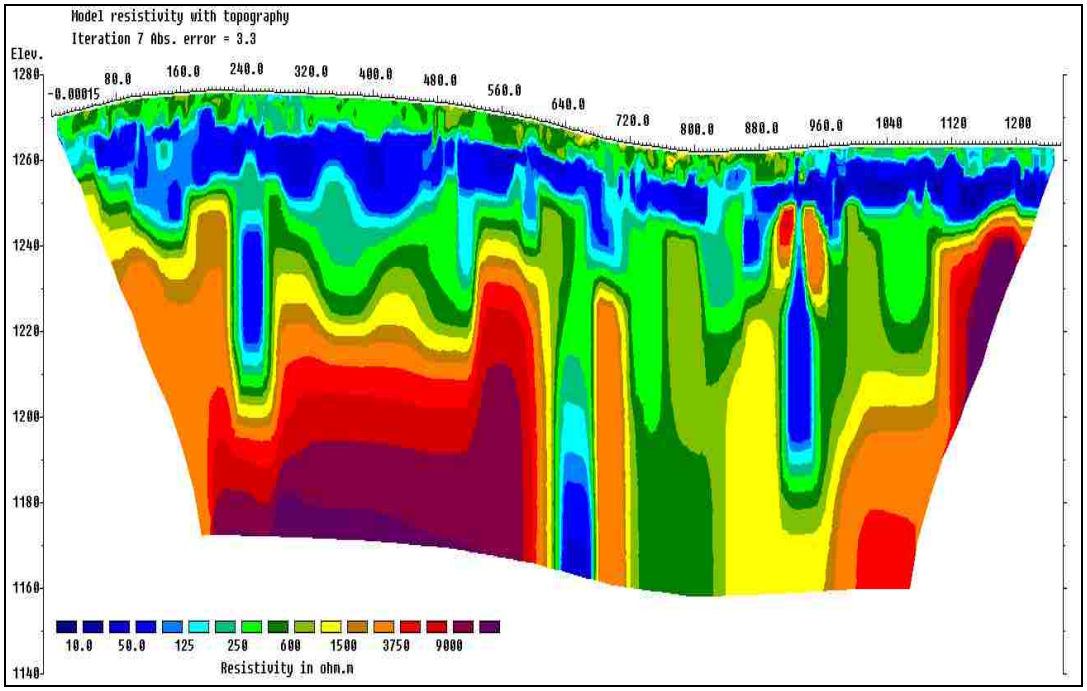

ERT Profile_506

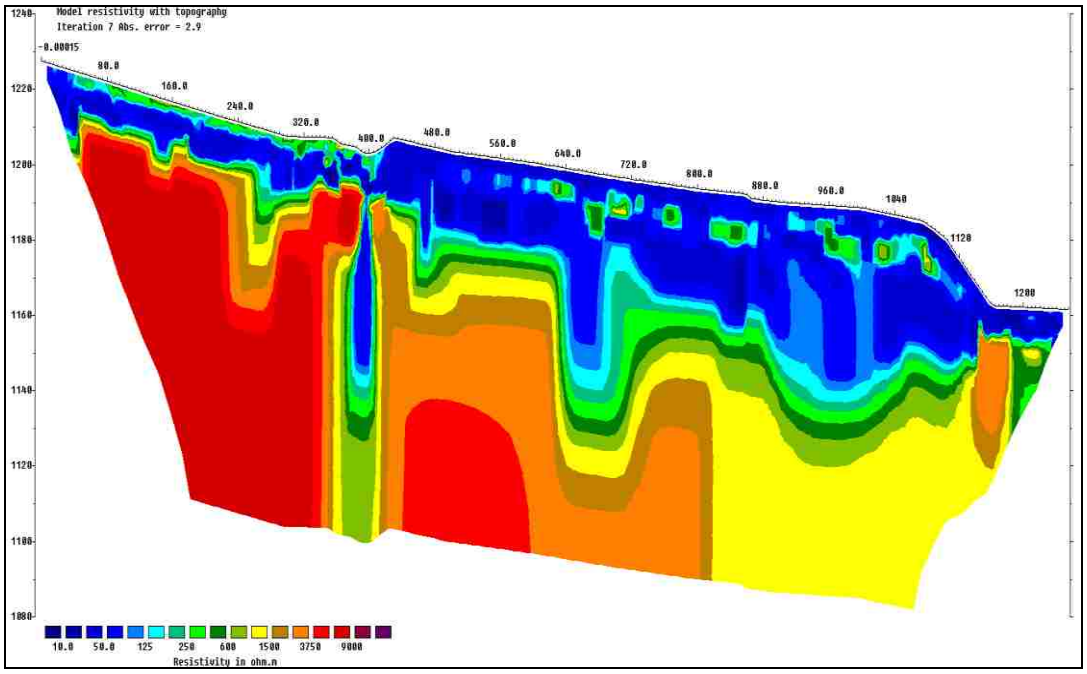

ERT Profile_601

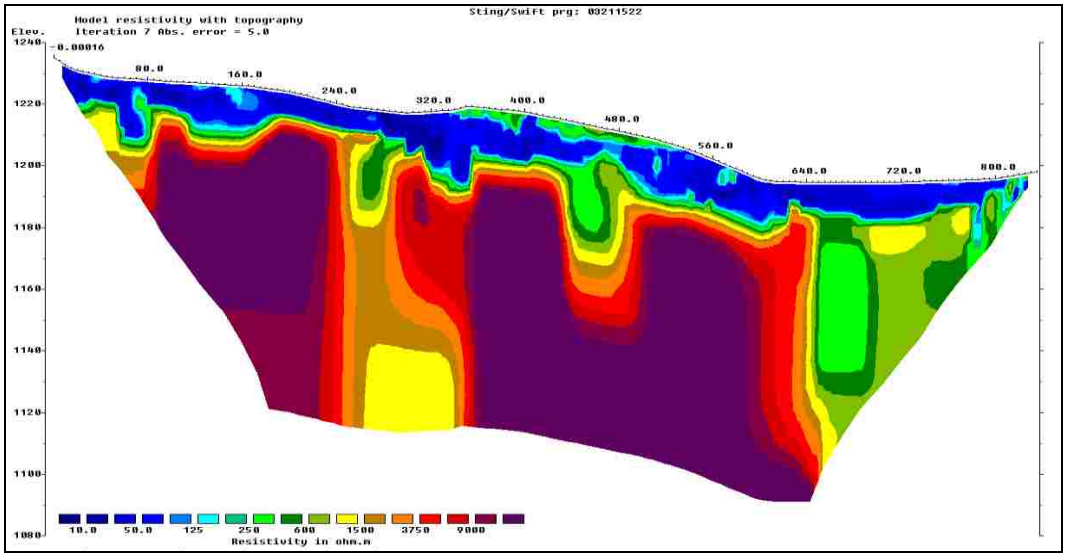

ERT Profile_604

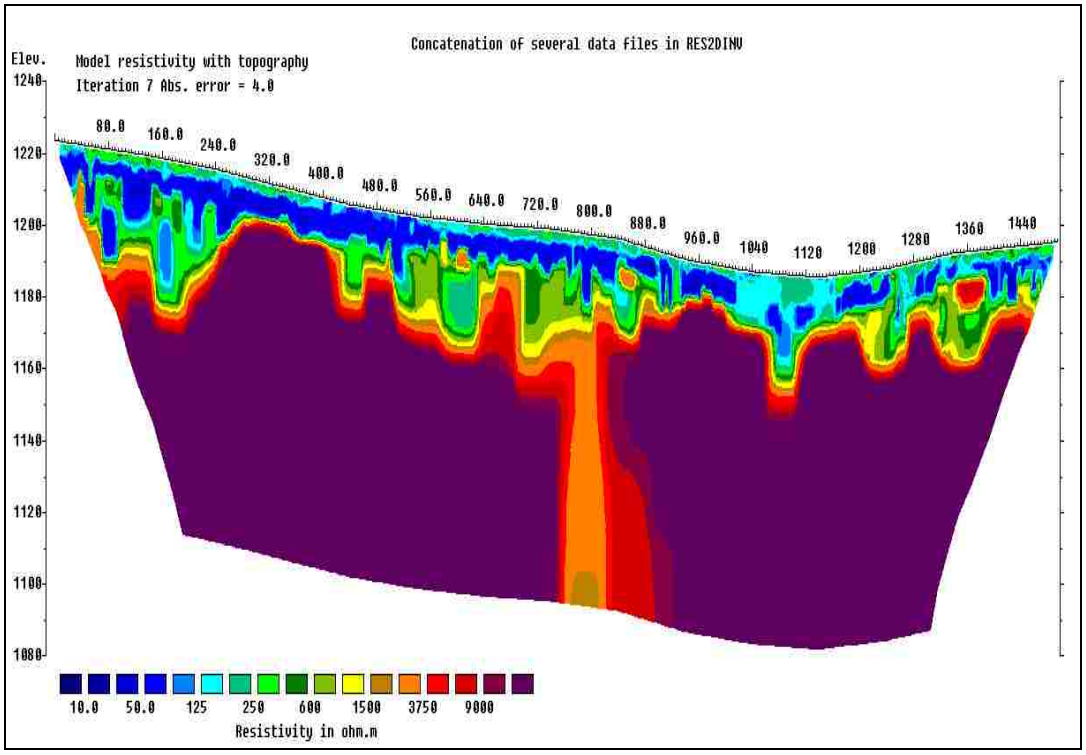

ERT Profile_608

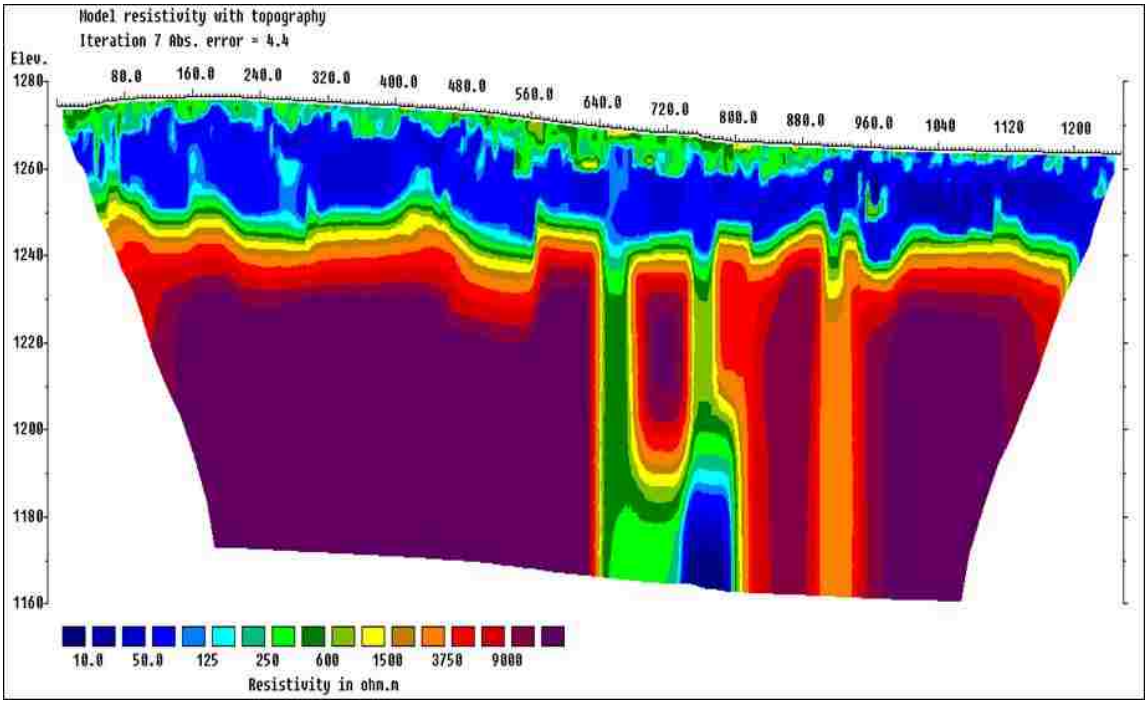

ERT Profile_701

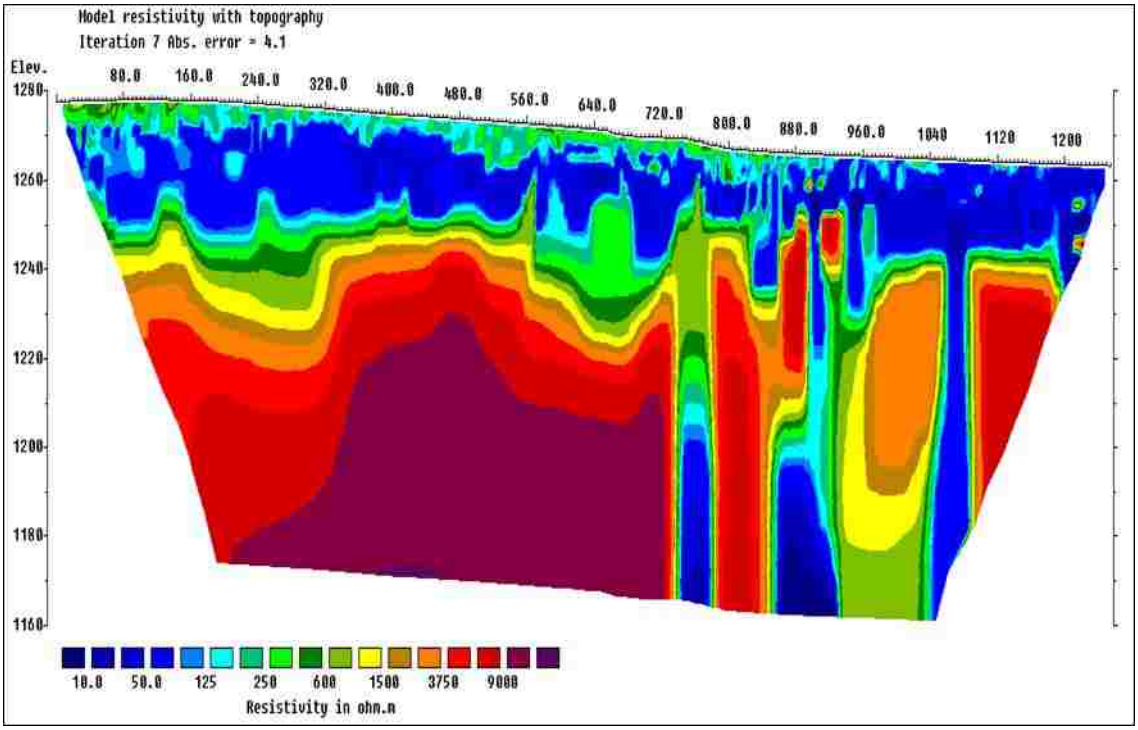

ERT Profile_702

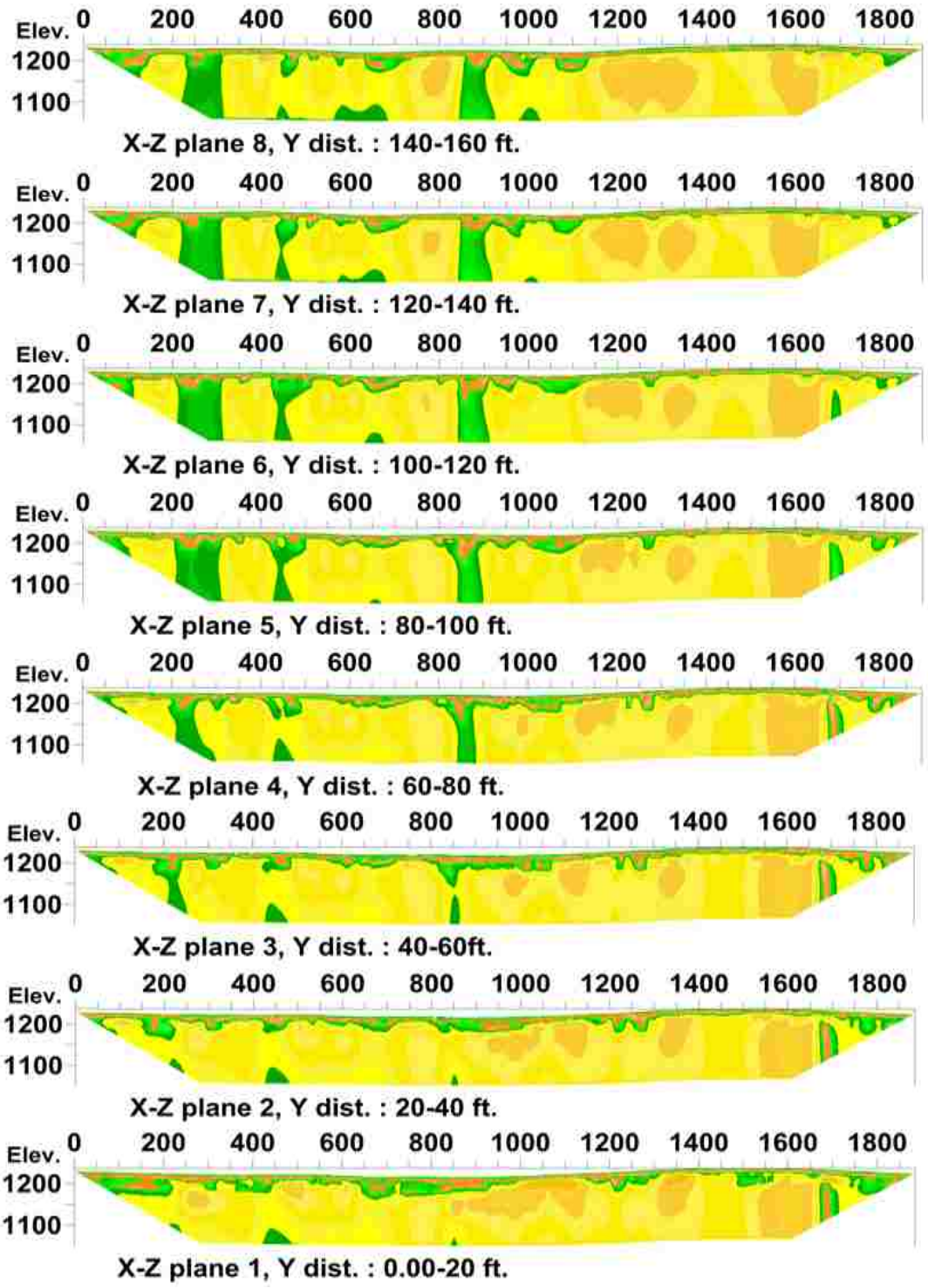
Elev.
0
200
400
600
800
1000
1200
1400
1600
1800
1200
1100
X-Z plane 8, Y dist. : 140-160 ft.
X-Z plane 7, Y dist. : 120-140 ft.
X-Z plane 6, Y dist. : 100-120 ft.
X-Z plane 5, Y dist. : 80-100 ft.
X-Z plane 4, Y dist. : 60-80 ft.
X-Z plane 3, Y dist. : 40-60ft.
X-Z plane 2, Y dist. : 20-40 ft.
X-Z plane 1, Y dist. : 0.00-20 ft.

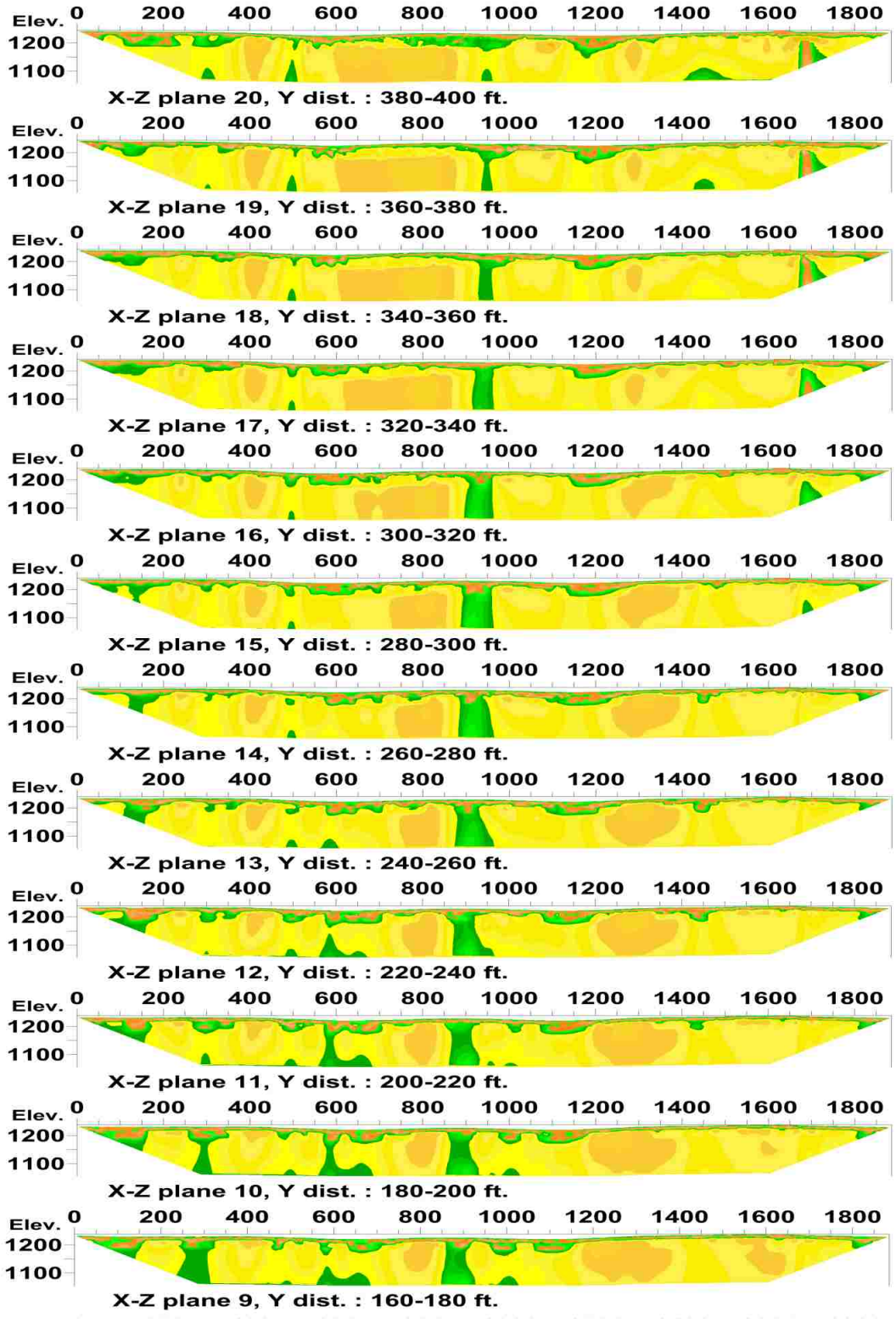

ERT Model of Northern Portion of Study Area

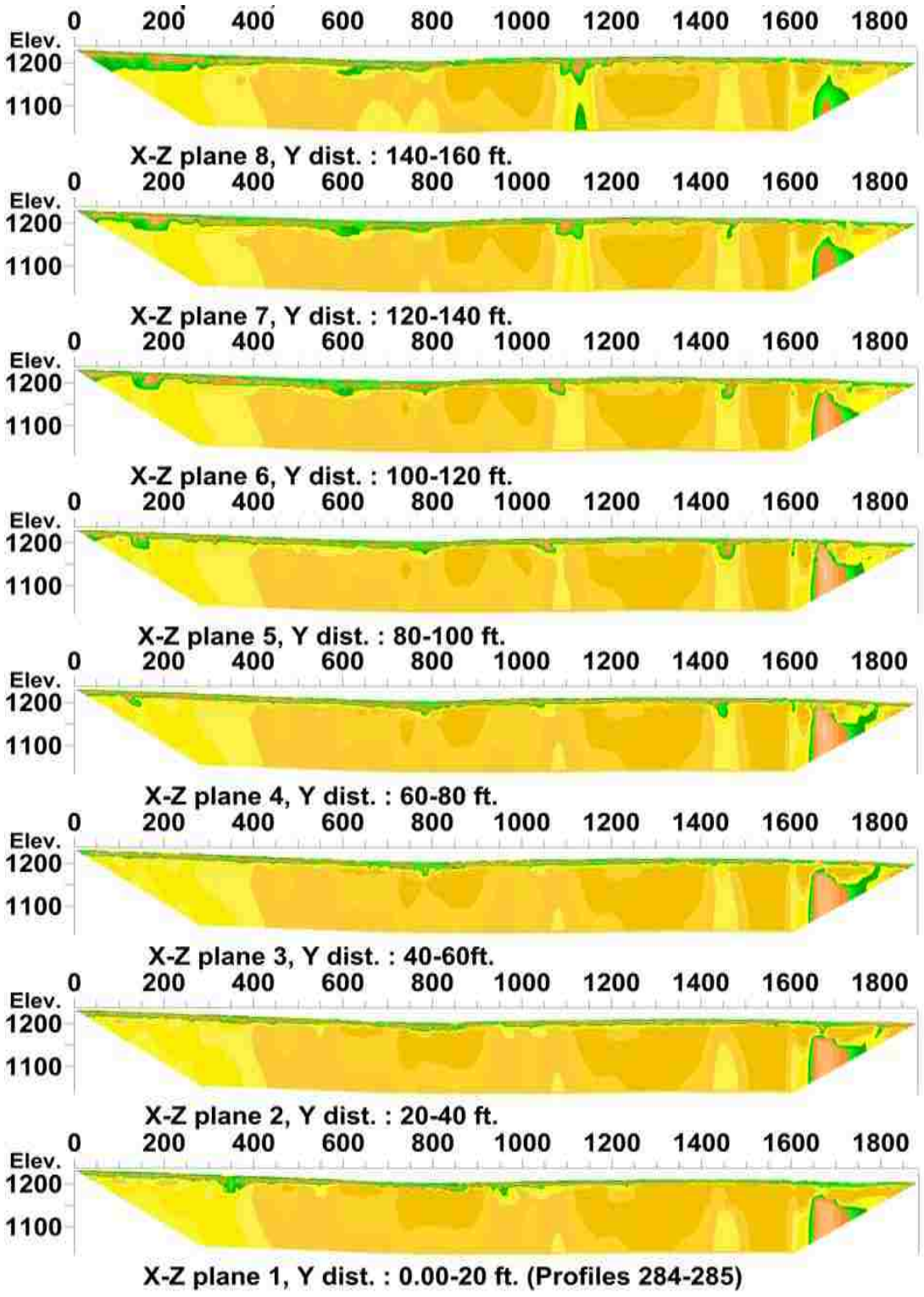
0 200 400 600 800 1000 1200 1400 1600 1800
Elev.
1200
1100
X-Z plane 8, Y dist. : 140-160 ft.
X-Z plane 7, Y dist. : 120-140 ft.
X-Z plane 6, Y dist. : 100-120 ft.
X-Z plane 5, Y dist. : 80-100 ft.
X-Z plane 4, Y dist. : 60-80 ft.
X-Z plane 3, Y dist. : 40-60ft.
X-Z plane 2, Y dist. : 20-40 ft.
X-Z plane 1, Y dist. : 0.00-20 ft. (Profiles 284-285)

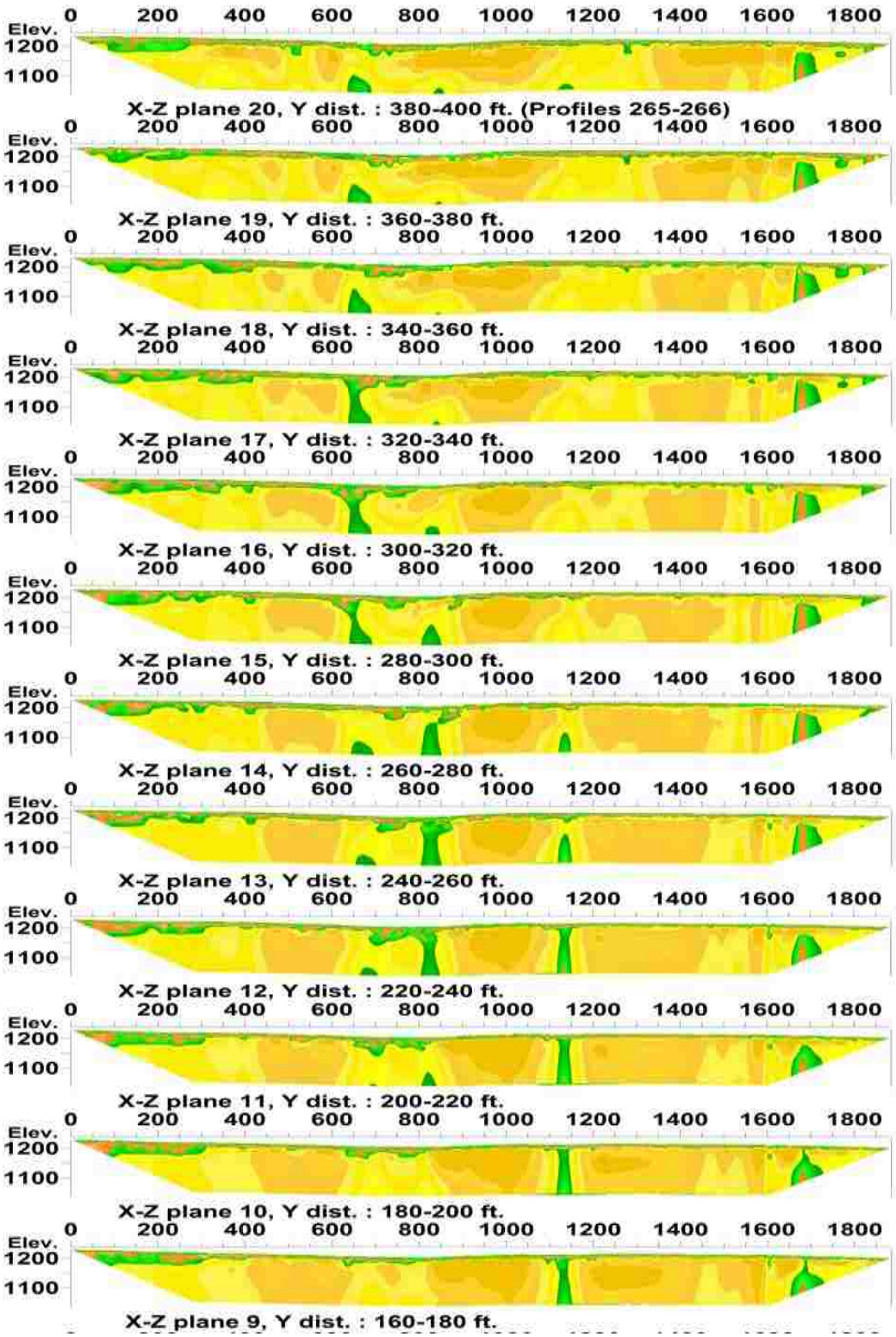

ERT Model of Southern Portion of Study Area

APPENDIX B.
BOREHOLE CONTROLS

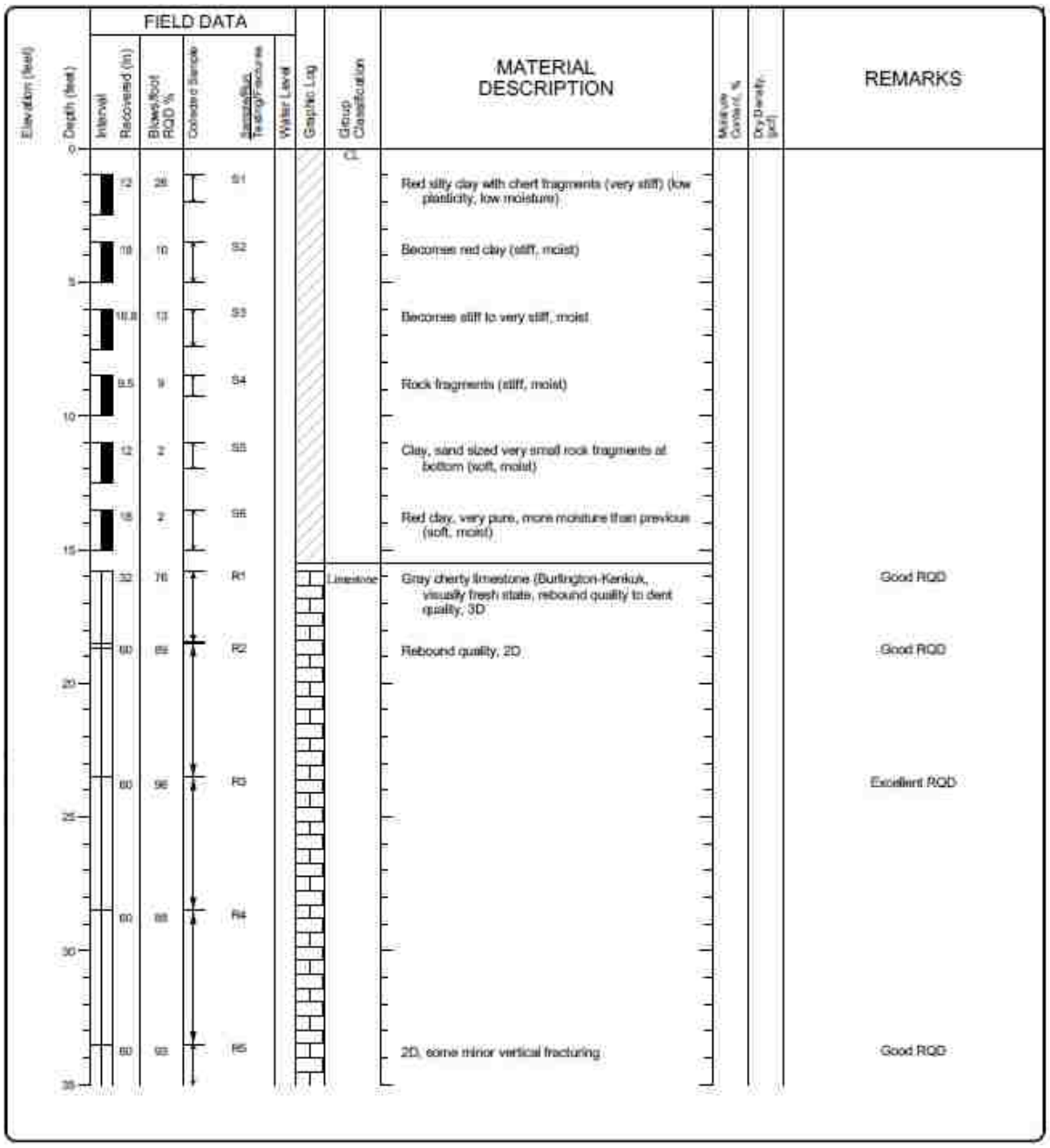

Borehole Control_BCI

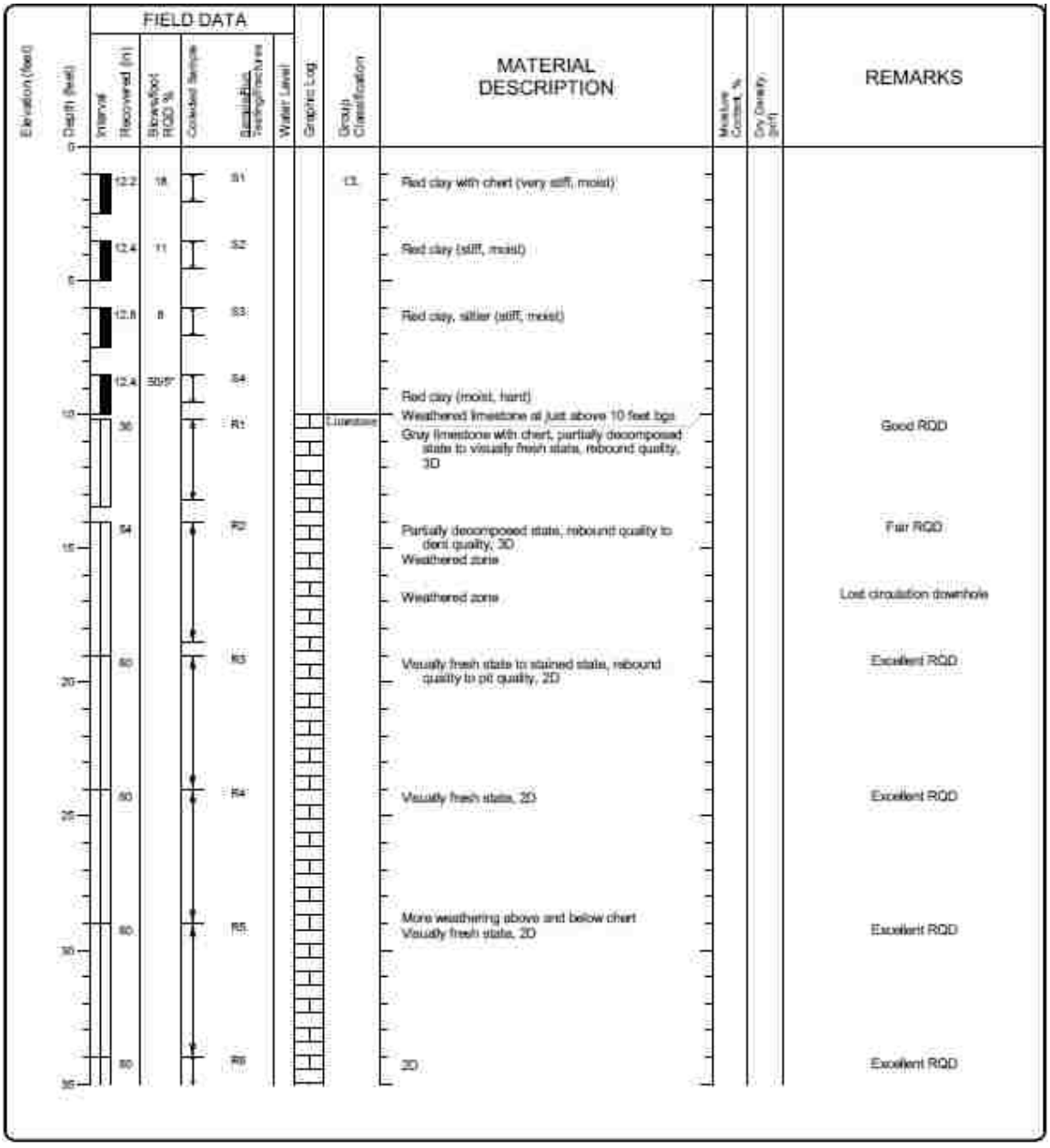

Borehole Control_BC2

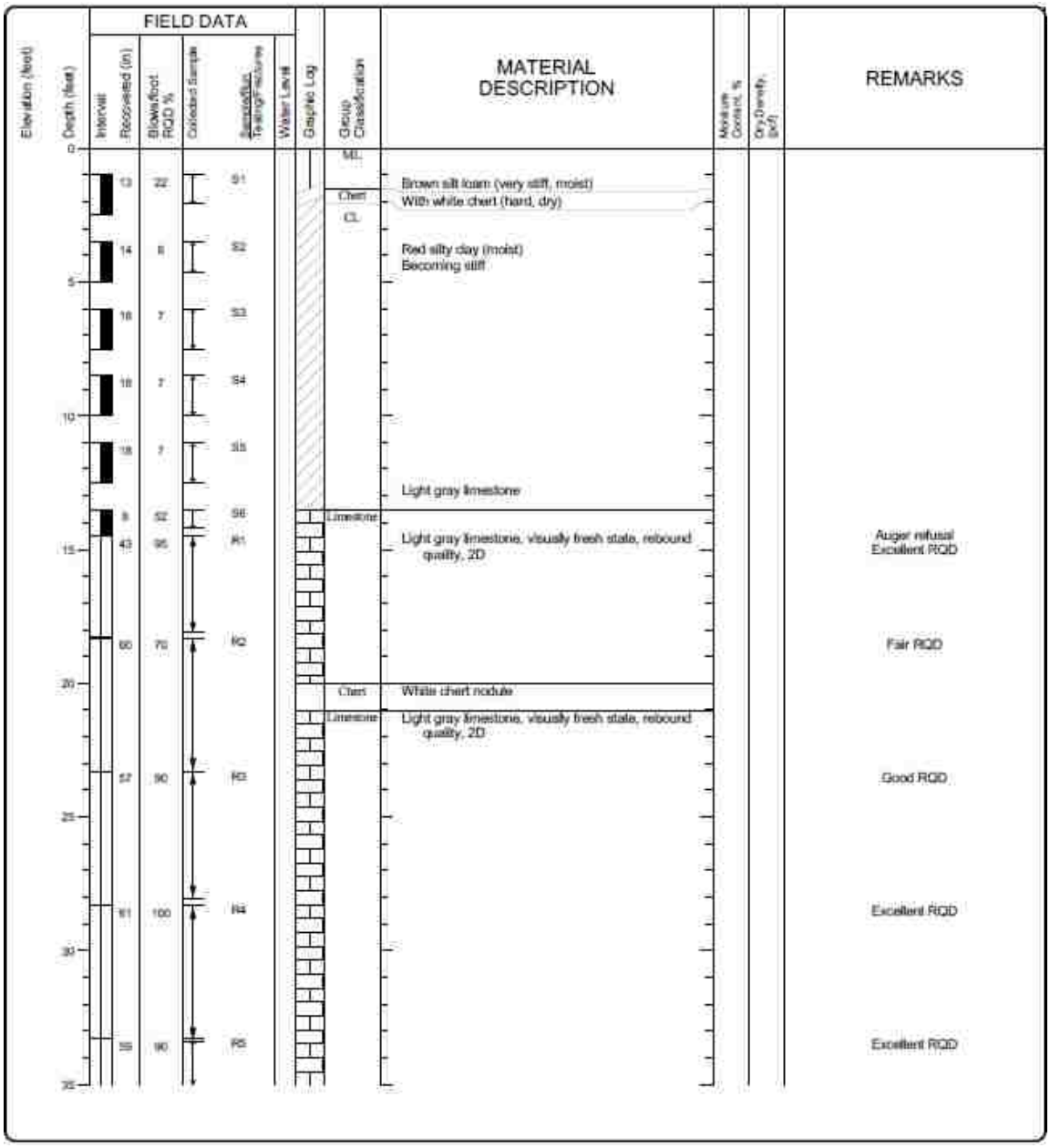

Borehole control_BC3

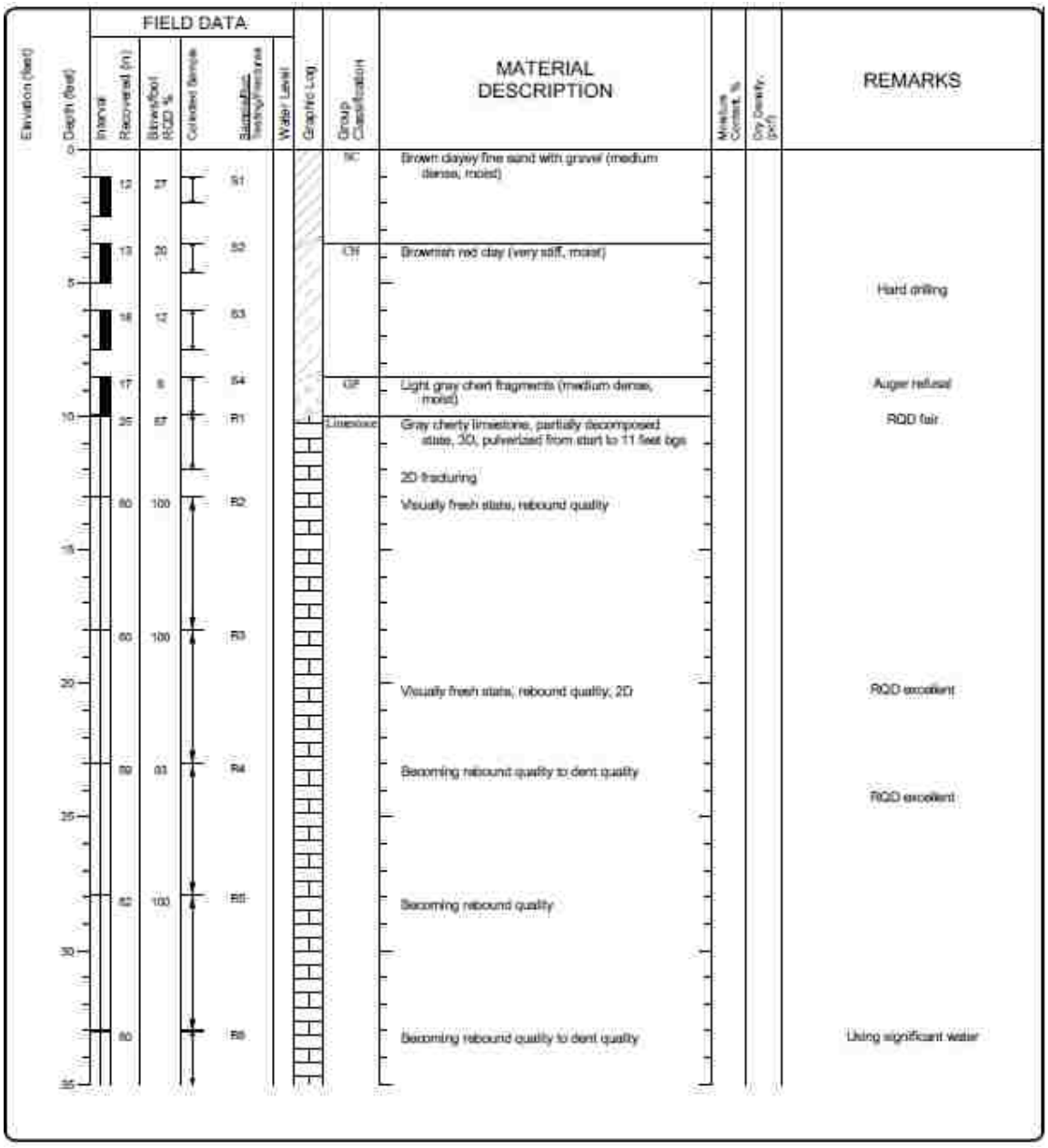

Borehole Control_BC4

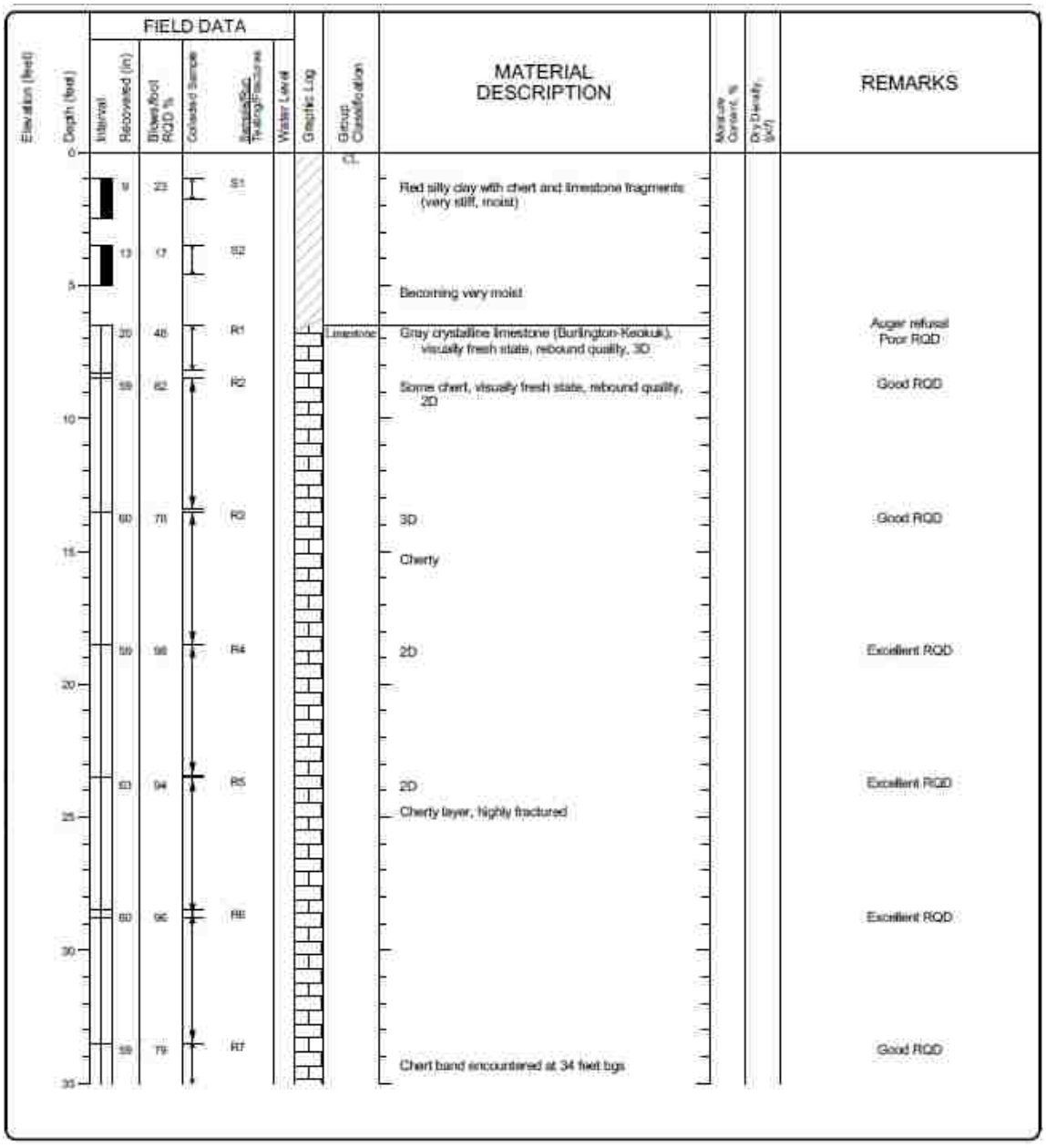

Borehole Control_BC5

APPENDIX C.

3-D SURFACE ELEVATION AND TOP OF ROCK MODELS

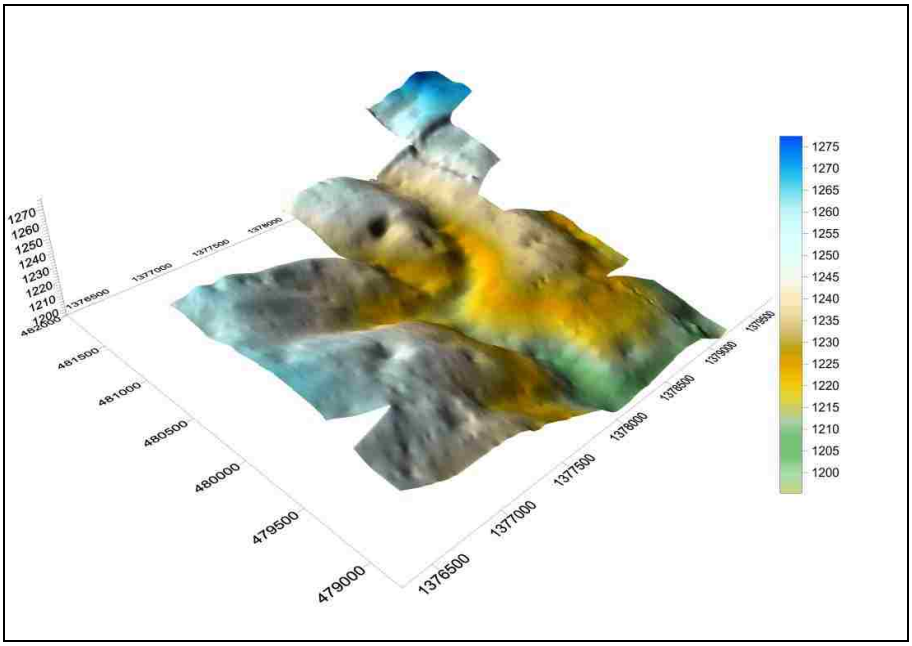

Surface Elevation Model of Study Area

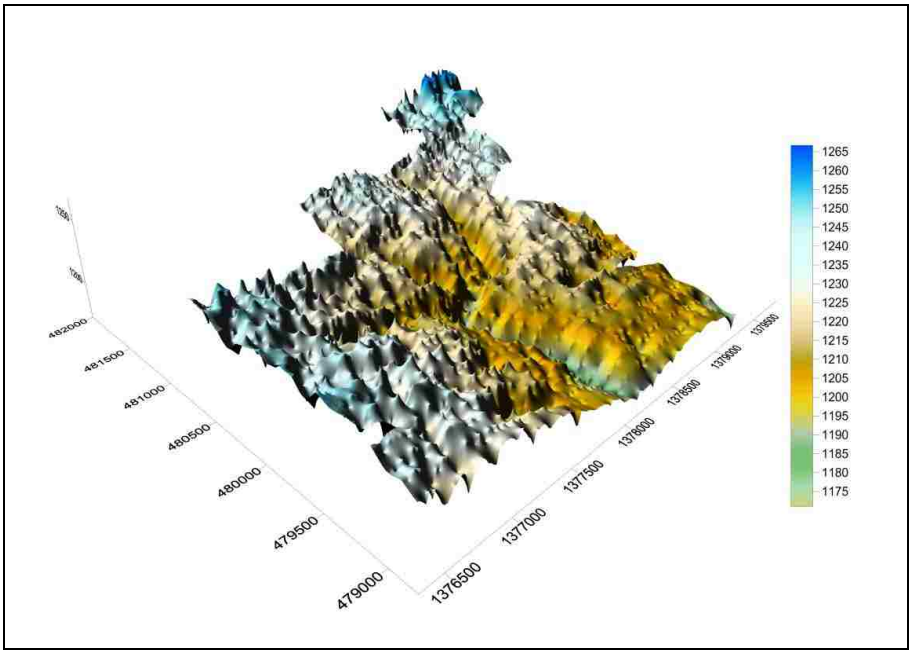

Top of Rock Elevation Model of Study Area

BIBLIOGRAPHY

Anderson, N. L. (2015). GPR and MASW lecture notes. Missouri University of Science and Technology, Missouri.

Anderson, N., Cardimona, S., & Newton, T. (2003). Application of innovative non-destructive methods to geotechnical and environmental investigation. *Final Report, RDT-008, Missouri Department of Transportation*, library.modot.mo.gov. Accessed 06.06.15.

Anderson, N., L., & Torgashov, E. (2010). Ground penetrating radar: Utility/REBAR/Cable detection and concrete/subgrade debonding. *SAGEEP 2010*, Keystone, Colorado, 13pp.

Andreychouk, V., & Tyc, A. (2013). Karst hazards. In *Encyclopedia of Natural Hazards*. *Springer Netherlands*, 571-576.

Andrejchuk, V. (2002). Collapse above the world's largest potash mine (Ural, Russia). *Int. J. Speleol.*, 31(1/4), 137-158.

Baines, D., Smith, D. G., Froese, D. G., Bauman, P., & Nimeck, G. (2002). Electrical resistivity ground imaging (ERGI): a new tool for mapping the lithology and geometry of channel-belts and valley-fills. *Sedimentology*, 49(3), 441–449.

Ballard, R. F., Cuenod, Y., & Jenni, J. P., (1983). Detection of karst cavities by geophysical methods. *Bulletin of the International Association of Engineering Geology*, 26–27, 153–157.

Bernard, J., Leite, O., Vermeersch, F., Instruments, I. R. I. S., & Orleans, F. (2006). Multi-electrode resistivity imaging for environmental and mining applications. *IRIS Instruments*, Orleans, France, 6.

Cardimona, S. (2002). Electrical resistivity techniques for subsurface investigation. *Geophysics 2002 Conference Proceedings*. Los Angeles, California, USA, 10.

Chalikakis, K., Plagnes, V., Guerin, R., Valois, R., & Bosch, F. P. (2011). Contribution of geophysical methods to karst-system exploration: an overview. *Hydrogeology Journal*, 19(6), 1169-1180.

Chen, J. (1988). Karst collapse in cities and mining areas, China, *Environmental Geology and Water Sciences*, 12(1), 29-35.

CNN (2015). Road rips open, 15 cars fall through. Retrieved from www.cnn.com/videos/us/2015/11/09/sinkhole-mississippi-drone-footage-newday.cnn/video/playlists/terrifying-sinkholes/. Accessed 18.12.2017.

Cook, J. C. (1965). Seismic mapping of underground cavities using reflection amplitudes. *Geophysics*, *30*(4), 527-538.

Cooper, A. H. (1998). Subsidence hazards caused by the dissolution of Permian gypsum in England: geology, investigation and remediation. *Geological Society, London, Engineering Geology Special Publications*, 15(1), 265-275.

Currens, J. C., Paylor, R. L., Beck, E. G., & Davidson, B. (2012). A method to determine cover-collapse frequency in the western pennyroyal karst of Kentucky. *Journal of Cave and Karst Studies*, 74(3), 292-299.

Daily, W., Ramirez, A., Labrecque, D., & Nitao, J. (1992). Electrical-resistivity tomography of vadose water-movement. *Water Resour. Res.*, 28(5), 1429–1442.

Daniels, F., & Alberty, R. A. (1966). Occam's inversion to generate smooth, two dimensional models from magneto telluric data. *Geophysics*, 55, 1613-1624.

De Giorgi, L., & G. Leucci. (2014). Detection of hazardous cavities below a road using combined geophysical methods. *Surveys in Geophysics*. 35(4), 1003-1021.

Debeglia, N., Bitri A., & Thierry, P. (2006). Karst investigations using microgravity and MASW; application to Orléans, France. *Near Surface Geophysics, European Association of Geoscientists & Engineers*, 215-225.

Del Prete, S., Iovine, G., Parise, M., & Santo, A. (2010). Origin and distribution of different types of sinkholes in the plain areas of Southern Italy. *Geodinamica Acta*, *23*(1-3), 113-127.

Dobecki, T. L., & Upchurch, B. S. (2006). Geophysical applications to detect sinkholes and ground subsidence. *The Leading Edge*, 25(3), 336-341.

Dobecki, T. L. (1990). Review: geophysical methods for karst detection and mapping, *Houston Geological Society Bulletin*, 32(5), 21-24.

Doerfliger, N., Jeannin, P. Y., & Zwahlen, F. (1999). Water vulnerability assessment in karst environments: a new method of defining protection areas using a multi-attribute approach and GIS Tools (EPIK method). *Environmental Geology*, 39(2), 165-176.

Epstein, J. B., Weary, D. J., Orndorff, R. C., Bailey, Z. C., & Kerbo, R. C. (2002). National karst map project, an update. *US Geological Survey Karst Interest Group Proceedings. Shepherdstown, West Virginia*, 43.

Gibson, P. (2004). *Application of resistivity and magnetometry geophysical techniques for near-surface investigations in karstic terranes in Ireland. Journal of Cave and Karst Studies*, 66 (2). 35-38.

Gómez-Ortiz, D., & Martín-Crespo, T. (2012). Assessing the risk of subsidence of a sinkhole collapse using ground penetrating radar and electrical resistivity tomography. *Engineering Geology*, 149, 1-12.

Grandjean, G., Gourry, J. C., & Bitri, A. (2000). Evaluation of GPR Techniques for Civil-Engineering Applications: Study on a Test Site. *Journal of Applied Geophysics*, 45(3), 141-156.

Gutierrez, F., Cooper, A. H., & Johnson, K. S. (2008). Identification, prediction, and mitigation of sinkhole hazards in evaporite karst areas. *Environmental Geology*, 53(5), 1007-1022.

Hoover, R. A. (2003). Geophysical choices for karst and mine investigations. Proceedings of International Conference on Applied Geophysics, 529-38.

Huisman, J. A., Hubbard, S. S., Redman, J. D., & Annan, A. P. (2003). Measuring soil water content with ground penetrating radar. *Vadose Zone Journal*, *2*(4), 476-491.

Kamal, H. A., Taha, M. F., & Al-Sanad, S. A. (2013). Microgravity application for detection of underground cavities in a desert karst terrain. In *Nondestructive Testing of Materials and Structures*, 949-955.

Geological Survey (2014). Introduction to MASW acquisition and processing. Kansas Geological Survey, Exploration Services. Retrieved from http://www.kgs.ku.edu/software/surfseis/masw.html Accessed 05.11.17.

Kaspar, M., & Pecen, J. (1975). Finding the caves in a karst formation by means of electromagnetic waves. *Geophys Prospect*, 23, 611–621

Keller, G. V., & Frischknecht, F. C. (1966). *Electrical Methods in Geophysical Prospecting*, Oxford, United Kingdom, Pergamon Press, 519.

Kidanu, S. T., Torgashov, E. V., Varnavina, A. V., & Anderson, N. L. (2016). ERT-based investigation of a sinkhole in Greene County. Missouri. *AIMS Geosciences*, 2 (2): 99-115.

Kruse, S. H., Grasmueck, M., Weiss, M., & Viggiano, D. (2006). Sinkhole structure imaging in covered karst terrain. *Geophysical Research Letters, 33*(2006).

Lange, A. L. (1999). Geophysical studies at Kartchner Caverns State Park, Arizona. *Journal of Cave and Karst Studies*, *61*(2), 68-72.

Loke, M. H. (2011). Tutorial: 2-D and 3-D electrical imaging surveys, 157.

Loke, M. H. (2004), Tutorial: 2-D and 3-D electrical imaging surveys, 136.

Loke, M. H. (2000). Electrical imaging surveys for environmental and engineering studies, *A Practical Guide to 2-D and 3-D Surveys*, 67.

Martínez-Moreno, F. J., Galindo-Zaldívar, J., Pedrera, A., Teixido, T., Ruano, P., Peña, J. A., ..., & Martín-Rosales, W. (2014). Integrated geophysical methods for studying the karst system of Gruta de las Maravillas (Aracena, Southwest Spain). *Journal of Applied Geophysics*, *107*, 149-162.

MASW (n.d.). Multichannel analysis of surface waves (MASW). Retrieved from http://www.masw.com/DataAcquisition.html. Accessed 11.05.2017.

Missouri Department of Natural Resources. (n.d.). Sinkholes in Missouri. Retrieved from https://dnr.mo.gov/geology/geosrv/envgeo/sinkholes.htm. Accessed 15.06.2017.

Moore, D. L., & Stewart M. T. (1983). Geophysical signatures of fracture traces in a karst aquifer (Florida, U.S.A.). *J Hydrol*, 61, 325-340.

Muchaidze, I. (2008). Imaging in karst terrain using electrical resistivity tomography. Masters Theses. 4623. www.scholarsmine.mst.edu/masters_thesis/4623. Accessed 15.01.18.

Munroe, J. S., Doolittle, J. A., Kanevskiy, M. Z., Hinkel, K. M., Nelson, F. E., Jones, B. M., Shur, Y., & Kimble, J. M. (2007). Application of ground-penetrating radar imagery for three-dimensional visualisation of near-surface structures in ice-rich permafrost, Barrow, Alaska. *Permafrost and Periglacial Processes*, 18(4), 309-321.

Nouioua, I., Rouabhia, A., Fehdi, C., Boukelloul, M. L., Gadri, L., Chabou, D., & Mouici, R. (2013). The application of GPR and electrical resistivity tomography as useful tools in detection of sinkholes in the Cheria Basin (northeast of Algeria). *Environmental Earth Sciences*, *68*(6), 1661-1672.

Obi, J. C. (2012). The use of electrical resistivity tomography (ERT) to delineate water filled vugs near a bridge foundation. *Masters Thesis*, Paper 5146, Curtis Laws Wilson Library, Missouri University of Science and Technology, Missouri.

Palmer, A. N. (1999). Origin and morphology of limestone caves. *Geological Society of America Bulletin*. 103, 1-21.

Parise, M., & Gunn, J. (2007). Natural and anthropogenic hazards in karst areas: an introduction. In: Natural and anthropogenic hazards in karst areas: recognition, analysis and mitigation. *Geological Society London*, Special Publications, 279, 1-3. DOI: 10.1144/SP279.1

Park, C. B, Miller, R. D., & Xia, J. (1999). Multichannel analysis of surface waves. *Geophysics*. 64(3), 800-808.

Park, C. B., & Miller, R. D. (2008). Roadside passive multichannel analysis of surface waves (MASW). *Journal of Environmental & Engineering Geophysics*. 13(1): 1-11.

Park, C. B., Miller, R. D., Xia, J., & Ivanov, J. (2007). Multichannel analysis of surface waves (MASW)—active and passive methods. *The Leading Edge*, 26(1), 60-64.

Peterson, E. W., Davis, R. K., & Orndorff, H. A. (2000). 17 β-Estradiol as an indicator of animal waste contamination in mantled karst aquifers. *Journal of Environmental Quality*, 29(3), 826-834.

Pueyo-Anchuela, Ó., Casas-Sainz, A. M., Soriano, M. A., & Pocoví-Juan, A. (2010). A geophysical survey routine for the detection of doline areas in the surroundings of Zaragoza (NE Spain). *Engineering Geology*, *114*(3-4), 382-396.

Reynolds International (2011). Multichannel analysis of surface waves (MASW), Technical summary sheet No. 13, *Reynolds International Limited*, Retrieved from http://www.reynolds-international.co.uk/. Accessed 09.03.16

Richardson, J. J. (2003). Local land use regulation of karst in the United States. In: Beck B. F (ed) Sinkholes and the engineering and environmental impacts of karst. ASCE Special Publication, 112, 492–501.

RSK Geophysics (2012). RSK Group PLC., *A reference for geophysical techniques and applications*, 46.

Saarenketo, T., & Scullion, T. (2000). Road evaluation with ground penetrating radar. *Journal of applied geophysics*, *43*(2), 119-138.

Siegel, T. C., Belgeri, J. J., & Terry, M. W. (1999). Compaction grouting versus cap grouting for sinkhole remediation in east Tennessee. *Hydrology and Engineering Geology of Sinkholes and Karst*, Balkema: Rotterdam, 157-163.

Sowers, G. F. (1996). Building on sinkholes: design and construction of foundations in karst terrain. *American Society of Civil Engineers*.

Stepišnik, U. (2008). The application of electrical resistivity imaging in collapse doline floors: Divača karst, Slovenia. *EVOLUTION*, *42*(33) 41-51.

Storz, H., Storz, W., & Jacobs, F. (2000). Electrical resistivity tomography to investigate geological structures of the earth's upper rrust. *Geophysical Prospecting*. 48, 455-471.

Styles, P., McGrath, R., Thomas, E., & Cassidy, N. J. (2005). The use of microgravity for cavity characterization in karstic terrains. *Quarterly Journal of Engineering Geology and Hydrogeology*, 38(2), 155-169.

Sudha, K., Israil, M., Mittal, S., Rai, J. (2009). Soil characterization using electrical resistivity tomography and geotechnical investigations. *Journal of Applied Geophysics*, 67(1), 74–79.

Šumanovac, F., & Weisser, M. (2001). Evaluation of resistivity and seismic methods for hydrogeological mapping in karst terrains. *Journal of Applied Geophysics*, 47(1), 13-28.

Šušteršič, F. (2002). Collapse dolines and deflector faults as indicators of karst flow corridors. *International Journal of Speleology*, 31(1/4), 115-127.

Telford, W. M., Geldart, L. P. & Sheriff, R. E. (1990). *Applied geophysics* (Vol. 1). *Cambridge University Press*.

The Guardian (2017). *Sinkholes*. Retrieved from https://www.theguardian.com/world/sinkholes. Accessed 08.05.17.

U.S. Geological Survey (2016). Sinkholes. Retrieved from https://water.usgs.gov/edu/sinkholes.html. Accessed 10.06.2017.

Vandike, J. E. (1993). Groundwater level data for Missouri: water year 1991-1992. *Missouri Department of Natural Resources. Division of Geology and Land Survey*. Water Resource Report No.42. Rolla, Missouri.

Waltham, A. C., & Fookes, P. G. (2003). Engineering classification of karst ground conditions. Quarterly Journal of Engineering Geology and Hydrogeology, 36 (2), 101-118. DOI: https://doi.org/10.1144/1470-9236/2002-33.

Weary, D. J. (2015). The cost of karst subsidence and sinkhole collapse in the United States compared with other natural hazards. NCKRI SYMPOSIUM 5: Proceedings of the *14th Multidisciplinary Conference on Sinkholes and the Engineering and Environmental Impacts of Karst*, National Cave and Karst Institute, 433 – 446.

Webb, D. J., Anderson, N. L., Newton, T., Cardimona, S., & Ismail, A. (2002). Ground penetrating radar (GPR): A tool for monitoring bridge scour. *Geophysics 2002, The 2nd Annual Conference on the Application of Geophysical and NDT Methodologies to Transportation Facilities and Infrastructure*, Los Angeles, California, 23.

Yassin, R. R., Muhammad, R. F., & Taib, S. H. (2013). Application of electrical resistivity tomography (ERT) and arial photographs techniques in geo hazard assessment of karst features in constructing sites in Perak, Peninsular Malaysia. *Journal of Environment and Earth Science*, 3(9), 91-125.

Zhou, W. (1997). The formation of sinkholes in karst mining areas in China and some methods of prevention. *Environmental Geology*, 31(1-2), 50-58.

Zhou, W., & Beck, B. F. (2008). Management and mitigation of sinkholes on karst lands: an overview of practical applications. *Environmental Geology*, *55*(4), 837-851.

VITA

Kenneth Bansah received his Ph.D. in mining engineering in May 2018 and Master of Science in geological engineering in December 2017 from Missouri S&T. He received a Master of Philosophy in mining engineering from the University of Mines and Technology (UMaT) in Tarkwa, Ghana and a bachelor's degree (First Class) in mining engineering from the Kwame Nkrumah University of Science and Technology in Kumasi, Ghana. He was a visiting scholar at Montana Tech in 2008 and was involved in multidisciplinary research in the areas of environmental and engineering applications of geophysics, artisanal and small-scale mining, sustainable development, occupational safety, and environmental issues.

While at Missouri S&T, Kenneth worked as a graduate research assistant and was appointed as a teaching fellow to the Saudi Mining Polytechnic in 2014. He was the director of Safety & Environmental Research Consultancy Limited, and provided consulting services to mining and related industries. In late 2016, he formed Mining & Community Research, a nonprofit organization that aims to use scientific rigor to promote sustainable development. He served as a faculty member at the mining engineering department of UMaT prior to joining Missouri S&T. Kenneth was a senior tutor at the Center for Continuing Education in the University of Cape Coast, Ghana. He was involved in the training of environmental, safety, and engineering professionals for the extractive and allied industries. Kenneth was a Tau Beta Pi Record Scholar and received the Grand Canyon SME award in 2018 for outstanding academic performance, leadership, and contributions towards the development of his community.